HIGH RESOLUTION UV SPECTROSCOPY
OF AROMATIC MOLECULES

Giel Berden

HIGH RESOLUTION UV SPECTROSCOPY
OF AROMATIC MOLECULES

HIGH RESOLUTION UV SPECTROSCOPY OF AROMATIC MOLECULES

EEN WETENSCHAPPELIJKE PROEVE OP HET GEBIED VAN
DE NATUURWETENSCHAPPEN

PROEFSCHRIFT

TER VERKRIJGING VAN DE GRAAD VAN DOCTOR
AAN DE KATHOLIEKE UNIVERSITEIT NIJMEGEN,
VOLGENS BESLUIT VAN HET COLLEGE VAN DECANEN
IN HET OPENBAAR TE VERDEDIGEN
OP WOENSDAG 21 JUNI 1995,
DES NAMIDDAGS TE 1.30 UUR PRECIES

door

WILHELMUS CAROLUS MARIA BERDEN

geboren op 12 mei 1966
te Tegelen

Promotor : **Prof. Dr. G.J.M. Meijer**

Co-Promotor : **Dr. W.L. Meerts**

aan mijn ouders

Voorwoord

Op deze plaats zou ik graag iedereen willen bedanken die op directe of indirecte wijze een bijdrage heeft geleverd aan het welslagen van het onderzoek en het tot stand komen van dit proefschrift.

- Alle (oud-)medewerkers van de afdeling Molecuul- en Laserfysica, en in het bijzonder:
- Mijn directe begeleider Leo Meerts, die een belangrijke bijdrage heeft geleverd aan het welslagen van dit onderzoek.
- Jörg Reuss, Dave Parker en natuurlijk Gerard Meijer voor hun altijd aanwezige belangstelling en voor de vele vruchtbare discussies.
- Erko Jalviste, tänan sind sinu suure osa eest selles dissertatsioonis. Algusest peale nägid sa imelikke intensiivsusi 'meie molekulide' spektrites. Sul oli õigus. Unustamattu sündmuseks on mulle siiamaani jäänud minu eelmise aasta reis Eestisse.
- Martien Kengen, Karen Remmers en Jack van Rooy voor de verstandige keuze van hun afstudeeronderzoek.
- De 'bewoners' van de altijd gezellige maar zeer rumoerige laatste-kamer-van-de-gang: permanente bewoner Harold Linnartz (hoewel je al een jaar in Bonn zit, staat de kamer nog steeds vol met je spullen), de altijd-in-Vlaardingen bewoner Michel Versluis (een directe telefoonlijn is inderdaad handig), de enige die-echt-mee-koffie-drinkt bewoner Marcel Drabbels (hoewel je het inmiddels een beetje verleerd bent), en natuurlijk de enige bewoonster Genie Stoffels (voor de vrouwelijke input; koelkast schoonmaken...).
- Johannes Heinze, Paul Uijt de Haag, Jean Schleipen, Maarten Ebben, Erik Zwart, Ad Marijnissen, Theo Brugman, LaTeX-koning Koen Schreel, Robert Klein-Douwel, Jules Spanjaars, Hans ter Meulen, Gina Cotti, Charles Spanjaars, Annemieke Kips, Maarten Boogaarts en Ger van den Hoek, voor de wetenschappelijke en maatschappelijke discussies tijdens de koffiepauzes, voor de hulp bij computer en experimentele problemen, en voor de gezellige sfeer op de laboratoria en zitkamers.
- John Holtkamp, Frans van Rijn, Chris Timmer, Eugène van Leeuwen en Cor Sikkens die altijd wel een oplossing hadden voor de vele grote en kleine electronische en technische problemen.
- Alec Wodtke for the sunny 'spectroscopy week' in Santa Barbara, en natuurlijk Marcel en Elly voor alles daar-om-heen (Viva la Fiesta!).
- Alle medewerkers van de Glasblazerij, de Instrumentmakerij, de Quick-service, de 'Ferry'-service, de afdeling Illustratie en Fotografie, het Universitair Centrum Informatievoorziening, en de afdeling Computer en CommunicatieZaken.
- Jaargenoten Jelle, Marc, en nu-jij-nog Kees.
- Welf Kreiner, within one week he doubled the amount of electronic equipment in my lab... David Pratt for the collaboration on 1-AN, and for critically reading the manuscript. Mike Schmitt and Karl Kleinermanns who introduced me in the fascinating, rotating, world of phenol and water.
- Alle vrienden voor de dingen buiten het werk. En natuurlijk mijn ouders en mijn zus, die mij altijd in alles hebben gesteund. Pap, mam en Leonie, bedankt!

Contents

Table of Contents

Chapter 1

Introduction

The combination of a supersonic molecular beam expansion and a narrow band UV laser is a powerful tool in experimental molecular spectroscopy. It can provide detailed information about the dynamics and structure of molecules and molecular complexes [1, 2, 3, 4] in both their ground and electronically excited states. Expanding volatilized organic molecules seeded in a carrier gas produces a cooling of the vibrational and rotational degrees of freedom [5]. The advantage for high resolution spectroscopy is two-fold. On the one hand, only the lowest rotational and vibrational levels in the electronic ground state are populated, leading to less congested excitation spectra. On the other hand, the low internal temperatures permit the stabilization of structural variants (tautomers or conformers) and the stabilization of molecular clusters (van der Waals and hydrogen bonded complexes).

Analysis of rotationally resolved laser induced fluorescence (LIF) spectra provides the molecular constants in both the ground and the electronically excited state. These constants are directly related to the geometrical structures in both states, giving access to information about intramolecular bond lengths, and in the case of a molecular complexes, intermolecular bond lengths and their changes upon excitation.

Unfortunately, the number of molecular constants is too small for the determination of the complete molecular structure. Consider, for example, a molecule with N atoms that can be described with an asymmetric rigid rotor Hamiltonian. There are only three rotational constants A, B and C available, while there are $3N-3$ unknown parameters. Recording the rotationally resolved LIF spectrum of an isotopically substituted molecule can give extra information to determine the position of the substituted atom *via* Kraitchman's equations [6]. Obviously, in the case of a molecule containing for example 30 atoms, determination of all atomic positions would be a very tedious process. This method is used if only a particular part of the molecule is interesting, such as the NH_2 group in 1-aminonaphthalene (Chapter 5).

If the molecule consists of parts with a well-known structure, the rotational constants of the entire molecule contain enough information to determine its structure. An example is triphenylamine (TPA), a molecule which consists of a nitrogen atom with three phenyl groups attached to it (see Chapter 2). Since the structure of each phenyl group is known, there are only a few unknown

parameters left, which are related to the relative orientation of the phenyl groups Therefore, it is possible to determine the structure of the entire molecule In all other cases the molecular constants have to be compared with other (related) molecules or with *ab initio* calculations to provide information about the structure This last comparison is very important, it is a sensitive check of the methods of calculation that are frequently used for providing a large amount of information about molecular properties

In addition to the molecular constants, one can determine the orientation of the electronic transition moment vector in the molecular frame from the high resolution spectrum This vector provides information about the direction of the electronic charge migration or displacement that occurs during the transition It is therefore related to the probability distribution functions in the involved electronic states Furthermore, from a deconvolution of the rotational line shape, the natural linewidth of the molecular transition can be obtained which gives the lifetime of the excited state

High resolution UV spectroscopy also can provide information about interactions between electronic states As an example, fluorescence excitation spectra can be perturbed by a coupling with 'dark' states (ISC, intersystem crossing) [7] The excitation spectrum of pyrazine contains many more lines than expected, owing to a coupling between single rovibronic levels of the S_1 state with many *quasi*-isoenergetic rovibronic levels of the lowest triplet state (T_1) [8, 9] Similar perturbations have been observed in the spectra of pyrimidine [10], *sym*-triazine [11] and acetylene [12]

Another interesting interaction is caused by the coupling of an internal hindered rotation with the overall rotation of the molecule Full analysis of the spectra can provide values for the barrier heights in the ground state and the excited state [13] The extent of complexity of the spectra depends strongly on the barrier heights, the direction of the internal rotation axis with respect to the overall inertial axis, and the (optical) selection rules (type of transition) In phenol, every rotational line is split into two barely resolved components due to the torsion of the hydroxyl group around the C–O bond (see Chapter 8) More complex is 1-methylnaphthalene internal rotation of the methyl group leads to a spectrum which consists of two bands (A and E lines), in which the E lines are further split by a K_a-dependent interaction [14]

In this thesis a number of high resolution UV experiments are described covering most of the aforementioned topics The spectrometer consists of a molecular beam apparatus and an intracavity frequency-doubled continuous-wave (cw) ring dye laser (265–340 nm), and has a spectral resolution of 1 part in 10^8 The studied molecular systems differ largely in size from a single molecule containing 12 atoms (phenol) to a cluster containing 41 atoms (the van der Waals complex of 1-cyanonaphthalene and triethylamine)

In Chapter 2, a spectroscopic study is presented of triphenylamine (TPA) and its van der Waals complex with argon Both the vibrationally and rotationally resolved spectra have been observed The latter spectrum for bare TPA can be fit to a symmetric top Hamiltonian This indicates that the molecule has a three-fold symmetry axis, which has important implications for its structure The high resolution spectrum of TPA-Ar is barely resolved, and could also be simulated using a symmetric top model This immediately implies that the argon atom is located on the three-fold symmetry axis of TPA

Chapter 3 describes a microwave-ultraviolet double resonance experiment on 1-cyanonaphthalene This experiment has been performed to explore the possibility of using this technique to label transitions in (dense) fluorescence excitation spectra of aromatic molecules This labeling is shown to facilitate the assignment of the UV spectrum

The limits of high resolution UV spectroscopy are almost reached in the experiment described in chapter 4 The barely resolved high resolution spectrum of the 0^0_0 band in the $S_1 \leftarrow S_0$ transition of the van der Waals complex of 1-cyanonaphthalene and triethylamine is shown This spectrum could be fit to a rigid rotor Hamiltonian Comparing the direction of the transition moment vector of the complex with that of bare 1-cyanonaphthalene, and using the rotational constants, we deduced the geometrical structure of the complex

Chapter 5 presents the results of a collaboration between the Nijmegen and the Pittsburgh high resolution groups The molecule under investigation is 1-aminonaphthalene High resolution spectra of 14 vibrational bands in the S_1 state of this molecule, and some bands of 8 isotopomers have been measured to determine the equilibrium geometry of the attached NH_2 group in both electronic states

In the next three chapters, the frequency range between 270 and 295 nm has been explored using BBO crystals for intracavity frequency doubling Chapter 6 presents the spectrum of benzotriazole All reported studies of the tautomerism in this molecule in literature show that in the solid state, in solution and in the gas phase, benzotriazole is predominantly found in the 1H-form Analysis of our rotationally resolved UV spectrum proves that 2H-benzotriazole also exists

Benzotriazole, benzimidazole, imidazole and indole form a group of molecules with similar electronic spectra The first two excited singlet states can be distinguished by the direction of the electronic transition moment vector In Chapter 7 we present accurate values for the rotational constants of the first excited singlet states of indole, indazole, and benzimidazole Furthermore, the direction of the transition moment vectors have been determined The spectra of all three molecules exhibit 'anomalous' rotational line intensities that are shown to results from an in-plane inertial axis reorientation which occurs when the molecules are electronically excited

Chapter 8 presents the spectra of phenol and the hydrogen bonded phenol/water complex The spectra are perturbed due to an interaction of a hindered internal motion with the overall rotation of the molecule In ground state of phenol, the hydroxyl group rotates around the C–O axis In the first excited state this rotation is absent due to an increase in the double-bond character of the C–O bond In the hydrogen bonded complex, the water molecule rotates around the hydrogen bond The barrier heights and the hydrogen bond lengths in the ground and excited state have been determined

The last chapter of this thesis presents the rotationally resolved fluorescence excitation spectra of several bands of the $S_1 \leftarrow S_0$ transition of 4-aminobenzonitrile (4-ABN) This molecule is closely related to the extensively studied molecule 4-N,N-dimethylaminobenzonitrile (DMABN) The rotationally resolved fluorescence excitation spectrum of DMABN is heavily perturbed due to rotation of the methyl groups The rather simple spectra of 4-ABN can provide information which will be helpfull in the analysis of the DMABN spectra

1.1 Experimental set-up

The high resolution spectrometer is represented schematically in Figure 1 1 It is composed of three parts the cw ring dye laser with its frequency calibration sources, the molecular beam machine and fluorescence detection system, and a computer system for recording, processing and analyzing the spectral data
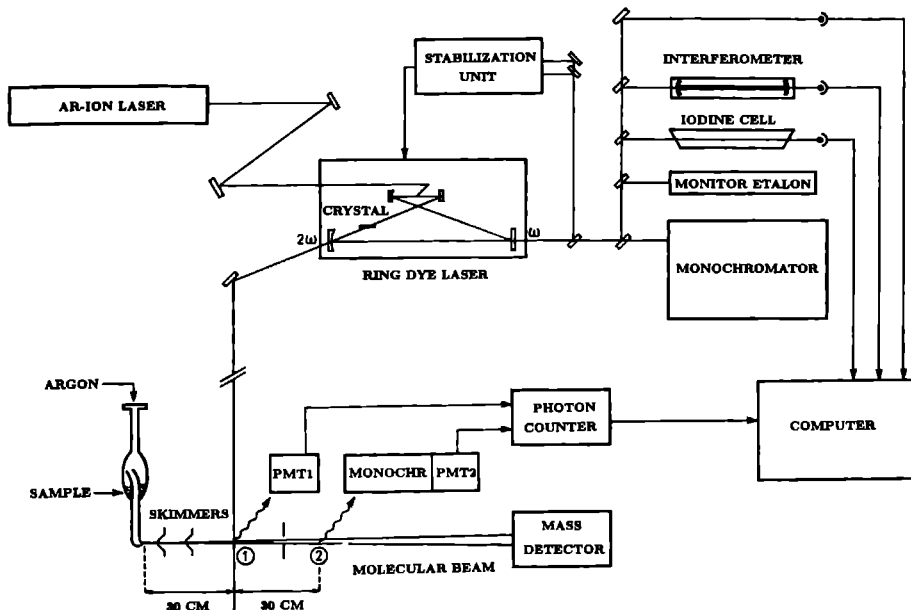
Figure 1.1: *Schematic overview of the experimental set-up.*

1.1.1 Laser system and frequency calibration

Narrow band UV radiation between 265 and 342 nm is generated by intracavity frequency doubling in a single frequency ring dye laser. This laser (a modified Spectra Physics Model 380D) is pumped by a Spectra Physics argon ion laser (Stabilite 2016) with an output power of 6 Watts (all lines). The dye laser operates between 530 and 685 nm by using three sets of specially coated mirrors and three different dyes: Rhodamine 110 (530–585 nm), Rhodamine 6G (565–630 nm), and DCM (610–685 nm).

The laser cavity is constructed by four mirrors and has two foci. In one of the foci the dye jet is positioned. If the cavity is aligned well, laser action can take place in two counter propagating directions making a figure eight. However, the laser will be unstable because there is no preference for one direction over the other. A unidirectional device consisting of a Faraday rotator and a quartz plate rotates the polarization vector of one of the travelling waves, while having no effect on the counterpropagating one. Since most of the optical devices in the laser cavity are positioned at Brewster's angle, the traveling wave with the rotated polarization will be attenuated and will never reach lasing threshold. Single mode operation is achieved by means of a single plate birefringent filter, a thin plate etalon, and a piezo-scanned thick etalon. The selected cavity mode can be scanned by changing the cavity length with two galvo-driven plates.

A small fraction of the intracavity power is coupled out of the resonator for calibration and stabilization purposes. The fundamental frequency is controlled by a modified Coherent CR 599 stabilization system. The frequency is locked to the transmission curve of a sealed-off, temperature-stabilized, low-finesse interferometer. The laser is scanned by adjusting the optical length of the

cavity of the interferometer with an inserted galvo-driven plate. The bandwidth of the laser is 3 MHz and is determined by the frequency jitter. Stabilized scans of 75 GHz at the fundamental frequency can be made.

A 30 GHz monitor etalon is used to check if the laser is single mode. A monochromator (Spex 1870) is utilized for a crude estimation of the absolute frequency (± 1 cm^{-1}). For an accurate absolute frequency calibration the absorption spectrum of the iodine molecule is recorded and compared with the well-documented reference spectrum [15]. The absolute laser frequency can be determined to an accuracy of about 100 MHz. The relative frequency is determined by measuring the transmission peaks of a high-finesse, temperature-stabilized, sealed-off Fabry-Perot interferometer with a free spectral range of 74.195 MHz. The drift of the interferometer can be as large as 50 MHz per hour. The free spectral range was calibrated in the microwave-ultraviolet double resonance experiment on 1-cyanonaphthalene (CNN) described in Chapter 3. Briefly, the fluorescence excitation spectrum of CNN was measured several times on various days. All spectra were analyzed and the UV transitions were fit together with 13 accurately measured microwave transitions. During the fit the free spectral range is one of the parameters that has to be determined. Since CNN has a very strong LIF spectrum, the total spectrum could be measured in less than 5 minutes to minimize the influence of the drift of the interferometer.

A second harmonic generating crystal is placed in the second focus (auxiliary waist) of the ring dye laser cavity to generate the desired UV radiation. The nonlinear response of the crystal to the high intensity (intracavity) fundamental wave ensures efficient generation of the frequency doubled wave. In order to minimize losses in the cavity, the crystal is cut at the Brewster angle. For generation of UV in the range of 295–342 nm LiIO$_3$ crystals are used. The crystals are angle tuned and are 1 2 mm thick. Typical UV output powers are between 1 and 10 mW, depending on the quality of the crystal, the frequency for which the crystal has been optimized, and the intracavity power at the fundamental frequency. A detailed discussion of intracavity frequency doubling in LiIO$_3$ crystals has been given by Majewski [16]. Due to self absorption of UV radiation at wavelengths below 300 nm, LiIO$_3$ cannot be used for generating UV below 295 nm. To cover this wavelength region β-BaB$_2$O$_4$ (BBO) crystals are used in the same way (angle tuning, Brewster cut, thickness) as LiIO$_3$. Output powers between 50 and 500 μW have been obtained.

1.1.2 Molecular beam machine and fluorescence detection system

The sample under investigation (a solid or a liquid at room temperature) is heated in a quartz oven to bring the molecules into the gas phase. This vapour is expanded supersonically together with 0.2–1.0 bar seeding gas (usually argon) through a quartz nozzle of 75–150 μm diameter. The quartz nozzle has the advantage that it is quite inert and can be heated up to 500 °C. The oven and the nozzle are separately wrapped with heating wire. The temperature of each part is monitored with a thermocouple. The nozzle is kept at a slightly higher temperature than the oven to prevent condensation in the orifice. A small removable quartz ball is used to partly close the entrance of the oven to prevent the sample from flowing in a backward direction where it could condense on colder parts. It is possible to fill the oven with the sample while maintaining vacuum conditions in the molecular beam machine.

The molecular beam apparatus consists of five differentially pumped vacuum chambers. The first chamber houses the quartz oven and the nozzle to generate a jet expansion. A molecular beam is formed out of this jet by two conical skimmers with a opening of 1.5 mm diameter. After passing through two interaction chambers the molecular beam enters the fifth chamber which
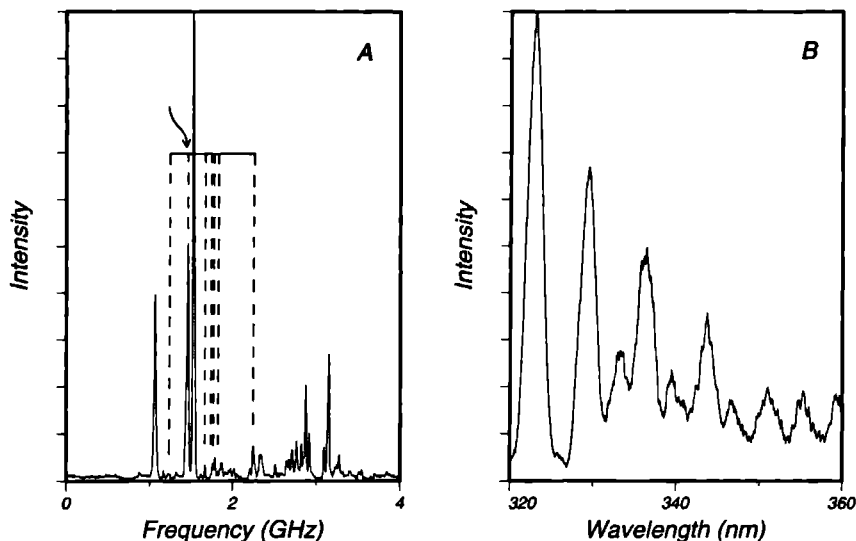
Figure 1.2: a) *High resolution fluorescence excitation spectrum of the P(2) band of pyrazine (vibronic origin of $S_1 \leftarrow S_0$). Lines belonging to the $(1,1,1) \leftarrow (2,2,1)$ transition are indicated with the horizontal bar. Instead of only a single line, 8 lines appear due to the coupling of the rotational $(1,1,1)$ state in S_1 with 7 rovibronic states in the triplet state (S_1–T_1 coupling, for a complete assignment see Ref. [9]). In literature these states are called molecular eigenstates (ME's). b) Dispersed fluorescence spectrum of pyrazine after excitation of one single ME (marked with an arrow) showing the vibrational structure in the electronic ground state. We have measured the dispersed fluorescence spectra of 11 different ME's. All spectra are identical within the experimental error.*

houses a quadrupole mass spectrometer. This detector is used for aligning the molecular beam through the skimmers and for monitoring the beam intensity during the measurements. The pressure in the interaction chambers is below 10^{-6} mbar, assuring collision free conditions.

The UV laser beam is crossed perpendicularly with the molecular beam in the third vacuum chamber at a distance of about 30 cm from the nozzle (position ① in Figure 1.1). The laser beam enters and leaves the vacuum chamber *via* windows of fused silica mounted at Brewster's angle on light baffles, which contain several diaphragms to reduce the stray light. The beam is focused to a spot size of about 1 mm at the position of the molecular beam. After excitation of the sample, the total undispersed laser induced fluorescence is collected with two spherical mirrors of equal radii. These image the fluorescence through a small hole in the upper mirror *via* a fused silica condenser onto the photomultiplier tube [17]. In this configuration the hole in the upper mirror serves as a spatial filter. The photomultiplier tube (EMI 9789QA) is placed in a cooled housing to reduce the dark counts and is connected to a photon counting system (ORTEC Brookdeal 5C1). As an example, part of the excitation spectrum of pyrazine is shown in Figure 1.2a.

In the fourth vacuum chamber, a second optical detection system is placed to disperse the fluorescence. The laser now interacts with the molecular beam at a distance of 60 cm from the

nozzle (position ② in Figure 1.1). The optical detection system is for the most part similar to the one described above. The condenser is now chosen to match the acceptance angle of a small monochromator (Oriel 77250). At the exit of this monochromator, the dispersed fluorescence is detected with a photomultiplier tube (EMI 9789QA) which is connected to the photon counting system. The transmittance of the monochromator is about 30%. Using a grating blazed at 280 nm (Oriel 77297), it was possible to measure a vibrationally resolved (resolution of 2.5 nm) dispersed fluorescence spectrum after excitation of a single molecular eigenstate of pyrazine (Figure 1.2b).

The spectral linewidth in the fluorescence excitation spectra is a convolution of two functions. First, there is a Lorentzian contribution due to the finite lifetime of the molecules in the excited state (natural line width). The molecules studied in this thesis have lifetime between 1 and 30 ns giving natural linewidths between 159 and 5 MHz. The second contribution is an experimental one. Broadening as a result of the finite interaction time of the molecules with the UV radiation and broadening due to the curvature of the wavefront are determined to be less than 1 MHz [18]. The frequency jitter of the excitation laser is about 3 MHz in the ultraviolet. The largest contribution to the experimental width is produced by residual Doppler broadening as a result of the divergence of the molecular beam, and is determined by the spatial sensitivity of the collection optics. The experimentally determined linewidth typically amounts to 12 MHz with argon as seeding gas.

1.1.3 Data acquisition, processing and analysis

Data acquisition is performed *via* a KDAC575 interface system from Keithley Instruments connected to a PC 286 AT. The KDAC575 system has 32 digital I/O channels, 8 differential analog input channels (12 bit A/D conversion) and 2 analog output channels (12 bit D/A). By software it is possible to select the gain that is used to pre-amplify the signals before conversion.

The photoncounter counts all photons within a preset time interval. The dynamic range is 8 digits. This result (and its sign) is transmitted through the digital channels to the KDAC575 in the form of a binary coded decimal (BCD) signal. The result is stored in memory of the computer as a long integer (4 bytes). The frequency markers from the interferometer, the iodine absorption spectrum, and the power, all analog signals, are after 12 bit A/D conversion stored as an integer (2 bytes). Other channels may be used to monitor other experimental parameters, such as the temperatures of the sample and the nozzle prior to the actual recording of the spectrum.

The number of samples to be taken for the various data channels while recording a spectrum need not to be the same. As a result of the high finesse of the interferometer, the markers are very narrow (5 MHz around 630 nm) and at least 10 samples should be taken of every marker. The experimental molecular linewidth is at least 12 MHz, but in most cases is larger depending on the natural linewidth of the molecule. Using the same sampling rate for every channel would give an exaggerated high sampling rate for all other channels. Therefore, two different timing sequences are used. The internal clock of the computer controls the sampling of the markers, while the sampling rate for the other channels is set equal to the sampling rate of the molecular signal (and is therefore controlled by the internal clock of the photoncounting system).

Normally four channels (molecular signal, markers, iodine and power) are read and stored. To increase the sampling rate and/or to reduce the amount of stored data, it is possible to reduce this number to two channels, the molecular signal and the markers.

Data is stored binary in a buffer block of 2000 bytes in the memory of the computer. Full blocks are written to a file on a RAM disk. When a measurement is finished the file is moved to the hard disk. Further data processing is performed on a PC 486 DX which is connected to the

data acquisition PC *via* the local network. In this way, a next measurement can be started while data from a previous measurement is being processed.

The next step is calibration and manipulation of molecular spectral data. This is done with the data analysis program *prepare*. First, the data file containing all the data channels is separated into several temporary files containing only one channel and a file that connects the data measured with different timing sequences. Then, a peak finding routine searches in the marker file for the marker positions. By interpolation *via* a third-order polynomial, the frequency scale in the other files (*e.g.*, the molecular spectrum) can be linearized. All files, linearized or unlinearized, can be viewed on the computer screen and can be manipulated. Possibilities are smoothing, normalization to the laser power, background subtraction, and fitting individual lineshapes.

Once the spectrum is linearized, it has to be analyzed. Most of the spectra in this thesis are rather complex and often contain more than 1000 spectral lines. Thus a software package has been written for simulating, assigning and fitting spectra, and viewing a simulation together with the experimental spectrum.

The first step in the analysis is determination of the band type by visual inspection of the rotational spectrum. Then, the spectrum is simulated using the appropriate Hamiltonian and selection rules, and rotational constants obtained from a structure calculation or, if available, from microwave experiments. This simulated spectrum is then visually compared with the experimental one. If no assignments can be made, the rotational constants are varied to generate a new simulation. After making a first assignment of several lines, the experimental frequencies together with quantum numbers act as input for a least-squares fitting program. The result of this fit (rotational constants, statistics, and observed minus calculated frequencies) are then examined, and a new simulation will be made based on these results, which can then be compared again with the experimental spectrum to further improve the assignments.

When viewing a simulated spectrum, it is possible to click with the mouse on a line to display the labels of this particular line. A label is a set of information such as the quantum numbers in ground and excited state, the band type, and the intensity of the rotational transition. This facilitates the assignment when viewing both the experimental and the simulated spectrum. One can click subsequently on an experimental line and a simulated line. A small panel appears on the display containing the labels of the simulated line. One can choose one or more of those labels, which are then stored in a file together with the experimental frequency. This file acts as an input file for the fitting program.

The rotational spectra of most molecules studied in this thesis can be described with an asymmetric top, rigid rotor Hamiltonian. An excellent discussion of the theory and methods for calculating frequencies and intensities of an asymmetric top has been given by Gordy and Cook [19].

References

1. W.M. van Herpen, *Ph.D. Thesis*, Katholieke Universiteit Nijmegen (1988)

2. P. Uijt de Haag, *Ph.D. Thesis*, Katholieke Universiteit Nijmegen (1990)

3. M. Drabbels, *Ph.D. Thesis*, Katholieke Universiteit Nijmegen (1993)

4. W.A. Majewski, J.F. Pfanstiel, D.F. Plusquellic and D.W. Pratt, in *Laser Techniques in Chemistry*, ed. by T. Rizzo and A.B. Myers, John Wiley & Sons, New York (1995)

5. D.H. Levy, Science **214** (1981) 263

6. J. Kraitchman, Am. J. Phys. **21** (1953) 17

7. For a recent review see W.L. Meerts, in *Jet Spectroscopy and Molecular Dynamics*, ed. by J.M. Hollas and D. Phillips, Blackie Academic & Professional, London (1995)

8. W.M. van Herpen, W.L. Meerts, K.E. Drabe and J. Kommandeur, J. Chem. Phys. **86** (1987) 4396

9. W. Siebrand, W.L. Meerts and D.W. Pratt, J. Chem. Phys. **90** (1989) 1313

10. J.A. Konings, W.A. Majewski, Y. Matsumoto and D.W. Pratt, J. Chem. Phys. **89** (1988) 1813

11. P. Uijt de Haag, W.L. Meerts and J.T. Hougen, Chem. Phys. **151** (1991) 371

12. M. Drabbels, J. Heinze and W.L. Meerts, J. Chem. Phys. **100** (1994) 165

13. For a recent review see L.H. Spangler and D.W. Pratt, in *Jet Spectroscopy and Molecular Dynamics*, ed. by J.M. Hollas and D. Phillips, Blackie Academic & Professional, London (1995)

14. X.-Q. Tan, W.A. Majewski, D.F. Plusquellic, D.W. Pratt and W.L. Meerts, J. Chem. Phys. **90** (1989) 2521
X.-Q. Tan, W.A. Majewski, D.F. Plusquellic and D.W. Pratt, J. Chem. Phys. **94** (1991) 7721

15. S. Gerstenkorn and P. Luc, *Atlas du spectroscopie d'absorption de la molecule d'iode*, CNRS, Paris (1978)
S. Gerstenkorn and P. Luc, Rev. Phys. Appl. **14** (1979) 791

16. W.A. Majewski, Optics Commun. **45** (1983) 201

17. W.A. Majewski and W.L. Meerts, J. Mol. Spectrosc. **104** (1984) 271

18. J.P. Bekooij, *Ph.D. Thesis*, Katholieke Universiteit Nijmegen (1983)

19. W. Gordy and R.L. Cook, *Microwave Molecular Spectra*, 3rd Ed., John Wiley & Sons, New York (1984)

Chapter 2

Spectroscopy of triphenylamine
and its van der Waals complexes

Gerard Meijer, Giel Berden and W. Leo Meerts
Department of Molecular and Laser Physics, University of Nijmegen,
Toernooiveld, 6525 ED Nijmegen, The Netherlands

Heinrich E. Hunziker, Mattanjah S. de Vries and H. Russell Wendt
IBM Almaden Research Center,
650 Harry Road, San José CA 95120, USA

Abstract

Both vibrationally and rotationally resolved spectra of the $S_1 \leftarrow S_0$ transition in jet-cooled triphenylamine (TPA) around 340-320 nm are reported. Medium resolution spectra (0.5-1.0 cm^{-1} resolution) are recorded using (1+1)-Resonance Enhanced Multi Photon Ionization (REMPI) with mass selective Time-Of-Flight (TOF) detection in a pulsed molecular beam apparatus. The origin of the $S_1 \leftarrow S_0$ transition is at 29520.7 cm^{-1}, higher than halfway to the ionization potential (IP) found at 6.89 eV. A vibrational progression in the symmetric torsion mode (114 cm^{-1}) as well as in the symmetric C N stretching mode (280 cm^{-1}) is observed in the electronic spectra. The spectrum of the most abundant isomer of the TPA–Ar (TPA–Kr) complexes is *blue*-shifted by 211 cm^{-1} (216 cm^{-1}) with respect to the spectrum of the free TPA molecule. High resolution spectra are recorded using Laser Induced Fluorescence (LIF) in a cw molecular beam apparatus. Individual rotational transitions are resolved and the spectrum shows unambiguously that TPA is a symmetric top molecule. The spectrum of the blue-shifted TPA–Ar isomer is the spectrum of a symmetric top molecule as well, and therefore the Ar atom has to be located on the C_3 symmetry axis, either on top of or underneath the umbrella formed by the phenyl rings. It appears that when Ar or Kr forms a complex with TPA, the first Ar, Kr, atom goes preferentially in a position on the C_3 symmetry axis of TPA, a position which causes an abnormal blue-shift of the spectrum. With the first rare gas atom located in this special position, the second rare gas atom is forced into a 'normal' position, *i.e.* above one of the phenyl-rings, causing a normal red-shift with respect to the TPA–Ar complex.

2.1 Introduction

A spectroscopic investigation of triphenylamine (TPA) is of special interest for the understanding of the interaction between the lone pair electron of the N atom and the π electrons of the adjoining aromatic phenyl groups (nπ conjugation) The interplay between nπ conjugation and steric hindrance becomes more important in going from aniline via diphenylamine to triphenylamine, the character of the lone pair electron in TPA will be strongly influenced by the molecular conformation Up to now several experiments have been performed to determine the geometrical structure of TPA in the gas-phase [1], in the liquid phase [2, 3, 4, 5] as well as in solid films [6], but a definite structure for TPA has not yet emerged from these measurements The geometrical structure of the TPA cation in the gas-phase and in solid films has also only been determined indirectly via a comparison of measured and calculated photoelectron spectra [7]

In the present work both vibrationally and rotationally resolved spectra of jet-cooled TPA are reported The geometrical structure of TPA in the S_0 and in the S_1 state is deduced from the measured rotational constants

Molecular beam techniques have been used extensively to study van der Waals complexes consisting of organic aromatic hydrocarbons bonded to rare gas atoms Such heteroclusters have provided an interdisciplinary testing ground for the energetics and the dynamics related to intermolecular potentials, cluster growth and solvent perturbations [8, 9] The microscopic solvent shifts of these heteroclusters are generally to lower energy, are linearly dependent on the polarizability of the rare gas atom and are additive for rare gas atoms in equivalent structural positions Different structural isomers have different spectral shifts A solvent shift towards higher energy has been reported for fluorobenzene [10], phenyl acetylene [11], paraxylene [12] and more recently for aniline [13, 14], the cluster of each of these molecules with three Ar atoms shows a blue-shift with respect to the cluster with two Ar atoms

In the present work we report spectra of various isomers of the TPA–Ar,Kr vdW complexes The spectra of the most abundant TPA–Ar,Kr isomers show a large anomalous blue shift with respect to the spectrum of the free TPA molecule The structure of these blue-shifted vdW complexes is determined, and the origin of the blue-shift is discussed

2.2 Vibrationally resolved (1+1)-REMPI spectroscopy

2.2.1 Experimental set-up

The search for the $S_1 \leftarrow S_0$ transition in TPA was made using pulsed lasers and a pulsed molecular beam apparatus at the IBM Almaden Research Center The vapour pressure of TPA at room temperature is about 10^{-5} Torr, and laser vaporization followed by supersonic cooling in a rare gas expansion was used to produce an intense pulsed beam of jet-cooled TPA The laser desorption jet cooling apparatus has been described in detail recently [15], and only a short experimental description will be given here

A KrF excimer laser (approx 50 μJ in a 0 25 mm diameter spot) is used to desorb the TPA from a piece of fritted glass placed very close (within two nozzle diameters) to the orifice of a supersonic jet The fritted glass acts as a matrix for the TPA, and yields a steady supply of TPA to the surface The supersonic jet is formed by expanding 8-10 atm of rare gas (Ar or Kr) through a 0 5 mm nozzle The laser desorbed molecules are entrained in the jet and their internal degrees of freedom are cooled by multiple collisions in the expansion region Rotational temperatures down to 5 K are obtained in this way The jet-cooled desorbed molecules obtain the same velocity as

the supersonically expanding rare gas, and arrive in the detection chamber after having passed through a 1 by 4 mm slit skimmer

In the detection chamber the laser desorbed TPA molecules are detected via resonant one photon $S_1 \leftarrow S_0$ laser excitation followed by one photon ionization, either by the same or by a longer wavelength laser Nd YAG pumped pulsed dye lasers with a typical bandwidth of 0 4 cm^{-1} are used for excitation and ionization The ions are formed between the extraction plates of a Wiley-McLaren type linear Time-Of-Flight (TOF) mass spectrometer A mass resolution M/ΔM of 300–400 is obtained, enough to separate TPA (245 amu) from its ^{13}C containing isotope Every single laser pulse yields a complete TOF mass-spectrum that is displayed on a digital oscilloscope and stored in a PC With the PC, gates are set over various mass-ranges, and wavelength spectra of several molecules (or molecular fragments) can be measured simultaneously

2.2.2 The $S_1 \leftarrow S_0$ transition of TPA

The origin of the lowest allowed singlet transition in TPA is found around 339 nm, the corresponding transitions in aniline and diphenylamine have their respective origins at 294 nm [16] and at 308 nm [15] In the upper part of Figure 2 1, the (1+1)-REMPI spectrum of jet-cooled TPA is shown A tunable, pulsed dye laser with a fluence of 1 0 mJ/cm^2 is used to induce the $S_1 \leftarrow S_0$ transition in TPA, and to subsequently ionize from the S_1 state Positive ions on the parent mass (245 amu) are detected Under these conditions, and even when two orders of magnitude higher laser fluences are used, no fragmentation of the TPA upon ionization is observed

In the TPA spectrum shown in Figure 2 1a, two vibrational progressions are visible, corresponding to vibrational modes at 114 cm^{-1} and 280 cm^{-1} Both of the progressions are very harmonic These are the only two low frequency modes that appear strongly when a low excitation fluence is used Although not indicated in the figure, other slightly weaker fundamental modes can be recognized in the low-fluence excitation spectrum around 383 cm^{-1}, 583 cm^{-1}, 715 cm^{-1} and 742 cm^{-1} All these modes combine again with the 114 cm^{-1} and the 280 cm^{-1} vibrations

When higher laser fluences are used for the resonant excitation step, a number of extra peaks appear A (1+1)-REMPI spectrum of jet-cooled TPA recorded with a laser fluence of 100 mJ/cm^2 is shown in Figure 2 2 The stronger peaks in the spectrum are all saturated by the excitation laser (they should thus be equally intense) and clipped by the detection electronics to better show the weaker features The peaks at 114 cm^{-1} and at 280 cm^{-1} are indicated again to aid in comparing this spectrum to the one shown in Figure 2 1a At low frequency there are extra peaks at 59 cm^{-1}, and at 131 cm^{-1}, 137 cm^{-1} and at 143 cm^{-1} All these weaker peaks combine again with the 114 cm^{-1} and the 280 cm^{-1} fundamentals The two weak peaks indicated with an asterix in the Figure show the same saturation behaviour as the strong fundamentals These peaks have always approximately 1% of the intensity of the main peaks, also when low excitation fluences are used Although these peaks are 23 cm^{-1} and 32 cm^{-1} to the blue of the TPA origin, we believe them to be hot bands, originating from vibrationally excited TPA, as will be discussed in section 2 4

In an experiment in which two frequency doubled pulsed dye lasers pumped with two independent Nd YAG lasers were used, we measured the ionization potential (IP) of TPA A low fluence dye laser (1 0 mJ/cm^2) was used to resonantly excite TPA from the S_0 to the S_1 state, whereas a second dye laser with two orders of magnitude higher fluence was used to ionize TPA from the S_1 state A wavelength scan of the second dye laser showing the onset of ionization is shown in Figure 2 3 In Figure 2 3a the onset of ionization is shown for jet-cooled TPA resonantly excited to the vibrationless level in the electronically excited S_1 state The onset of ionization is seen around
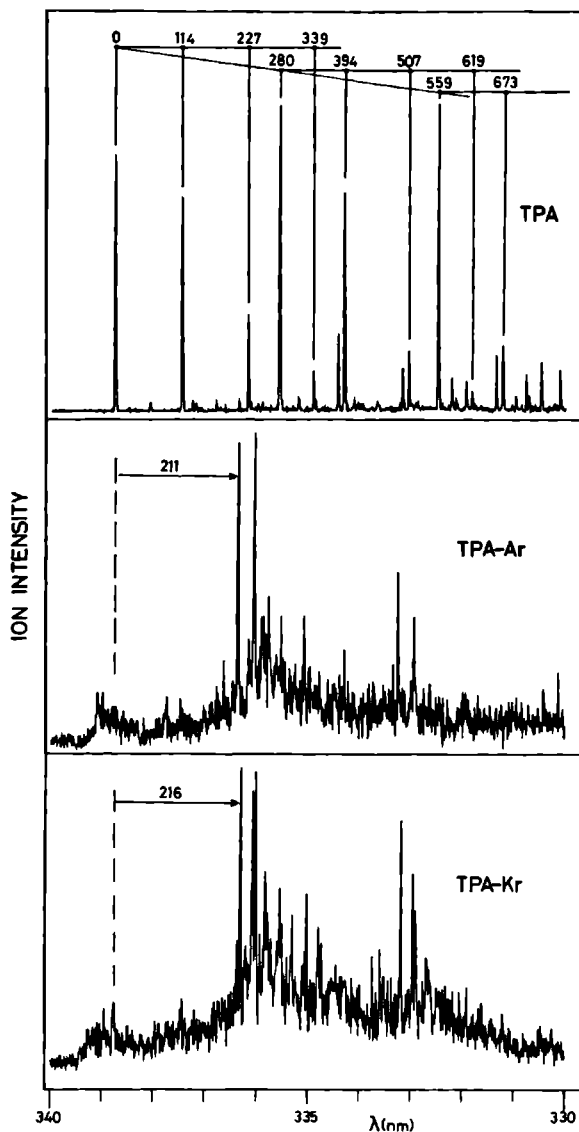
Figure 2.1: *Vibrationally resolved (1+1)-REMPI spectrum of jet-cooled TPA (A), TPA- Ar (B) and TPA–Kr (C). In all cases the parent ion is mass-selectively detected. In the spectrum of TPA, two vibrational progressions are indicated (values in cm^{-1}). In the lower panels the shift of the van der Waals complexes relative to the free TPA is indicated (in cm^{-1}).*
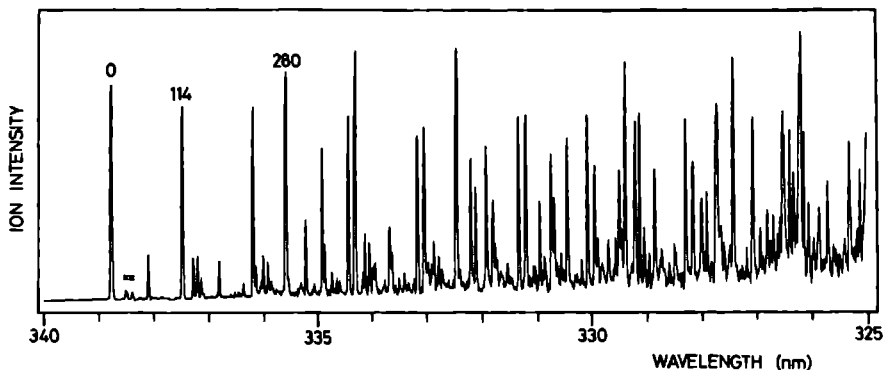
Figure 2.2: *Vibrationally resolved (1+1)-REMPI spectrum of jet-cooled TPA using 100 mJ/cm² for excitation and ionization. The stronger peaks in the spectrum are all off scale. Clear structure is observed up to at least 1000 cm⁻¹ above the S₁ origin*

385 nm, at 25968 cm^{-1} to be more precise. If TPA is resonantly excited to the 114 cm^{-1} vibration in the S$_1$ state one would expect the onset of ionization to appear when the ionizing laser has an 114 cm^{-1} lower frequency, i e around 386 7 nm. In Figure 2 3b this spectrum is shown and there is only a 10 cm^{-1} red-shift of the strongest onset of the IP, however. This indicates that the Franck-Condon factors for the transition from the S$_1$ state of the neutral to the ground state of the positive ion are more or less diagonal for this mode, from the one quantum excited 114 cm^{-1} vibration in the TPA S$_1$ state preferentially TPA ground state ions that have one quantum excited in the corresponding vibration are produced. Moreover, it can be deduced from the spectrum in Figure 2 3b that the frequency of the vibration in the ion that corresponds to the vibration of 114 cm^{-1} in the neutral is approximately 10 cm^{-1} lower, i e around 104 cm^{-1}. In Figure 2 3c something similar is seen when TPA is resonantly excited to the 280 cm^{-1} vibration in the S$_1$ state, and the ionization laser is scanned over the ionization onset. Although now a weak onset of ionization is observed around 389 nm, as expected, it can be concluded from the strong step in the ionization continuum around 385 nm that again preferentially ions that have one quantum of the corresponding vibration excited are formed. The frequency of this vibration in the ion is just a few cm^{-1} larger than 280 cm^{-1}.

The apparent IP of TPA as deduced from the spectra shown in Figure 2 3 and from the absolute frequency of the origin of the S$_1$ ← S$_0$ transition (29521 cm^{-1}) is at 6 880 eV, in good agreement with a previously estimated value [17]. It should be noted that the measurements of the IP are performed in an electric field of approximately 300 V/cm, and so the actual field-free value for the IP will be several thousandths of an eV higher [18].

From a measurement of the double resonance TPA-ion signal as a function of the time delay between the two pulsed lasers an upper limit of 6 ns is deduced for the lifetime of the TPA S$_1$ state, an exact value for the lifetime can not be determined in this way as the pulse-length of each of the dye-lasers is already 4-5 ns.
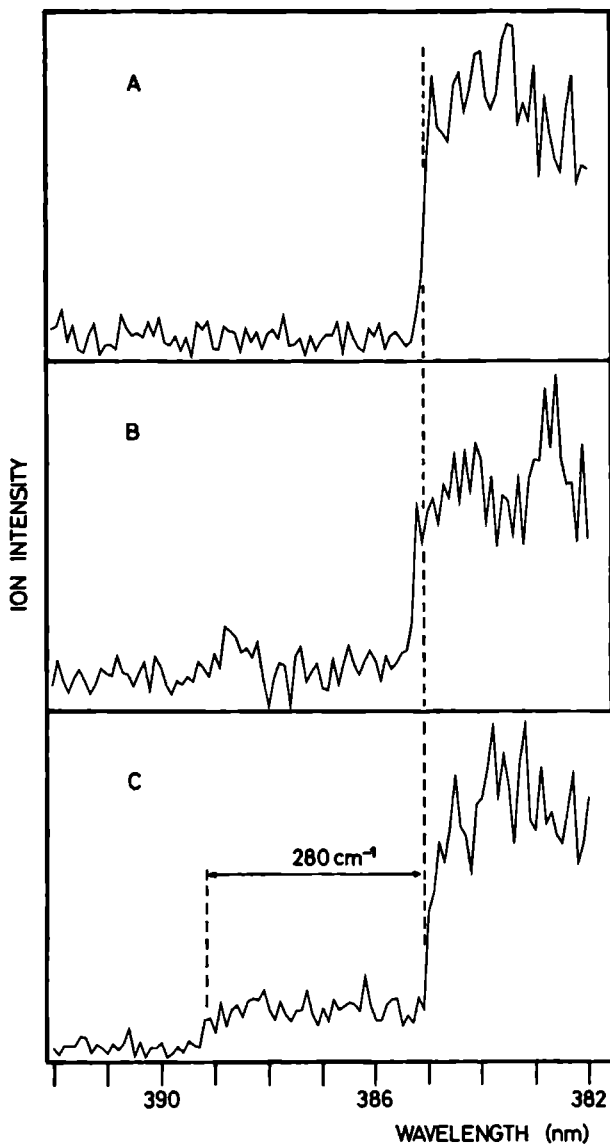
Figure 2.3: *Wavelength dependence of the TPA ion signal showing the onset of ionization after resonant excitation of TPA to (A) the vibrationless level in the S_1 state (B) the 114 cm^{-1} vibration in the S_1 state and (C) the 280 cm^{-1} vibration in the S_1 state.*

2.2.3 Spectra of TPA–Ar,Kr van der Waals complexes

We have reported previously that under slightly different desorption conditions, complexes between the laser desorbed molecules and the carrier gas can be produced, internally cooled and mass-selectively detected [19]. (1+1)-REMPI spectra of TPA–Ar and TPA–Kr obtained that way are shown in Figures 2.1b and 2.1c, respectively. Both spectra are measured at the parent mass, i.e. at 285 amu for TPA–Ar and at 329 amu for TPA–Kr, ^{84}Kr being the most abundant Kr isotope. In these spectra the intensity of the strongest peaks is about 200-500 times smaller than of those in the TPA spectrum. The most striking observation in both the spectrum of TPA–Ar and of TPA–Kr is both the size and the sign of the spectral shift with respect to the TPA origin. Never before has a blue shift been observed in the complex of an aromatic molecule with either one Ar or one Kr atom, let alone a blue shift of over 200 cm^{-1}.

One has to be careful in assigning the correct spectral features to the specific size cluster, even if mass selective detection is applied; higher TPA–Ar$_n$ clusters will fragment and give rise to a signal on the TPA–Ar$_m$ mass (m≤n) as well. There are two approaches commonly used to overcome this problem. In the first approach care is taken not to detect the fragments of larger clusters, although they are still formed [20, 21]. In the other approach, soft ionization (*i.e.* bringing the molecule just barely above the ionization limit) is applied to strongly limit the fragmentation process itself [14]. For this latter approach two different lasers would have to be used for TPA, as one-color (1+1)-REMPI of TPA can bring the ion about 3500 cm^{-1} above the IP. In our measurements of the cluster spectra we recorded the spectra of TPA–Ar$_n$,Kr$_n$ for n=0–4 simultaneously, thereby being able to trace the origin of the various lines. All the spectral features observed in Figure 2.1b and 2.1c are due to the TPA complexed with one Ar, Kr, respectively. Although there was severe fragmentation of these complexes (which made the spectra of these complexes appear just as strong at the TPA mass as at the parent mass of the complex) distinctly different spectral features were observed at the higher cluster masses.

About 30 cm^{-1} red-shifted from the TPA origin, the TPA–Ar spectrum displayed in Figure 2.1b shows a broad structure. As this is the position where we expected the origin of the $S_1 \leftarrow S_0$ transition in the TPA–Ar complex to appear, *i.e.* it is the 'normal' red-shifted position for an aromatic molecule complexed to an Ar atom, we tried very hard to optimize on this signal. There was no way, however, to get clearly resolved single sharp lines. Sharp structure does appear 211 cm^{-1} *blue*-shifted from the TPA origin. We believe this to be the origin of one of the possible, and apparently one of the most stable, TPA–Ar isomers. The TPA fundamental modes at 114 cm^{-1} and at 280 cm^{-1} are seen in the spectrum of the Ar complex as well, and from this a lower limit of 280 cm^{-1} can be deduced for the binding energy of this TPA–Ar isomer in the S_1 state.

There is another strong peak at 239 cm^{-1} to the blue of the TPA origin, which might be the origin of another isomer of TPA–Ar. Again, the main vibrational modes in the TPA molecule are built on top of this. One might also argue that this extra peak is due to a vdW Ar–TPA stretching mode at 28 cm^{-1}. In that case, however, more of these modes should appear with comparable intensity, but they don't. In addition, the relative intensity of the 211 cm^{-1} and the 239 cm^{-1} shifted peaks changes with changing laser-desorption/jet-cooling conditions, *i.e.* with changing production conditions for the van der Waals complexes. Some extra peaks that we do observe at a slightly larger frequency are attributed to vdW stretching modes of the TPA–Ar complex.

One might argue, that the structure observed for the TPA–Ar complex to the blue of the TPA origin, is due to a complex that is actually 69 cm^{-1} red shifted, and of which we only see the TPA vibrational progression (-69 + 280 = 211). Although there is absolutely no signal visible
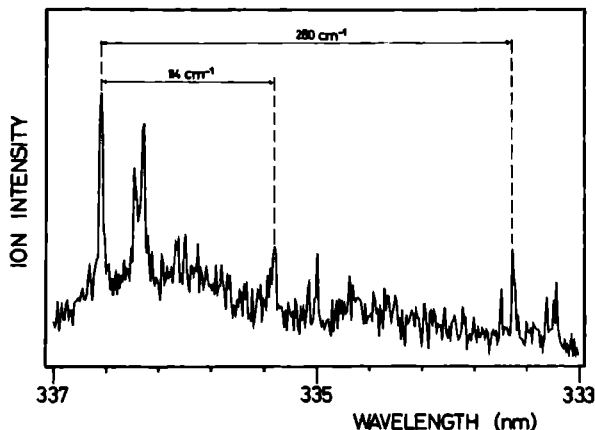
Figure 2.4: *(1+1)-REMPI spectrum of the TPA–Ar$_2$ complex. The indicated origin is 187 cm^{-1} blue-shifted from the origin of free TPA.*

at the thus predicted origin, we can also find strong experimental evidence against this conjecture by looking at the TPA–Kr complex. Kr has a larger polarizability than Ar (by a factor 1.5), and consequently a larger red-shift of the hypothetical origin (and of the TPA modes built on top of this) should be visible. Instead, a somewhat larger blue-shift (216 cm^{-1}) is observed for TPA-Kr than for TPA–Ar, ruling out this hypothesis.

All in all the spectrum of TPA–Kr looks very similar to the TPA–Ar spectrum. There is some sign of a red-shifted isomer (somewhat further red shifted than the TPA–Ar complex, as expected), but the strongest signal is from a 216 cm^{-1} blue shifted isomer. Again, the two strongest TPA modes are seen in the Kr complex as well. There is a set of two peaks visible that are approximately 21.5 cm^{-1} and 26 cm^{-1} blue-shifted from the origin of this TPA–Kr complex. It might well be that one of them is actually the origin of another TPA–Kr isomer while the other is due to a vdW TPA–Kr stretching mode.

We also measured the spectrum of the TPA–Ar$_2$ complex, and this spectrum is shown in Figure 2.4, albeit on a different wavelength scale. The origin of the strongest TPA–Ar$_2$ isomer was found at 29708 cm^{-1}, about 24 cm^{-1} red-shifted with respect to the strongest TPA- Ar origin, but still with an overall blue-shift of 187 cm^{-1} with respect to the TPA origin. As indicated in the Figure, the fundamental vibrations of TPA are seen in the spectrum of the Ar$_2$ complex as well. Again, there are some extra peaks at low frequencies, 22 cm^{-1} and 28 cm^{-1} further to the blue of the forementioned TPA–Ar$_2$ origin, which might either be due to vdW vibrations in the complex or due to other TPA–Ar$_2$ isomers.

A first conclusion from these measurements is that when Ar or Kr forms a complex with TPA, the first Ar, Kr, atom goes preferentially in a 'special' position, a position which causes an abnormal blue-shift of the spectrum. With the first rare gas atom sitting in this special position, the second rare gas atom is forced into a 'normal' position, *i.e.* above one of the phenyl-rings, causing a normal red-shift with respect to the TPA–Ar complex.

2.3   High resolution LIF spectroscopy

2.3.1   Experimental set-up

In the Nijmegen laboratory high resolution spectroscopy was performed to determine both the geometrical structure of TPA itself as well as that of the TPA–Ar complexes. Again, details of both the molecular beam machine as well as of the narrow bandwidth UV radiation source have been given in Chapter 1, and only a short description is given here.

TPA is heated in a quartz oven to approximately 200 °C (10 Torr vapour pressure) and is expanded supersonically together with 0.6–1.0 atm Ar through a 0.15 mm nozzle, kept at a slightly higher temperature. The molecular beam is skimmed twice and enters a differentially pumped LIF detection chamber about 30 cm away from the beam orifice. There the molecular beam is crossed perpendicularly with the weakly focused UV laser beam. The TPA molecules are resonantly excited from the S_0 to the S_1 state, and total fluorescence back to the ground state is detected. The UV radiation is obtained by frequency doubling in a $LiIO_3$ crystal inside the cavity of a single frequency ring dye laser, operating on DCM. By pumping the dye laser with 6 W of an Ar ion laser (all lines), 0.2–0.5 mW of tunable radiation in the 339–336 nm range with an effective bandwidth of about 3.0 MHz is obtained. A single mode laser scan can be made over 50 GHz, enough to record the whole envelope of a single ro-vibronic band in the $S_1 \leftarrow S_0$ electronic transition of TPA in a single scan. The TPA spectra are recorded together with the transmission peaks of a pressure and temperature stabilized interferometer with a free spectral range (in the UV) of 150 MHz. The absolute frequency of the transmission peaks of the interferometer, and thereby the absolute frequency of the TPA lines, is determined by the simultaneous recording of the I_2 absorption spectrum in a cell at the fundamental laser frequency. Although the I_2 absorption spectrum is relatively sparse in this region, an accuracy better than 0.1 cm^{-1} can still be obtained for the absolute frequency, the error being mainly due to the determination of the centre of the broad and not always symmetric I_2-lines. Relative line positions are measured to an accuracy of 10 MHz.

2.3.2   The rotationally resolved spectrum of TPA

In the top portion of Figure 5 the measured high resolution spectrum of the origin of the TPA $S_1 \leftarrow S_0$ transition is shown. The absolute frequency of the origin (0.0 on the scale in the Figure) is at ν_{vac}=29520.7 cm^{-1}. The signal intensity of the strongest peak is around 5000 counts/sec whereas there is a continuous background of about 200 counts/sec due to scattered laser radiation. This high resolution spectrum is clearly that of a parallel transition of a symmetric top molecule. There is a strong Q branch, blue degraded, a R branch and a P branch with a band-head. The lower portion of Figure 2.5 shows a fit to the data. Formulas for a rigid oblate symmetric top molecule are used, and these fit the data perfectly well. The constants we used are the rotational constant B'' in the S_0 state, and ΔB and ΔC, the differences of constants in the S_1 and S_0 state. The rotational constant determined by the moment of inertia around the symmetry axis of TPA, the c-axis, cannot be determined in a parallel transition of a symmetric top molecule. The values that we used in the fit are given in Table 2.1. It should be noted that the values of ΔB and ΔC are much more precise than the value of B''; the inaccuracy in the latter constant is due to a slight drift of the interferometer during the scan of the spectrum, and is the standard deviation in the value of B' obtained on various days, scanning in either frequency direction. For the C'' constant a value of 230 MHz was assumed, based on an estimate of the geometrical structure of
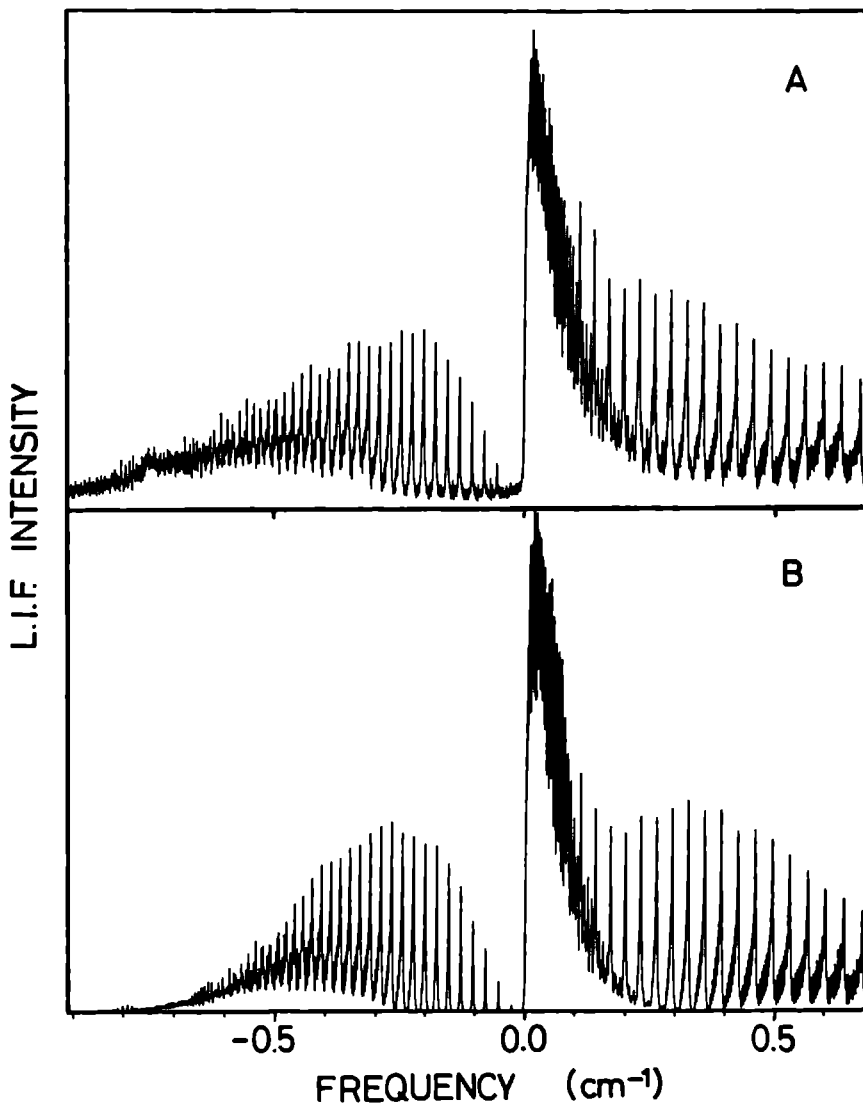
31

Figure 2.5: *High resolution LIF spectrum of the origin of the $S_1 \leftarrow S_0$ transition in jet-cooled TPA The experimentally observed spectrum (A) can be fitted into the smallest detail, using the formulas for a rigid oblate symmetric top molecule, as shown in (B) Note the band head in the P-branch for large J'',K'' values*

Rotational constants		TPA	TPA–Ar
B''	(MHz)	403.7(5)	280.0(5.0)
C''	(MHz)	230.0[a]	230.0[b]
$\Delta B \equiv B' - B''$	(MHz)	7.4(1)	-8.5(5)
$\Delta C \equiv C' - C''$	(MHz)	2.8(1)	2.8[b]

[a] Calculated value for a TPA geometry with $\phi = 50.0$ and $\angle CNC = 120.0$ degrees.
[b] Kept fixed to the value as obtained for TPA
[c] Calculated value for a TPA geometry with $\phi = 50.0$ and $\angle CNC = 120.0$ degrees.
[d] Calculated value for a TPA geometry with $\phi = 50.0$ and $\angle CNC = 120.0$ degrees.

Table 2.1: *Rotational constants for TPA and TPA–Ar as determined from the high resolution LIF spectrum of the origin of the TPA $S_1 \leftarrow S_0$ transition at 29520.7 cm^{-1} and of the 211 cm^{-1} blue-shifted origin of TPA–Ar at 29731.2 cm^{-1}.*

TPA, as will be discussed later. The exact value for this constant is not critical anyway; it only influences to a minor extent the intensities of the various lines. A perpendicular transition, which is intrinsically weak in the TPA $S_1 \leftarrow S_0$ band, has to be measured to determine the absolute value of C'' in TPA. To obtain the fit shown in Figure 2.5b, a rotational temperature of 4.0 K was assumed, a value that we typically find for the rotational temperature in large aromatic molecules using this molecular beam apparatus. J-values up to $J=100$ were included in the fit; to reproduce the observed band head in the P-branch more accurately even higher J-values have to be included.

In Figure 2.6 an enlargement of a part of the experimental (upper) and fitted (lower) R branch of TPA is shown. Individual J,K lines are resolved. In the fit a Lorentzian lineshape with a full width at half maximum (FWHM) of 40 MHz is assumed. The contribution to the linewidth due to residual Doppler broadening in the molecular beam (*i.e.* the Gaussian contribution to the linewidth) is known to be 12 MHz. The largest contribution to the observed linewidth therefore has to come from lifetime broadening. Deconvolution of the experimentally observed Voigt profile yields a Lorentzian contribution to the linewidth of around 36 MHz, implying a lifetime for individual J',K' levels in the vibrationless S_1 state of TPA of 4.5±0.5 ns.

In the fit to the experimental data the spin statistical weights have not been taken into account, as they are very close to one with 5 fermions present in each phenyl ring. No splitting is observed due to the isomeric right-hand-rotating and left-hand-rotating forms of TPA.

In addition to the origin of the $S_1 \leftarrow S_0$ transition we also measured the transitions to the 114 cm^{-1} and the 280 cm^{-1} vibrations under high resolution. We found the same rotational constants within the quoted error bars. As the spectrum of the transition to either one of these vibrations is also that of a parallel transition of TPA, both vibrations are due to symmetric modes.
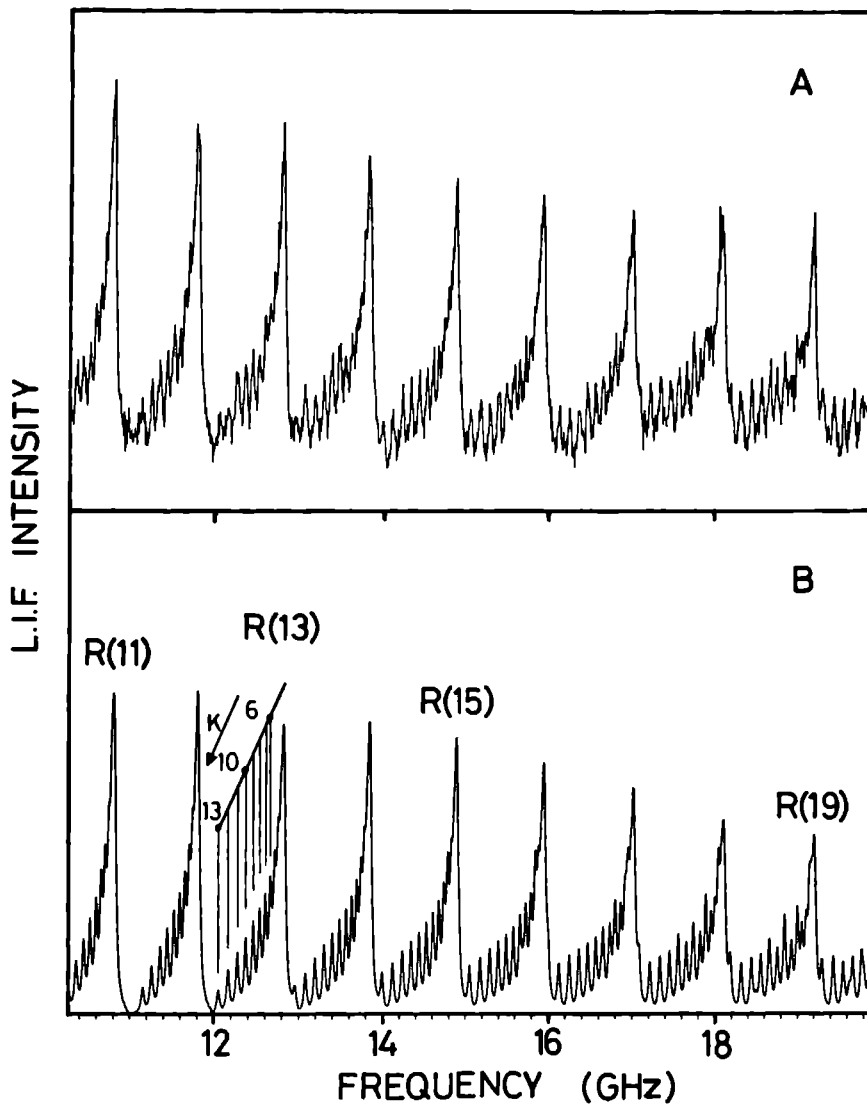
Figure 2.6: *Part of the R-branch of the experimental (A) and fitted (B) spectrum of TPA. As explicitly indicated in the figure, individual J,K lines can be resolved and assigned. The width (FWHM) of individual lines is about 40 MHz.*

34
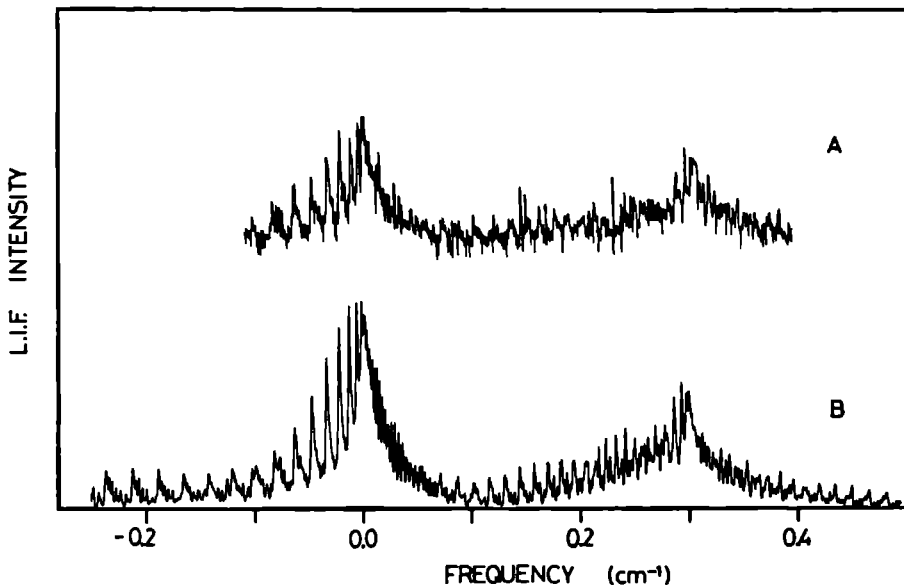
Figure 2.7: *Experimentally observed (A) and simulated (B) high resolution LIF spectrum of the origin of the 211 cm^{-1} blue-shifted TPA–Ar complex at 29731.2 cm^{-1}. The simulated TPA–Ar spectrum is for a van der Waals complex that is a symmetric top, i.e. a vdW complex in which the Ar atom is sitting on the c-axis. In the simulation the same rotational temperature (4.0 K), the same lineshape (Lorentzian, 40 MHz FWHM) and the same values for C'' and ΔC were taken as found for TPA. The simulated spectrum is for B'' = 280±5 MHz and ΔB = -8.5 ± 0.5 MHz. As now ΔB is negative, the R-branch has a band head, and the Q-branch degrades to the red.*

2.3.3 High resolution spectra of TPA–Ar

To determine the geometrical structure of especially the blue-shifted TPA–Ar complex we measured its spectrum under high resolution, as had been done previously for other vdW clusters between aromatic molecules and rare gas atoms in the same molecular beam apparatus [22, 23]. The best experimental spectrum which we managed to obtain reproducibly for the 211 cm^{-1} blue-shifted TPA–Ar isomer is shown in the upper part of Figure 2.7. Although it looks hopeless at first sight, there is some clear structure visible that we managed to simulate as shown in the lower portion of the Figure. Most importantly, the observed TPA–Ar spectrum can be simulated using the formulas for a rigid symmetric top.

In our simulation we assume the Ar atom to be located on the c-axis of the TPA molecule. Then neither C'' nor ΔC will change in going from TPA to TPA–Ar. Furthermore, we assume the individual lines to have a Lorentzian shape with a width (FWHM) of 40 MHz, just as for the free TPA. A rotational temperature of 5.0 K is taken for the simulation of the TPA–Ar complex. This leaves only two constants that have to be varied, B'' and ΔB, of which B'' can be reasonably estimated from the calculated position of the Ar atom on the c-axis in the minimum energy

configuration, as will be discussed in section 4.3. Because the observed blue shift indicates that the TPA–Ar complex is less bound in the excited state than in the ground-state one expects the N–Ar distance to increase upon $S_1 \leftarrow S_0$ excitation, producing a negative value of ΔB. Having only these two parameters to vary, the simulated spectrum shown in Figure 2.7b is obtained with $B'' = 280$ MHz and $\Delta B = -8.5$ MHz, as also indicated in Table 2.1. Since ΔB is negative, the R branch shows a band head, whereas the Q branch runs into the P branch. The apparently single sharp lines around the origin are due to a coincidental bunching of a large number of lines, and no individual J'', K'' assignments can be made. The absolute frequency of the origin of the spectrum of this TPA–Ar isomer is 29731.2 cm^{-1}, so the spectrum of this isomer is blue-shifted by 210.5 cm^{-1} with respect to the transition in TPA. The total number of lines included in the simulated part of the spectrum that is shown is about 5000.

Up to now we did not succeed in measuring the high-resolution spectrum of the (possibly) TPA–Ar isomer that is even 28 cm^{-1} further blue-shifted nor of the less-structured red-shifted TPA–Ar isomer. Both in view of the low signal to noise ratio on the TPA–Ar complex that we *did* observe as well as in view of the fact that the production conditions in the cw beam machine are very different from those in the laser desorption jet cooling apparatus, this is not too surprising.

2.4 Discussion

2.4.1 The geometrical structure of TPA

As already mentioned in the section 2.1 there is some ambiguity in the literature on the geometrical structure of free TPA in the gas-phase. The high resolution spectra reported here give a straight answer to this question: within our present accuracy of 0.1 MHz, two of the rotational constants for TPA are identical implying a symmetric top structure for TPA. This means that the TPA molecule has at least C_3 symmetry. For the rest of the discussion we will therefore use the geometry of TPA as depicted in Figure 2.8.

The three phenyl rings are assumed to be flat and identical to each other, with fixed C–C (1.379 Å) and C–H (1.070 Å) distances and ∠CCC angles and ∠CCH angles of exactly 120 degrees. The values for the bondlengths are the averaged values as obtained from a X-ray crystallographic study of TPA in the solid [6]. Then there are only three other parameters left that are allowed to vary, *i.e.* the C–N distance (taken as 1.419 Å in the S_0 state of TPA), the angle ϕ by which the phenyl groups are rotated around the C–N bond and the ∠CNC angle. The angles are defined such that a fully planar geometry of TPA means $\phi = 0$ and ∠CNC = 120 degrees. If ∠CNC is exactly 120 degrees TPA has additional C_2 symmetry axes through each of the three phenyl rings, yielding a D_3 symmetry for the molecule. In the literature up to now no definite values for either ϕ or ∠CNC have been obtained, although averaging of the existing literature values would give a ϕ somewhere between 15 and 60 degrees and a ∠CNC angle that is is quite large, between 120 and 114 degrees.

The $S_1 \leftarrow S_0$ transition in TPA is probably best described as a $\pi^* \leftarrow n$ transition, which means that if TPA is electronically excited from S_0 to S_1, one of the lone pair electrons on the N atom is moved towards the phenyl rings. Therefore, upon excitation a change is mainly expected in the bonds and the angles involving the N atom. More specifically, the C N bonds are expected to shorten and to get stiffer upon $S_1 \leftarrow S_0$ excitation.

The vibrationally resolved electronic $S_1 \leftarrow S_0$ spectrum of TPA shown in Figure 2.1a shows a progression in two low frequency modes, indicating a substantial change in the geometry of TPA
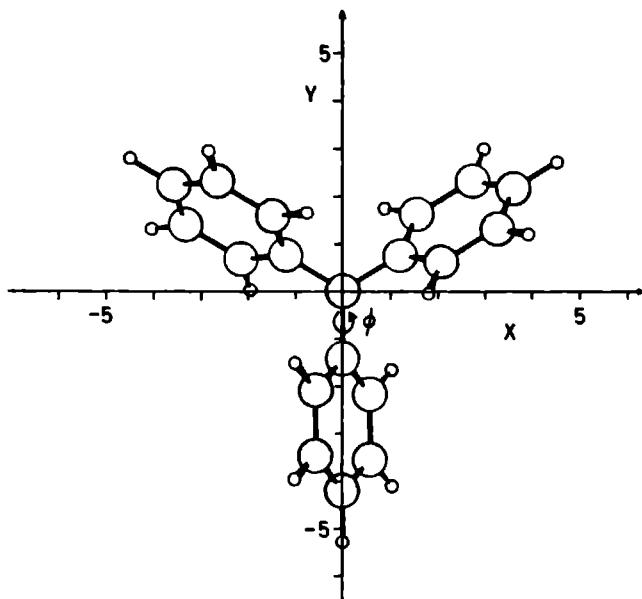
Figure 2.8: *Schematic of the TPA geometry, and the axes system used in the calculation of the TPA–Ar potential energy surface The N atom is taken to be in the origin of a right handed (x,y,z) coordinate system The scale along the x and y axis is in Å All three phenyl rings are rotated in a symmetric fashion around the C–N bonds by an angle ϕ The angle ϕ is defined such that $\phi = 90$ degrees means that all three phenyl rings are perpendicular to the plane of the paper If $\angle CNC = 120$ degrees, the molecule looks the same from the top (pos z-values) and the bottom (neg z-values) For $\angle CNC$ smaller than 120 degrees, the phenyl rings are bend down, so that positive z-values correspond to a position above the umbrella whereas negative z-values correspond to positions underneath the umbrella*

upon excitation The 280 cm^{-1} mode, which we know to be symmetric from its high resolution spectrum, is most likely due to the symmetric N-phenyl stretch mode This mode has been observed at 290 cm^{-1} in Raman spectra of TPA in a CS$_2$ solution [2] More recently, the frequency of this mode has been calculated in the S$_0$ state as well as in the ground state of the positive ion of TPA to be around 300 cm^{-1} [24] A long progression in this mode is in full agreement with the expected shortening of the C N bonds upon excitation The other low frequency vibrational mode at 114 cm^{-1} is also symmetric and is most likely due to the symmetric torsion of the phenyl rings around the C–N bond The frequency of this mode has also been calculated [24], and there is a large difference between the calculated frequency of this mode in the S$_0$ state of the neutral (74 cm^{-1}) and in the ground state of the positive ion (104 cm^{-1}) From the IP measurements as described in section 2 2 we know that the frequency of the mode corresponding to the 114 cm^{-1} vibration in the S$_1$ state *is* around 104 cm^{-1} in the ground state of the ion Apparently the frequency for the symmetric torsion mode increases substantially in going from S$_0$ to S$_1$, indicating an increased

Possible $(\phi,\angle CNC)$ combinations	TPA–Ar vdW min Above umbrella	TPA–Ar vdW min Under umbrella	Ar position $(\pm 0\ 10\ \text{Å})$
(50 0 , 120 0)	$-438\ \text{cm}^{-1}$, $+4\ 22$ Å	$-438\ \text{cm}^{-1}$, $-4\ 22$ Å	$+4\ 01$ Å, $-4\ 01$ Å
(54 5 , 119 0)	$-391\ \text{cm}^{-1}$, $+4\ 24$ Å	$-420\ \text{cm}^{-1}$, $-4\ 56$ Å	$+3\ 74$ Å, $-4\ 28$ Å
(59 0 , 118 0)	$-359\ \text{cm}^{-1}$, $+4\ 34$ Å	$-400\ \text{cm}^{-1}$, $4\ 78$ Å	$+3\ 63$ Å, $-4\ 39$ Å
(64 0 , 117 0)	$-331\ \text{cm}^{-1}$, $+4\ 44$ Å	$-383\ \text{cm}^{-1}$, $-4\ 98$ Å	$+3\ 54$ Å, $-4\ 48$ Å
(70 0 , 116 0)	$307\ \text{cm}^{-1}$, $+4\ 56$ Å	$-367\ \text{cm}^{-1}$, $-5\ 18$ Å	$+3\ 47$ Å, $-4\ 55$ Å
(80 0 , 115 0)	$-284\ \text{cm}^{-1}$, $+4\ 69$ Å	$-351\ \text{cm}^{-1}$, $-5\ 38$ Å	$+3\ 41$ Å, $-4\ 62$ Å

Table 2.2: *In the first column, various possible (ϕ, $\angle CNC$) combinations that yield a rotational constant along the b axis that is in agreement with the experimentally found value for B'' are given In the electronic ground state of TPA, ϕ and $\angle CNC$ are the only variables, for all the bondlengths as well as for all the other angles, values as obtained from X-ray analysis of solid TPA are taken In the second and thirth column the calculated minimum value for the TPA Ar van der Waals potential on the c-axis as well as the distance of the Ar atom to the N nucleus are given, for an Ar atom above and underneath the umbrella, respectively In the last column the measured value for the Ar position, i e the position as deduced from the measured B'' value for the complex, is indicated*

stiffness in the C–N bonds in the excited state The observed Franck-Condon intensity pattern in the progression of this mode is in agreement with a change in the angle ϕ of 2 to 3 degrees in going from S_0 to S_1 A Franck-Condon analysis does not give the sign of this change

In the recent theoretical calculation [24] two low frequency modes are found for TPA in the S_0 state around 20–25 cm^{-1} In the ground state of the ion these modes are at a much larger frequency, around 45–50 cm^{-1} It is expected that the frequency of the corresponding modes in the S_1 state of TPA is close to the frequency of those in the ion Under our experimental conditions these low frequency modes are certainly populated to some extent, and transitions from these non-symmetric low frequency modes in the S_0 state to the corresponding modes in the S_1 state will be blue-shifted with respect to the TPA origin The 23 and 32 cm^{-1} blue-shifted lines that are observed in the TPA spectra are therefore probably hot-bands, as mentioned in section 2 2 2

The rotational constants for TPA as determined from the high resolution spectroscopy of TPA and as given in Table 2 1, can be fitted to several geometries If it is assumed that only the C–N bondlength and the angle ϕ change upon excitation, then ΔB and ΔC indicate a decrease of the angle ϕ of 2 to 3 degrees, and a decrease in the C–N bondlength of 0 03 Å in going from S_0 to S_1 This change in ϕ is in perfect agreement with the observed Franck-Condon intensity distribution in the progression for the symmetric torsion mode The change in C–N bond length is very moderate, compared with for instance the situation in aniline [14] The absolute value of B'' can be fitted to a set of (ϕ, $\angle CNC$) angles, as indicated in Table 2 2 For all sets the changes in ϕ and the C N bond length are as mentioned before As seen in Table 2 2, if the N atom is in the plane of the three adjacent C atoms the angle ϕ is 50 0 degrees A more pyramidal structure of TPA is only in agreement with the measured B'' value if at the same time the angle ϕ increases, so if at the same time the phenyl rings turn towards a more staggered geometry Instead of the $\angle CNC$ often

the 'umbrella-angle' Θ, *i.e.* the angle by which the C–N bonds are bent out of the x,y-plane, is used. These angles are related via: $\cos(\angle CNC) = 1 - \frac{3}{2}\cos^2\Theta$.

2.4.2   The geometry of the various TPA–Ar,Kr isomers

For the 210.5 cm^{-1} blue-shifted TPA–Ar isomer the Ar atom is located on the C_3 axis, as is unambiguously shown by the high resolution spectrum of this complex. There are of course two positions possible, one underneath and one above the umbrella; these positions are equivalent if $\angle CNC$ equals 120 degrees. The positions for the Ar atom on the C_3-axis as deduced from the measured B'' value for the TPA–Ar complex are indicated in the last column of Table 2.2. The exact positions are of course strongly dependent on the choices that are made for the angles (ϕ, $\angle CNC$). In all cases, however, the magnitude and sign of ΔB for TPA-Ar imply that in the electronically excited state of the complex the Ar atom has moved considerably further away from the N-atom, approximately by (0.20±0.02) Å.

Qualitatively, the fact that the Ar atom moves further away from the N-atom upon electronic excitation is in agreement with the observed blue shift of the spectrum; both facts indicate that the Ar atom is less bound in the S_1 state than in the S_0 state.

The question remains, however, which effect causes this abnormal blue-shift. As the electronic transition in TPA is probably best described as a $\pi^* \leftarrow n$ transition, there is a larger electron density on the C_3 axis, due to the lone pair electrons of the N-nucleus, in the ground state of the TPA molecule than in the electronically excited state. Therefore a stronger overlap of the Ar atom with the electron density of TPA is expected in the ground state than in the electronically excited state. If attractive forces between the Ar atom and the TPA molecule are more important than the repulsive contributions, this would explain the sign of the observed electronic shift of the TPA–Ar complex. An explanation analogous to the one given by Hermine *et al.* to explain the blue-shift for one of the observed aniline-Ar$_3$ isomers [14] holds for the TPA–Ar complex; the Ar atom sitting on the C_3-axis slightly hinders the electron density on the N nucleus to be hybridized with the π system of the phenyl rings as much as it would like to, *i.e.* as much as it is in the free TPA. This then causes a kind of a chemical shift in the complexed TPA, bringing its spectrum more in the direction of the lowest singlet-singlet transition in benzene, this is, to the blue. It should be noted that the shift of TPA–Ar relative to TPA is about 2.5 % of the shift of TPA relative to benzene.

2.4.3   Calculations on the minimum energy TPA–Ar complex geometries

To rationalize the position of the Ar atom on the C_3 axis in TPA, as well as to rationalize the apparent existence of various TPA–Ar isomers, the potential energy surface for an Ar atom around a TPA molecule in its electronic ground state is calculated. For this, atom-atom potentials of the Lennard-Jones type are summed over all the atoms in TPA, as prescribed by Ondrechen *et al.* [25]. For the ground state of TPA interacting with an Ar atom, we use the same C–Ar, H–Ar and N–Ar interaction parameters as used in the calculation of aniline-Ar$_n$ cluster geometries [13]. The geometry of TPA in the electronic ground state is taken as discussed in section 2.4.1, and as shown in Figure 2.8. For all the different (ϕ, $\angle CNC$) combinations shown in Table 2.2, the two dimensional minimum-energy surface for an Ar atom attached to the TPA molecule is calculated. The plane defined by the N atom and the three adjacent C atoms (if $\angle CNC$ is 120.0 degrees) is taken to be the x,y plane. The z-axis is along the C_3 symmetry axis of TPA, positive z-values indicating a position above the umbrella. In (more or less) planar molecules, a two-dimensional

picture of the binding energy versus position of the Ar atom relative to the molecular framework is often given by taking a cut through the potential energy surface at a certain height above the molecule. In the case of TPA this would not make any sense, as the molecule is not planar at all. Therefore, the two-dimensional contour plots shown for two different sets of possible (ϕ, $\angle$CNC) angles in Figure 2.9, are 2-D projections from the 3-D minimum energy surface on the x,y-plane. The minimum energy values in a certain point (x,y) are calculated along the z-coordinate, from $z=\infty$ to $z=0$, and from $z=0$ to $z=-\infty$. The values for the energy minima thus obtained are plotted in a contour plot in the left and right column of Figure 2.9, respectively. Different values of z belong to each of the points in the Figure. Contour lines are drawn in 40 cm^{-1} intervals, and the contour lines at -320 cm^{-1} are indicated in each of the plots.

A first inspection of Figure 2.9 shows that it is indeed energetically favourable for the Ar atom to sit on the C$_3$ symmetry axis of the TPA molecule, although there are also some other, and even deeper, minimum energy configurations possible. In Figure 2.9a the minimum energy on the C$_3$ symmetry axis is -438 cm^{-1}, and this value is obtained for a z-value of $z=\pm4.22$ Å. The even deeper off-axis minima, indicated with numbers (1), (2) and (3), belong to z-values closer to the x,y-plane. The minimum numbered (1) is for a z value around $z=+1.0$ Å, and the minimum numbered (3) is an equivalent mimimum on the other side of the TPA, so for $z=-1.0$ Å; because in Figure 2.9a the $\angle$CNC is equal to 120 degrees, positions above and below the TPA are identical. The equivalent minima numbered (2) are in the $z=0$ plane, and these act as 'gateways' for the Ar atom to move to the other side of the molecule. A closer inspection of the contour plots learns that the minimum energy surface is critically dependent on the chosen TPA geometry. In going from the flat geometry (Figure 2.9a) towards a more umbrella like geometry (Figure 2.9b) several features change. First of all, as $\angle$CNC decreases, the 'top' and 'bottom' of TPA are no longer identical. The minimum on the symmetry axis for both positive and negative values of z becomes less deep, distinctively more so for the minimum on top of the umbrella (positive z-values) than for the one underneath. (Note that the first contour line away from the C$_3$-axis in Figure 2.9b is at -320 cm^{-1} and at -360 cm^{-1} for the left and right column, respectively.) Secondly, the various minima between the phenyl rings gradually merge together and get deeper and deeper, much deeper than the minima on the C$_3$-axis. For (ϕ, $\angle$CNC) combinations further down in Table 2.2, first the minimum on the C$_3$ axis above the umbrella but eventually also the minimum on the C$_3$-axis underneath the umbrella completely disappear.

Care should be taken in the interpretation of these contour plots. The Lennard-Jones model is too simplistic to describe the complicated vdW interactions. The atom-atom interaction parameters have been used extensively and have been optimized for a number of aromatics, but in practically all of these systems the rare-gas atom is located more or less above the center of a benzene ring. It has been pointed out recently [26] that in this case the simple Lennard-Jones atom-atom potential model works remarkably well, but that this is no longer true when the rare gas atom is further off to the side of the benzene plane. In the case of TPA–Ar, minima are found either on the symmetry axis, *i.e.* far away from the centerlines through the phenyl rings, or above one of the phenyl-rings. For the latter minima the interaction with one of the rings is probably described quite correctly, but this is certainly not the case for the interaction with the other two rings. Therefore, care should be taken especially when the relative depths of the various minima for the TPA–Ar complex are compared, as now binding to different positions in the TPA molecule is compared.

The position of the various minima is more likely to be correct, however, and it is clear from
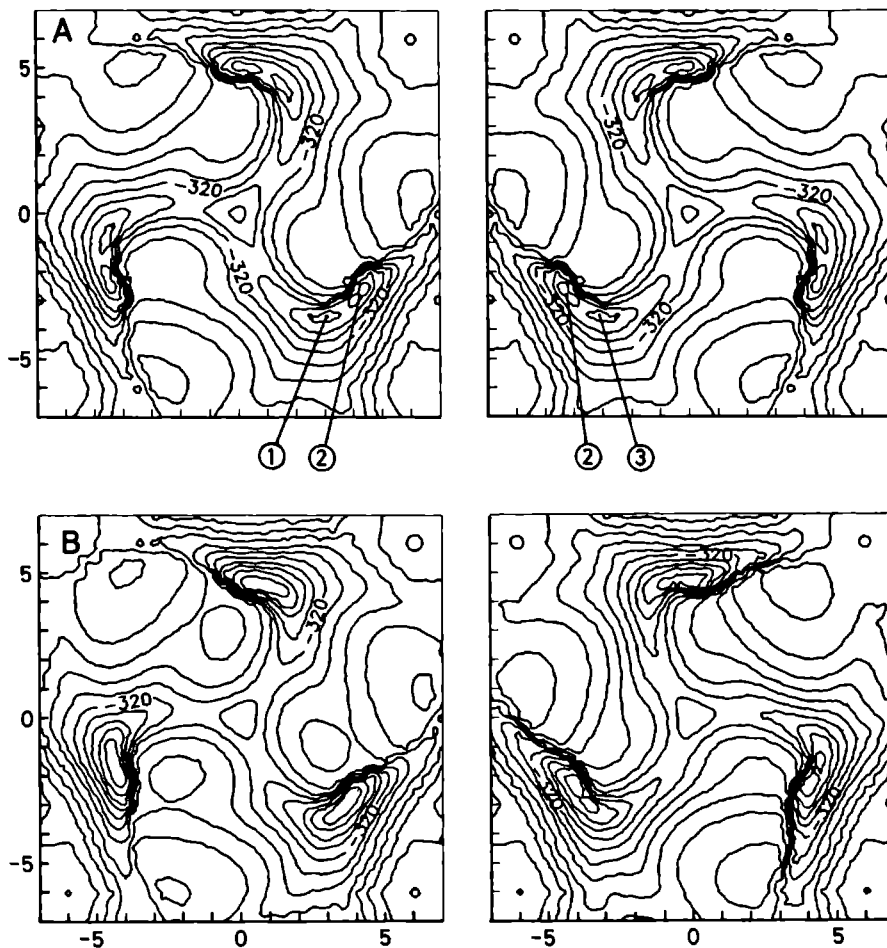
Figure 2.9: *Topographic plots of the TPA–Ar potential energy surface for two possible (ϕ, $\angle CNC$) combinations For the combination A (50 0, 120 0) and B (59 0, 118 0) the minimum energy for the TPA–Ar complex for a certain value of (x,y) is calculated as a function of z, for z-values from $+\infty \rightarrow 0$ (left column) and for z-values from $0 \rightarrow -\infty$ So the left column shows contour plots for positive z-values (positions above the umbrella) whereas in the right column the corresponding TPA Ar potential energy surface for negative z-values is projected on a 2D plane Contour lines are 40 cm^{-1} apart*

the calculations that, generally speaking, only two types of TPA -Ar complexes will be possible, *i.e.* either with the Ar atom on the C_3 symmetry axis or with the Ar atom above one of the phenyl rings. Experimentally we do observe the isomer with the Ar on the C_3-axis to be the most abundant (this is the blue-shifted complex), although there is a sign of the presence of the other type of TPA–Ar complex as well (the slightly red-shifted complex).

For each set of (ϕ, $\angle$CNC) indicated in Table 2.2, the depth of the calculated potential energy minima on the C_3 axis, as well as the z coordinate for which these minima appear are given in the second and thirth column. The measured Ar· N distance, *i.e.* the Ar–N distance inferred from the high resolution LIF spectrum of the 211 cm^{-1} blue-shifted TPA–Ar isomer, is given in the last column of Table 2.2. Of course, two positions are always possible, and the fitted Ar–N distance is dependent on the chosen TPA geometry. Best agreement between the calculated and observed Ar position is obtained if a planar TPA geometry is assumed, although a slightly bent TPA geometry can not be ruled out.

2.5 Conclusions

The rotationally resolved spectrum of the $S_1 \leftarrow S_0$ transition of jet-cooled TPA is the spectrum of a symmetric top molecule. The identical phenyl-rings are rotated around the C–N bonds out of the planar geometry over an angle ϕ of about 50 degrees. The $\angle$CNC angle is close to or equal to 120 degrees for gas-phase TPA. Upon electronic $S_1 \leftarrow S_0$ excitation, there is only a minor change in the geometry of the molecule; the C–N bondlength decreases by approximately 2% whereas the phenyl rings rotate over 2-3 degrees towards a flatter geometry.

The spectrum of the most abundant TPA–Ar complex shows an abnormal blue-shift with respect to the spectrum of the free TPA molecule. The high resolution spectrum of this blue-shifted complex is again that of a symmetric top molecule, indicating that the Ar atom is located on the C_3 symmetry axis of TPA. The spectrum of another possible TPA–Ar complex shows a 'normal' red-shift, and in this case the Ar atom is most likely located above one of the phenyl-rings.

The detailed interaction mechanism responsible for the observed blue-shift of the TPA–Ar complex is not understood yet. The TPA molecule, being a symmetric top molecule, should be perfectly suited to study the effect of an aromatic molecule-rare gas interaction in which the rare gas atom is bound to a less common place of the aromatic molecule. Moreover, the data presented here can be used to test various (empirical) models for the vdW interactions.

Acknowledgements

References

1. J. Sasaki, K. Kimura and M. Kubo, J. Chem. Phys. **31** (1959) 477

2. A.N. Rodionov, N. I. Ruch'eva, K.L. Rogozhin and D.N. Shigorin, Zhur. Prikl. Spektr. **20** (1974) 534

3. I. Janic and M. Kakas, J. of Mol. Struct. **114** (1984) 249

4. S. Higuchi, H. Tsuyama, S. Tanaka and H. Kamada, Spectr. Acta **30A** (1974) 463

5. C.W.N. Cumper and A.P. Thurston, J. Chem Soc. **B** (1971) 422

6. A.N. Sobolev, V.K. Belsky, I.P. Romm, N.Y. Chernikova and E.N. Guryanova, Acta Cryst. **C41** (1985) 967

7. C.B. Duke, J.W.-P. Lin, A. Paton, W.R. Salaneck and K.L. Yip, Chem. Phys. Lett. **61** (1979) 402

8. E. Shalev, N. Ben-Horin, U. Even and J. Jortner, J. Chem. Phys. **95** (1991) 3147, and references therein.

9. Th. Troxler and S. Leutwyler, J. Chem. Phys. **95** (1991) 4010, and references therein.

10. K. Rademann, B. Brutschy and H. Baumgärtel, Chem. Phys. **80** (1983) 129

11. P.D. Dao, S. Morgan and A.W. Castleman Jr., Chem. Phys. Lett. **111** (1984) 38

12. P.D. Dao, S. Morgan and A.W. Castleman Jr., Chem. Phys. Lett. **113** (1985) 219

13. E.J. Bieske, A.S. Uichanco, M.W. Rainbird and A.E.W. Knight, J. Chem. Phys. **94** (1991) 7029

14. P.Hermine, P. Parneix, B. Coutant, F.G. Amar and Ph. Brechignac, Z. für Physik D **22** (1992) 529

15. G. Meijer, M.S. de Vries, H.E. Hunziker and H.R. Wendt, Appl. Phys. **B 51** (1990) 395

16. N. Mikami, A. Hiraya, I. Fujiwara and M. Ito, Chem. Phys. Lett. **74** (1980) 531

17. R.A. Holroyd, J.M. Preses, E.H. Böttcher and W.F. Schmidt, J. Phys. Chem. **88** (1984) 744

18. M.A. Duncan, T.G. Dietz and R.E. Smalley, J. Chem. Phys. **75** (1981) 2118

19. G. Meijer, M.S. de Vries, H.E. Hunziker and H.R. Wendt, J. Chem. Phys. **92** (1990) 7625

20. E.J. Bieske, M.W. Rainbird and A.E.W. Knight, J. Chem. Phys. **90** (1989) 2068

21. V. Beushausen, *Ph.D. Thesis*, University of Göttingen, Germany, (1990)

22. W.L. Meerts, W.A. Majewski and W.M. van Herpen, Can. J. Phys. **62** (1984) 1293

23. W.M. van Herpen, W.L. Meerts and A. Dymanus, J. Chem. Phys. **87** (1987) 182

24. J. Pacansky, unpublished results.

25. M.J. Ondrechen, Z. Berkovitch-Yellin and J. Jortner, J. Am. Chem. Soc. **103** (1981) 6586

26. A.T. Amos, T.F. Palmer, A. Walters and B.L. Burrows, Chem. Phys. Lett. **172** (1990) 503

Chapter 3

High resolution laser induced fluorescence and microwave-ultraviolet double resonance spectroscopy on 1-cyanonaphthalene

Giel Berden and W. Leo Meerts
Department of Molecular and Laser Physics, University of Nijmegen,
Toernooiveld, 6525 ED Nijmegen, The Netherlands

Welf Kreiner
Department of Physical Chemistry, University of Ulm,
Einstein Allee 11, D-7900 Ulm, Germany

Abstract

The rotationally resolved fluorescence excitation spectrum of the 0_0^0 band in the $S_1 \leftarrow S_0$ transition of 1-cyanonaphthalene (CNN), at $\sim$318 nm, has been recorded using laser induced fluorescence in a molecular beam apparatus. This band exhibits pure a-type character and consists of $\sim$600 lines at a rotational temperature of 2.5 K, each with a linewidth of 17 MHz. A microwave-ultraviolet double resonance experiment on the 0_0^0 band of CNN has been performed to verify the rotational assignments of the fluorescence excitation spectrum and to obtain more accurate rotational constants in both the ground and electronically excited states. The band origin of the 0_0^0 band is at $31\,411.114\pm0.003$ cm^{-1} and the rotational constants are (in MHz) A''=1478.65(2), B''=956.75(1), C''=580.989(7), $A'-A''$=-21.363(9), $B'-B''$=-13.305(5), and $C'-C''$=-8.167(2).

3.1 Introduction

The combination of supersonic molecular beam expansions and very narrow band lasers is a very powerful tool in experimental molecular spectroscopy. Expanding volatilized organic molecules seeded in a carrier gas gives a cooling of vibrational and rotational degrees of freedom. The advantage for high resolution spectroscopy is twofold. On the one hand, only the lowest rotational and vibrational levels in the electronic ground state are populated, leading to less dense excitation spectra. On the other hand, owing to the low temperature, stabilization of molecular clusters can occur.

Rotationally resolved laser induced fluorescence (LIF) spectra can provide detailed information about the geometrical structures in both ground and electronically excited states. Analysis of rotational bands becomes difficult in two cases. First, when the natural lifetime of the excited state is too short, rotational lines become too broad to be resolved resulting in a band contour [1]. Secondly, when the molecule is very large the rotational constants are too small to resolve all the rotational structure in the spectrum. If the molecule under investigation can be described as a rigid symmetric top, the analysis of a partially resolved spectrum is still possible; *e.g.*, triphenylamine and its van der Waals complex with argon [2]. But in the case the molecule has to be described as an asymmetric top, analysis can be difficult due to the large number of unknown molecular parameters; *e.g.*, tetracene-argon complex [3], or due to the presence of hybrid bands [4].

The application of double resonance spectroscopy can be very useful for identifying transitions in spectra of asymmetric rotors [5]. The present paper demonstrates the microwave-ultraviolet double resonance technique for 1-cyanonaphthalene (CNN). This molecule is taken as a test case because it is expected to have a partially resolved spectrum; the rotational constants are expected to be somewhat smaller than those of naphthalene, 1-fluoronaphthalene, 1-hydroxynaphthalene and 1-methylnaphthalene whose spectra have already been measured [6, 7, 8, 9], and the natural lifetime of CNN is known to be 22.4 ± 0.2 ns [10], short compared to 1-fluoronaphthalene (110 ns [11]) and 1-methylnaphthalene (353 ns [11]). Therefore, the Lorentzian contribution to the total experimental linewidth in CNN will be 7.1 MHz. The resolution of our UV spectrometer, which consists of a strongly collimated molecular beam and an intracavity frequency doubled ring dye laser, is 12 MHz [12], so that the experimental linewidth is expected to be on the order of 17 MHz (Voigt profile). Hollas and Thakur [13] showed that several 1-substituted naphthalenes have a transition moment not (totally) parallel to the a-inertial axis. Since the CN substituted group exhibits rather similar electronic properties, CNN could be regarded as a possible candidate for a hybrid band.

3.2 Experimental

An extensive description of the molecular beam apparatus and the narrow band UV laser system has been given in Chapter 1. Crystalline 1-cyanonaphthalene (Aldrich-Chemie, 98%) was heated in a quartz nozzle to approximately 100 °C. A molecular beam was formed by a continuous expansion of a mixture of CNN vapor and argon (500–600 Torr) through a nozzle with a diameter of 0.15 mm. The nozzle was kept at a slightly higher temperature to prevent condensation of CNN in the orifice. The molecular beam was skimmed twice in a differential pumping system.

The CNN molecule was resonantly excited from the S_0 to the S_1 state at a distance of 30 cm from the nozzle orifice. The total fluorescence back to the electronic ground state was imaged onto a photomultiplier connected to a photon counting system interfaced with a computer. Narrow band

UV radiation was generated by intracavity frequency doubling a single frequency ring dye laser (a modified Spectra Physics 380D). By using a 2 mm thick $LiIO_3$ crystal, 2 mW of tunable radiation was obtained in the 312–320 nm range with an effective bandwidth of 3 MHz. The excitation spectra of CNN were recorded together with the transmission peaks of a pressure and temperature stabilized interferometer with a free spectral range of 75 MHz. This value was determined in a microwave-ultraviolet double resonance experiment as will be discussed later. For absolute frequency calibration, the iodine absorption spectrum [14] was recorded.

To perform microwave-ultraviolet (MW-UV) double resonance experiments, microwave radiation was fed into the region where the UV laser interacts with the molecular beam. Microwave radiation with a frequency range between 2 and 10 GHz was generated by a backward wave oscillator (BWO) whose frequency was phase locked to a harmonic of a synthesizer. The radiation was transported to the vacuum chamber by a coaxial cable and coupled into the excitation region by an antenna mounted on the inner core of the coaxial cable. This antenna was an open loop with a diameter of about 1.5 cm and was positioned in such a way that the laser beam can pass through it. Although this method introduced a lot of stray light, this was the only way to get the MW radiation into the desired region without changing the UV collecting system drastically.

Because of the poor coupling, the intensity of the MW radiation at the crossing point of laser and molecular beam is not known. By amplitude modulation of the MW radiation it is possible to resolve the double resonance signal through digital lock-in techniques. First the UV excitation spectrum is measured. Then the UV frequency is fixed to a (not necessarily totally resolved) rotational transition $(J, K_-, K_+)' \leftarrow (J, K_-, K_+)''$, and the MW frequency is varied until the double resonance signal is found. This MW frequency corresponds to a transition in the vibrationless electronic ground state $(J, K_-, K_+)''_u \leftrightarrow (J, K_-, K_+)''_l$ in which $(J, K_-, K_+)''$ is either the upper (subscript u) or lower (l) level. Keeping the MW frequency fixed to this transition and scanning the UV laser while monitoring the double resonance signal gives a spectrum belonging exclusively to electronic transitions originating from $(J, K_-, K_+)''_u$ and $(J, K_-, K_+)''_l$, the last ones with opposite phases.

3.3 Results

In Figure 3.1 the electronic origin of the $S_1 \leftarrow S_0$ fluorescence excitation spectrum of 1-cyanonaphthalene is shown. The absolute frequency of the band origin (0.0 on the scale of the Figure) is at $31\,411.114 \pm 0.003$ cm^{-1}. The fluorescence is very strong. The signal intensity of the strongest peak is around 700,000 counts/sec per mW laser power, whereas there is a continuous background of about 10,000 counts/sec per mW due to scattered light. The spectrum contains more than 600 lines and was recorded in less than 10 minutes. In this way the drift of the interferometer during the scan is minimized.

The spectrum shows the characteristic P, Q, and R branch structure and can be identified as an a-type band with selection rules $ee \leftrightarrow eo$ and $oo \leftrightarrow oe$ for $K'_- K'_+ \leftrightarrow K''_- K''_+$.

As a starting point for the analysis a spectrum was simulated using an asymmetric rotor Hamiltonian and calculated rotational constants obtained from a crude geometrical structure. This spectrum was then compared with the experimental spectrum and an initial assignment was made. The assigned lines were then returned into the fitting program. At the end 170 lines were included in the fit and all parameters were varied simultaneously resulting in a fit with a standard deviation of 4.0 MHz. All lines could be fitted within the experimental accuracy.
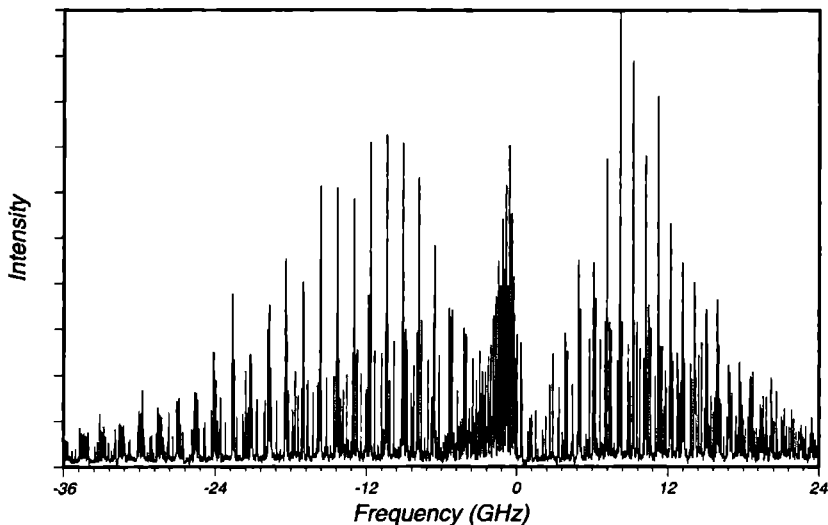
Figure 3.1: *High resolution LIF spectrum of the origin of the $S_1 \leftarrow S_0$ transition of 1-cyanonaphthalene. The absolute frequency of the origin (0.0 on the scale of the figure) is at $31\,411.114 \pm 0.003$ cm^{-1}.*

Although there is no doubt of the correctness of the assignments a double resonance measurement has been performed for two reasons. In the first place we wanted to investigate this technique for new applications; *i.e.*, to rotationally resolve the electronic excitation spectrum of aromatic molecules in a molecular beam. Secondly, the observation of a number of microwave transitions and fitting simultaneously the microwave and ultraviolet data allows a more accurate determination of the free spectral range of our interferometer that is used for relative frequency calibration of the UV excitation spectra. In addition, more accurate values are obtained for the rotational constants.

Because there were no accurate ground state rotational constants available from other microwave experiments we calculated microwave transitions from the rotational constants resulting from the fit of the $S_1 \leftarrow S_0$ transition, assuming that the dipole moment in the electronic ground state has a component along the a-axis. Then, the MW frequency was scanned around the predicted value and continued as has been discussed in the previous section.

Some double resonance spectra are shown in Figures 3.2 and 3.3. Individual rotational levels are labeled according to the convention $(J, K_-, K_+)''$ and $(J, K_-, K_+)'$ where the double prime denotes the vibrationless electronic ground state and the single prime the electronically excited state.

In the upper panel of Figure 3.2 the MW frequency has been fixed to the $(5,1,4)'' \leftrightarrow (6,1,5)''$ transition and the UV laser has been scanned over a large frequency interval. One would expect to see two lines with opposite phase in every branch: $(4,1,3)' \leftarrow (5,1,4)''$ and $(5,1,4)' \leftarrow (6,1,5)''$ in the P-branch, $(6,1,5)' \leftarrow (5,1,4)''$ and $(7,1,6)' \leftarrow (6,1,5)''$ in the R-branch, and $(5,1,5)' \leftarrow (5,1,4)''$
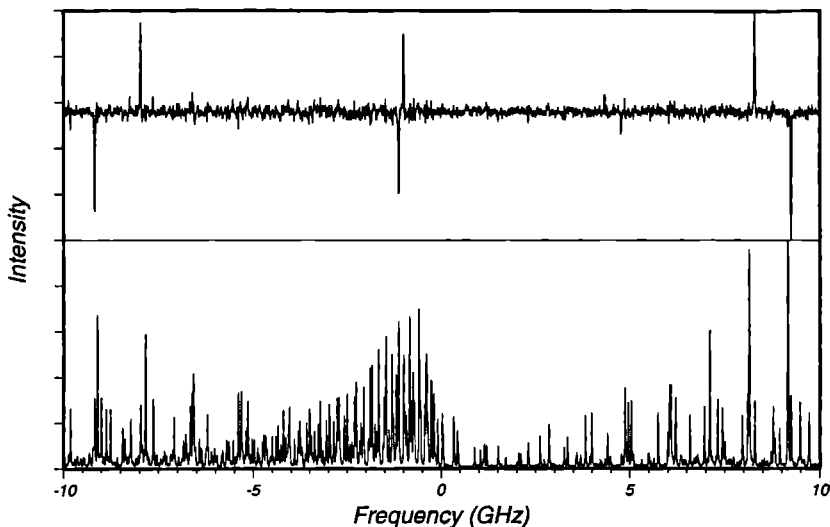
Figure 3.2: *Central part of the microwave-ultraviolet double resonance spectrum of CNN (upper panel). The MW frequency is fixed at 8828 MHz, the UV laser is scanned. The lower panel shows the corresponding part of the UV excitation spectrum. The lines in the double resonance spectrum can be assigned as (from left to right): $(5,1,4)' \leftarrow (6,1,5)''$ and $(4,1,3)' \leftarrow (5,1,4)''$, $(7,7,0)' \leftarrow (7,7,1)''$ and $(7,6,1)' \leftarrow (7,6,2)''$, $(6,1,5)' \leftarrow (5,1,4)''$ and $(7,1,6)' \leftarrow (6,1,5)''$. See text for further details.*

and $(6,1,6)' \leftarrow (6,1,5)''$ in the Q-branch. However, a-type electronic transitions in the Q-branch involving low K_--values, with respect to J, have very low intensities and are not detectable in our case. Therefore only the two lines on the right and left side of the spectrum can be attributed to a transition involving either $(5,1,4)''$ or $(6,1,5)''$ in the electronic ground state. The origin of the two lines in the center will be discussed later. In the lower panel of Figure 3.2 part of the UV excitation spectrum in the same frequency range is shown. The reduction of the number of lines in the double resonance spectrum is evident; instead of 600 lines, only 6 lines (in this particular case) are observed.

In Figure 3.3 an example in the dense part of the Q-branch is given. The MW frequency is fixed to a transition with high K_- (with respect to J), $(5,5,0)'' \leftrightarrow (6,5,1)''$. It is clearly seen that the $(5,5,1)' \leftarrow (5,5,0)''$ and $(6,5,2)' \leftarrow (6,5,1)''$ transitions can be resolved from the UV spectrum.

Because the two lines in the middle of the double resonance spectrum of Figure 3.2 have intensities on the same order of magnitude as lines in the P and R branch, they have to arise from a transition in the Q-branch involving high K_- values (with respect to J). Since there are no other a-type microwave transitions (with high K_-) at exactly (*i.e.*, within 1 MHz) the same frequency as the $(5,1,4)'' \leftrightarrow (6,1,5)''$ transition, there could be a microwave b-type transition accidentally at the same frequency. Although one can immediately see that CNN possesses a permanent dipole moment component parallel to the a inertial axis it cannot be ruled out that there exists also a perpendicular component in the plane of the naphthalene molecule , *i.e.*, parallel to the b-axis.
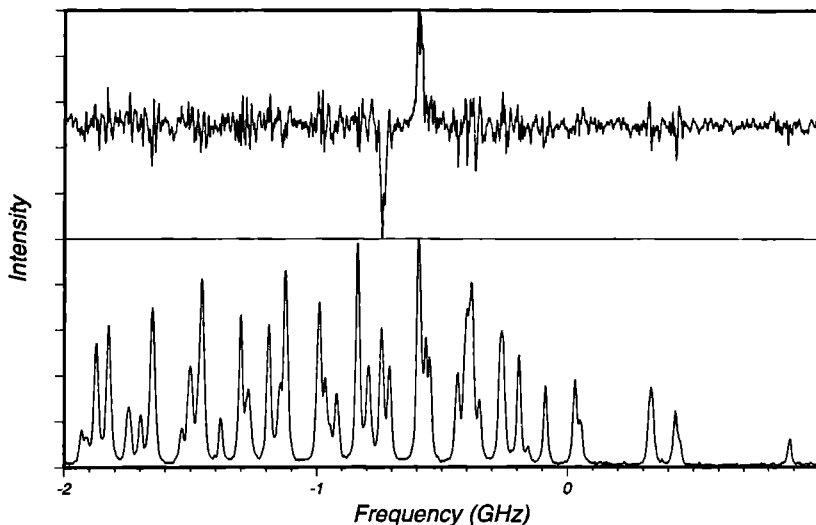
Figure 3.3: *Part of a MW-UV double resonance spectrum of CNN (upper panel) showing UV transitions in the dense part of the Q-branch. The microwave frequency is fixed to the (5,5,0)″ ↔ (6,5,1)″ transition. The lower panel shows the corresponding part of the UV excitation spectrum. The lines in the double resonance spectrum can be assigned as (from left to right): (6,5,2)′ ← (6,5,1)″ and (5,5,1)′ ← (5,5,0)″.*

Indeed the two lines in the center of Figure 3.2 can be assigned to an a-type UV transition originating from one of the levels involved in the b-type microwave transition $(7,6,2)'' \leftrightarrow (7,7,1)''$. For a b-type transition the selection rules are $ee \leftrightarrow oo$ and $oe \leftrightarrow eo$ for $K'_- K'_+ \leftrightarrow K''_- K''_+$. The UV transitions can thus be assigned as $(7,6,1)' \leftarrow (7,6,2)''$ and $(7,7,0)' \leftarrow (7,7,1)''$. Note that the phases of the lines are correct as compared to those of the P and R lines.

With the double resonance technique we measured 13 microwave transitions (12 a-type, 1 b-type) with an accuracy of about 1 MHz. This last value depends on the lineshape and linewidth of the microwave transition. These 13 transitions and 170 UV transitions have been included in a fitting program in which an extra parameter (a correction factor for the free spectral range of the interferometer) was varied simultaneously, resulting in a fit with a standard deviation of 1.5 MHz. It should be noted that including only 1 b-type MW transition increases the accuracy of the A rotational constant by a factor of four.

However, the overall precision of the UV data is limited by thermal drift of the frequency markers during the scan of the laser. The magnitude of this error can be determined by scanning the spectrum several times on various days. From the fit, we obtain the origin of the transition and the rotational constants A, B, and C in the ground state as well as in the excited state. The constants are listed in Table 3.1 together with the asymmetry parameters and the inertial defects.

With these constants one can calculate the microwave frequencies for the above mentioned a-type $(5,1,4)'' \leftrightarrow (6,1,5)''$ and b-type $(7,6,2)'' \leftrightarrow (7,7,1)''$ transitions. The results are 8828.0 and

Molecular Constants			
A''	1478.65(2)	ΔA	−21.363(9)
B''	956.75(1)	ΔB	−13.305(5)
C''	580.989(7)	ΔC	−8.167(2)
κ''	−0.16280(3)	$\Delta\kappa$	0.0009(1)
$\Delta I''$	−0.15(1)	$\Delta(\Delta I)$	−0.05(2)
Band origin	31 411.114±0.003 cm^{-1}		

Table 3.1: *Molecular constants of 1-cyanonaphthalene; the rotational constants A, B, and C (in MHz), the asymmetry parameter κ, and the inertial defect $\Delta I = I_c - I_a - I_b$ (in amu Å^2) in the electronic ground state and their differences with the first excited state ($\Delta A = A' - A''$, etc.).*

8827.4 MHz respectively, both within the experimentally determined linewidth.

The shape of the UV excitation spectrum due to line intensities and linewidths can be simulated by assuming a rotational temperature of 2.5±0.5 K and a linewidth of 17 MHz. The linewidth of our spectrometer is known to be 12 MHz owing to residual Doppler broadening, transit time effects, fluorescence collection optics and laser linewidth, leaving a contribution owing to the lifetime of CNN. This lifetime can be estimated to be about 19 ns, in agreement with the value of 22.4±0.2 ns found by Saigusa *et al.* [10].

3.4 Discussion

The rotational constants of 1-cyanonaphthalene have a value of about 75–80% of those found for other 1-substituted naphthalenes like 1-fluoronaphthalene (FN) [7], 1-methylnaphthalene (MN) [9], 1-hydroxynaphthalene (HN) [8] and 1-aminonaphthalene (AM) [13]. This is not surprising since the attached CN group is heavier than the attached groups in the above mentioned molecules. The value of the inertial defect of the vibrationless electronic ground state of CNN is equal to that of naphthalene (−0.14 amu Å^2) [6]. The geometrical structure in this state can thus be described as planar. Exciting CNN to the vibrationless first electronically excited state changes the structure only slightly. The molecule remains planar and, since the rotational constants in the excited state are only a little bit smaller, there is a small increase in the dimensions of the molecule in all directions of the plane.

A more interesting result from our measurements is the direction of the transition moment (TM). Because the experimental spectrum only shows a-type character the TM is parallel to the a-inertial axis. This axis makes an angle of 45° with the x-axis (*i.e.*, the long axis in naphthalene, see Figure 3.4). A number of other 1-substituted naphthalenes exhibit hybrid bands. Knowing the intensity ratio of the a and b-type bands makes it possible to calculate the magnitude (however, not the sign) of the angle θ between the a-axis and the TM by using the relation [15]:

$$\tan^2 \theta = I(b)/I(a) \tag{3.1}$$

Both FN and MN have 75±5% a-type and 25±5% b-type, giving $\theta = \pm30 \pm 5°$ [7, 9]. For
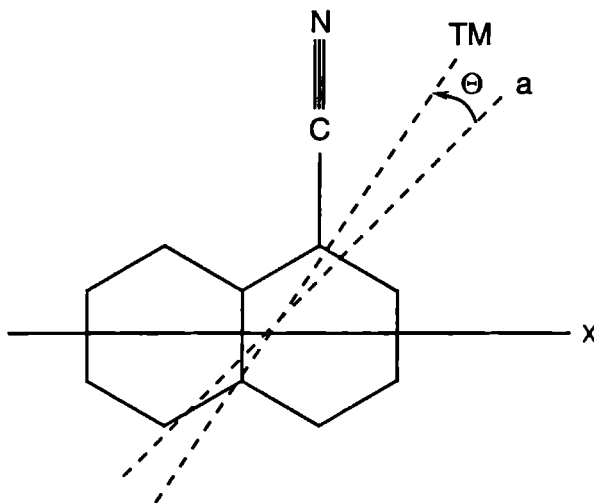
Figure 3.4: *Schematic of the 1-cyanonaphthalene geometry and the axis system used. The axis labeled with a is the a-inertial axis, the one labeled with TM is the transition moment axis. The angles measured in the counterclockwise sense are taken to be positive.*

HN, two rotamers have been distinguished [8]. The *trans*-rotamer (*t*-HN) has 71±5% *a*-type character resulting in $\theta = \pm 33 \pm 5°$, and *cis*-hydroxynapthalene (*c*-HN) is for more than 99% *a*-type thus having a transition moment parallel to the *a*-axis. A rotational contour analysis performed by Hollas and Thakur [13] of the rather featureless 0_0^0 band of 1-aminonaphthalene (AN) gives a predominant *a*-type character but the existence of 25% *b*-type cannot be ruled out. PPP calculations performed by Singh and Thakur [16] show that FN, AN, HN (they did not distinguish the two rotamers) and 1-chloronaphthalene all have the same direction for the transition moment. Their calculation also indicates that one should take the minus sign for θ. Because the *a*-axis makes an angle of 16°-18° with the *x*-axis in the case of FN, HN, AN and MN, the transition moment then will make an angle of −13° to −16° with the *x*-axis (supposing that AN has hybrid character and regarding only *t*-HN). However, both *c*-HN and CNN have their transition moment (almost) parallel to the *a*-axis. In this case there is no ambiguity for the direction of the TM. The angles between TM and *x*-axis are 16° and 45°, respectively.

If, however, we take the opposite sign of θ for FN, *t*-HN, AN and MN the transition moment of all these molecules make an angle between 47° and 48° with the *x*-axis. Although we are speculating , this choice of θ leads to an interesting point of view; all transition moments of the presently studied 1-substituted naphthalenes have a transition moment pointing in the same direction. The different angle for *c*-HN can be attributed to the influence of the lone pair electrons at the oxygen as has been pointed out by Johnson *et al.* [8].

In this paper we have shown that microwave-(narrow band) ultraviolet double resonance spectroscopy can be applied to aromatic molecules in a strongly collimated molecular beam. However, owing to the large number of populated levels, even at very low rotational temperatures, one has to

be careful in the assignment because of accidentally coinciding microwave transitions as has been demonstrated for 1-cyanonaphthalene. For this molecule we have deduced the rotational constants and the direction of the electronic transition moment. Since the dipole moment in the electronic ground state possesses components along both the a-axis and b-axis, MW-UV double resonance spectroscopy especially improves the accuracy of the rotational A constant. Comparison of the direction of the transition moment of 1-cyanonaphthalene with other 1-substituted naphthalenes shows that this molecule is one of the few examples having a transition moment parallel to the a-inertial axis.

Acknowledgements

References

1 B B Champagne, D F Plusquellic, J F Pfanstiel, D W Pratt, W M van Herpen and W L Meerts, Chem Phys **156** (1991) 251

2 G Meijer, G Berden, W L Meerts, E Hunziker, M S de Vries and H R Wendt, Chem Phys **163** (1992) 209

3 W M van Herpen, W L Meerts and A Dymanus, J Chem Phys **87** (1987) 182

4 L A Philips and D H Levy, J Chem Phys **85** (1986) 1327

5 W Gordy and R L Cook, *Microwave Molecular Spectra*, 3rd Ed , John Wiley & Sons, New York (1984)

6 W A Majewski and W L Meerts, J Mol Spectrosc **104** (1984) 271

7 W A Majewski, D F Plusquellic and D W Pratt, J Chem Phys **90** (1989) 1362

8 J R Johnson, K D Jordan, D F Plusquellic and D W Pratt, J Chem Phys **93** (1990) 2258

9 X Q Tan, W A Majewski, D F Plusquellic and D W Pratt, J Chem Phys **94** (1991) 7721

10 H Saigusa, M Itoh, M Baba and I Hanazaki, J Chem Phys **86** (1987) 2588

11 B A Jacobson, J A Guest, F A Novak and S A Rice, J Chem Phys **87** (1987) 269

12 P Uijt de Haag, *Ph D Thesis*, Katholieke Universiteit Nijmegen (1990)

13 J M Hollas and S N Thakur, Molec Phys **27** (1974) 1001

14 S Gerstenkorn and P Luc, *Atlas du spectroscopie d'absorption de la molecule d'iode*, CNRS, Paris (1978)
S Gerstenkorn and P Luc, Rev Phys Appl **14** (1979) 791

15 J M Hollas, *High Resolution Spectroscopy*, Butterworths, London (1982)

16 R A Singh and S N Thakur, J Cryst Mol Struct **11** (1981) 197

Chapter 4

Rotationally resolved spectroscopy on the 1-cyanonaphthalene/triethylamine van der Waals complex in a molecular beam

Giel Berden and W. Leo Meerts
Department of Molecular and Laser Physics, University of Nijmegen,
Toernooiveld, 6525 ED Nijmegen, The Netherlands

Abstract

The rotationally resolved fluorescence excitation spectrum of the 0_0^0 band in the $S_1 \leftarrow S_0$ transition, at $\sim$318 nm, of the 1-cyanonaphthalene/triethylamine van der Waals complex has been recorded using laser induced fluorescence in a molecular beam apparatus. This spectrum could be fitted to a pure a-type band. From the rotational constants a T-shaped geometry could be deduced.

4.1 Introduction

Exciplex formation in jet-cooled 1-cyanonaphthalene/triethylamine (CNN/TEA) was first reported by Saigusa and Itoh [1, 2]. The excitation spectrum of CNN/TEA consists of only narrow band spectral features and resembles that of the CNN monomer. This indicates that the initially excited state of the complex is located in CNN. The efficiency of exciplex formation depends strongly on the excitation energy [2, 3]. Excitation of the complex into the origin band shows only resonant emission, while excitation into vibronic bands with increasing excess energy (>400 cm^{-1}) shows that the resonant emission is decreasing in favour of broad and structureless emission, characteristic for exciplex formation.

Recently, Zingher and Haas [4] reported a multiphoton ionization study of the jet-cooled CNN/TEA system. They showed that under suitable stagnation conditions a large number of cluster ions of the type [CNN/TEA$_n$]$^+$ are formed. The 1 1 cluster ion (n=1) appears to be more prominent than all others. Zingher and Haas suggest that this observation indicates the presence of an energetically stable species, with the same mass as the CNN/TEA ion, possibly due to the formation of a chemical bond. They also discussed the possible role of the exciplex intermediate in the sequence leading to the production of this species.

These results suggest that the van der Waals complex of CNN and TEA plays an important role. Information about the geometrical structure of this complex in both the ground state and first electronically excited state can provide a more detailed insight in the step leading to exciplex formation. Rotationally resolved laser induced fluorescence, using a very narrow bandwidth laser in combination with a molecular beam, can provide this information. Recently, we reported the high resolution excitation spectrum of 1-cyanonaphthalene [5]. From this spectrum, the rotational constants and the direction of the electronic transition moment were obtained.

In this contribution, the rotationally resolved excitation spectrum of the origin in the S$_1$ ← S$_0$ transition of the CNN/TEA van der Waals complex is reported. By comparing the direction of the electronic transition moment of the complex with that of the CNN monomer, and by comparing the rotational constants obtained from the experimental spectrum with those obtained from a crude geometry calculation, possible geometries for the CNN/TEA van der Waals complex will be discussed.

4.2 Experimental

The experimental set-up for high resolution measurements has been described in Chapter 1. Only the relevant features are given here. Crystalline 1-cyanonaphthalene (Aldrich-Chemie, 98%) was heated in a quartz nozzle to approximately 100 °C. A molecular beam was formed by a continuous expansion of CNN vapor and pre-mixed TEA in argon (backing pressure 0 8 bar) through a nozzle with a diameter of 0 15 mm. The nozzle was kept at a slightly higher temperature to prevent condensation of CNN in the orifice. The pre-mixture consists of 90 mbar TEA in 6 bar argon. The molecular beam was skimmed twice in a differential pumping system and was crossed perpendicularly with a UV laser beam at about 30 cm from the beam orifice.

UV radiation with a bandwidth of 3 MHz was generated by intracavity frequency doubling in a single frequency ring dye laser operating on DCM. By using a 2 mm thick Brewster cut LiIO$_3$ crystal, 2 mW of tunable radiation was obtained. For relative frequency calibration a temperature stabilized Fabry-Perot interferometer was used with a free spectral range of 75 MHz. For absolute frequency calibration, the iodine absorption spectrum [6] was recorded simultaneously.
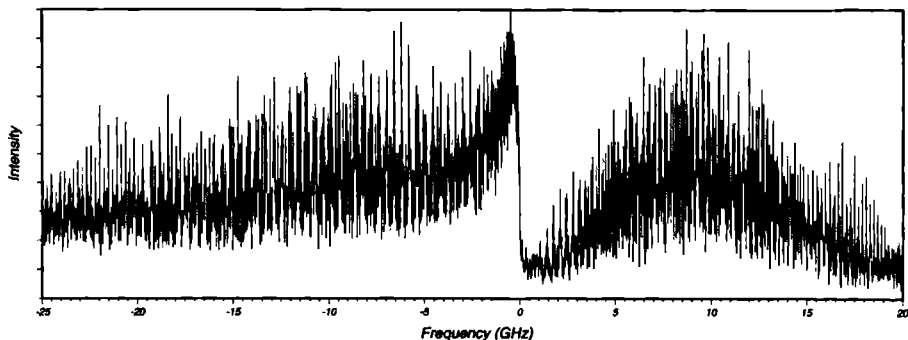
Figure 4.1: *High resolution LIF spectrum of the origin of the $S_1 \leftarrow S_0$ transition of 1-cyanonaphthalene/triethylamine. The absolute frequency of the origin (0 on the scale of the figure) is at 31 425.022±0.003 cm^{-1}.*

The total undispersed fluorescence was collected by two spherical mirrors and imaged on a photomultiplier connected to a photon counting system interfaced with a computer. The instrumental linewidth of our spectrometer is 12 MHz and is mainly determined by residual Doppler broadening.

4.3 Results

From the vibrationally resolved excitation spectra, it is known that the 0_0^0 band of the CNN/TEA van der Waals complex is blue shifted from the CNN monomer origin by 13.8 cm^{-1} [7]. The absolute frequency of the origin of CNN is known very accurately from high resolution measurements and amounts 31 411.114±0.003 cm^{-1} [5]. Adding the aforementioned blue shift gives the frequency region of the complex.

In Figure 4.1, the high resolution excitation spectrum of the electronic origin of the $S_1 \leftarrow S_0$ transition of CNN/TEA is shown. The absolute frequency of the band origin (0 on the scale of the figure) is at 31425.022±0.003 cm^{-1}. The blue shift is therefore 13.908±0.004cm^{-1}. Because of the characteristic P, Q, and R branch, one can immediately identify the band as dominated by an a-type. The spectrum is not totally resolved. The part with the least amount of spectral features, the beginning of the R branch, is shown in Figure 4.2a. This part is most useful to start the assignment. Since the van der Waals complex is very large it is difficult to start with calculating rotational constants from an estimated geometry because these constants are very sensitive to the (unknown) intermolecular distance.

To estimate the B constant, the spectrum was smoothed over 100 MHz. The result is a spectrum with lower resolution and unresolved K structure, from which one can determine a B constant of about 180 MHz. The a-type character of the excitation spectrum indicates that the electronic transition moment vector (TM) is parallel to the a-axis (*i.e.* the long inertial axis). Since the complex is locally excited in the CNN chromophore, the TM of CNN/TEA will point in the same direction as the TM of the CNN monomer. That the orientation of the TM of the bare chromophore is relatively unaffected by complex formation is shown by Plusquellic and Pratt [8]
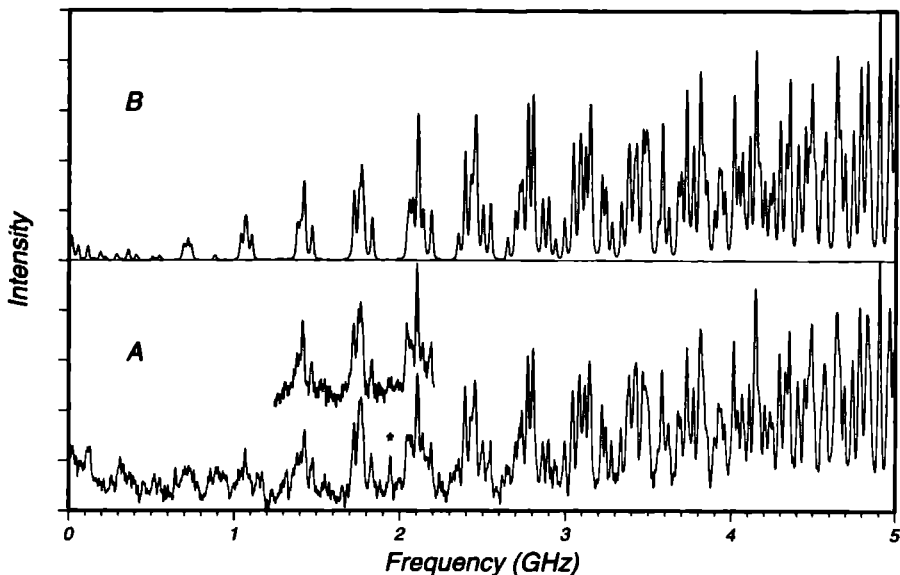
Figure 4.2: *The beginning of the R branch; a) experimental spectrum (same as in Figure 4.1); b) simulated spectrum. The inset of a) shows a small part of an experimental spectrum obtained with a slightly higher backing pressure.*

for the hydrogen bonded complex of *trans*-2-hydroxynaphthalene and ammonia. The orientation of the TM in CNN is known to be parallel to its a-axis [5]. Therefore, the a-axis of the CNN/TEA complex has to be parallel to the a-axis of the CNN monomer. To ensure that both a-axes are parallel, TEA has to be located on that axis. By making a crude calculation of the rotational constants as a function of the intermolecular distance (assuming several geometries) and matching the B constant to the above mentioned value, we obtained also estimated values for the rotational constants A and C.

With these estimated rotational constants, a spectrum was simulated using an asymmetric rotor Hamiltonian. This spectrum was then compared with the experimental one and an initial assignment was made. The assigned lines were then returned into the fitting program, giving new rotational constants which were used to generate a new simulation, and so on. Since, even for low J values, the K structure is not totally resolved, one has to compare the experimental spectrum and the simulation very carefully. At the end 130 lines were included in the fit and all parameters were varied simultaneously resulting in a fit with a standard deviation of 3 MHz. It should be noted that the included lines are not only from the part which is shown in Figure 4.2a, but also from the P branch and the remainder of the R branch. However, owing to thermal drift of the frequency markers, the overall precision of the line frequencies is limited. The magnitude of this error can be estimated by scanning the spectrum several times on various days. The rotational constants A'', B'', and C'', and the inertial defect $\Delta I''$ ($\Delta I = I_c - I_b - I_a$) in the ground state, as well as their differences with those in the excited state are listed in Table 4.1.

Molecular Constants			
A''	683(8)	ΔA	−4 712(7)
B''	192 4(3)	ΔB	−0 98(1)
C''	170 4(1)	ΔC	−1 048(9)
$\Delta I''$	−400(10)		
Band origin		31 425 022±0 003 cm^{-1}	

Table 4.1: *Molecular constants of 1-cyanonaphthalene/triethylamine, the rotational constants A, B, and C (in MHz), and the inertial defect $\Delta I = I_c - I_b - I_a$ (in amu $Å^2$) in the electronic ground state and their differences with the first excited state ($\Delta A = A' - A''$, etc)*

In Figure 4 2b the simulation of the beginning of the R branch is shown using the fitted rotational constants, a rotational temperature of 7 K and a line width of 16 MHz Deconvolution of this lineshape gives a contribution owing to the lifetime of CNN/TEA This lifetime can therefore be estimated to be between 24 ns and 34 ns, which is in agreement with the value of 29 5±0 3 ns obtained from fluorescence decay measurements [3] It should be noted that a large part of the 'noise' in the experimental spectrum actually consists of real rotational lines from $\Delta J = 0$ transitions with very high rotational quantum numbers ($J > 30$) These lines still have intensity because the cooling for these high J levels is less efficient The line marked with an asterisk is a pile up of several high Q lines, which disappears in a colder spectrum, which is shown in the inset of Figure 4 2a This spectrum has been obtained with a slightly higher backing pressure

The resemblance between the total experimental experimental spectrum and the simulation is very good, taking into account the higher rotational temperature for high J transitions There is no indication that the experimental spectrum has a hybrid character This has been confirmed by simulation The excitation spectrum of the origin of CNN/TEA is a pure a-type band

4.4 Discussion

From the rotational constants and the character of the band (i e the direction of the electronic transition moment vector), it is possible to estimate the geometrical structure of the CNN/TEA van der Waals complex An important observation is the a-type character of the band This means that the TM points along the a-axis of the complex Since the direction of the TM in the complex is the same as the known direction of the TM in the CNN monomer, the direction of the a-axis in CNN/TEA is also known If we take a coordinate system with CNN in the xy plane and the x-axis along the long axis of the naphthalene frame, the a-axis of CNN/TEA makes an angle of 45° with the x-axis, pointing towards the CN group and lying in the xy plane [5]

This observation leads to a restriction in possible geometries for the complex TEA is located on the a-axis of the CNN monomer, or is located above the center of mass of CNN in a so called *sandwich* geometry In the latter case the intermolecular distance must be small so that the intermolecular axis can not take over the role of the a-axis The consequence of this restriction in intermolecular distance is that the rotational constants B and C would be much larger than the

experimental values, ı e the *sandwich* structure ıs not prolate enough (the asymmetry parameter κ'' calculated from the rotatıonal constants ın Table 4 1 ıs −0 91) Thus the *sandwich* structure for the complex can be rejected and TEA ıs therefore located on the a-axıs of the CNN monomer

There are now two possible structures left the complex ıs planar or T-shaped If the complex ıs planar, the ınertıal defect of CNN/TEA would have more or less the same value as the ınertıal defect of TEA, sınce the ınertıal defect of CNN ıs very small ($\Delta I''$=−0 15 amu Å^2) [5] Takeuchı *et al* have determıned the molecular structure of TEA by gas electron dıffractıon, *ab ınıtıo* calculatıons and vıbratıonal spectroscopy at room temperature [9] They also reported that TEA has three conformers wıth C_1, C_s, and C_3 symmetry and that theır populatıons are respectıvely 33%, 11%, and 56%, from whıch the C_3 conformer ıs most stable We therefore used the structure of the C_3 conformer ın our calculatıons Then, the ınertıal defect of bare TEA (and of CNN/TEA ıf ıts structure ıs planar) ıs −23 amu Å^2, much smaller (ı e closer to zero) than the experımentally derıved value of −400 amu Å^2 A planar structure ıs therefore rejected

One geometry ıs left a T-shape structure ın whıch the nıtrogen atom of TEA ıs located on the a-axıs of the CNN monomer and the C_3 symmetry axıs of TEA ıs ın the CNN plane (xy plane) The calculated ınertıal defect ıs then −387 amu Å^2 and ıs ın the same order as the measured value $\Delta I''$=−400 amu Å^2 It ıs easıly seen that the rotatıonal constants B and C are sensıtıve to the ıntermolecular dıstance and the A constant ıs sensıtıve to the orıentatıon of the C_3 axıs of TEA wıth respect to the a-axıs of CNN

A more general and quantıtatıve search for possıble complex geometrıes was obtaıned by calcu-latıng the rotatıonal constants and prıncıpal ınertıal axes as a functıon of sıx parameters, whıch are necessary to descrıbe all possıble orıentatıons of TEA wıth respect of CNN, and comparıng these calculated values wıth those obtaıned from the fitted spectrum The result ıs the above mentıoned T-shape ın whıch the C_3 axıs of TEA (almost) coıncıdes wıth the a-axıs of CNN (thıs C_3 axıs also coıncıdes wıth the a-axıs of the complex) Matchıng the experımental data, there are two possıbılıtıes TEA ıs located near the CN group (see Fıgure 4 3), or at the opposıte sıte (between the hydrogens at the 5- and 6-posıtıon), wıth an ıntermolecular dıstance (between the center of mass of CNN and TEA) of about 5 7 Å, The latter orıentatıon can be rejected because TEA ıs too close to CNN It should be noted that the rotatıonal constants are not sensıtıve to rotatıon of TEA around ıts C_3 axıs and also not to whıch of the two sıdes of TEA ıs facıng CNN Summarızıng, the structure of the CNN/TEA complex ıs most probably T-shaped ın a way that the C_3 symmetry axıs of TEA coıncıdes wıth the a-axıs of CNN The ıntermolecular dıstance, between the center of mass of CNN and TEA ıs about 5 7 Å The calculated rotatıonal constants are A=690 MHz, B=189 MHz and C=167 MHz

Recently, Brenner *et al* [10] reported an experımental and theoretıcal study of 1-cyanonaphtha-lene clustered wıth acetonıtrıl (AN) and water (W) They calculated the geometry of CNN/AN, CNN/W and CNN/AN/W and showed that these complexes are planar, and that there exısts a strong, maınly electrostatıc, ınteractıon ınvolvıng a hydrogen atom and an electronegatıve atom (N or O) For CNN/AN two conformers are calculated ın whıch the ınteractıon ıs between the N of CNN and a hydrogen atom of AN, and between the N of AN and the hydrogen atom ın the 8-posıtıon of CNN for one conformer and the 2-posıtıon for the other one The geometry of the latter conformer resembles that of the aforementıoned geometry of CNN/TEA

Excıtatıon of CNN/TEA to the vıbratıonless first electronıcally excıted state changes the struc-ture only slıghtly It ıs known [5] that on excıtıng the CNN monomer there ıs a small ıncrease ın the dımensıons of CNN ın all dırectıons of the molecular plane Comparıng the change ın rota-
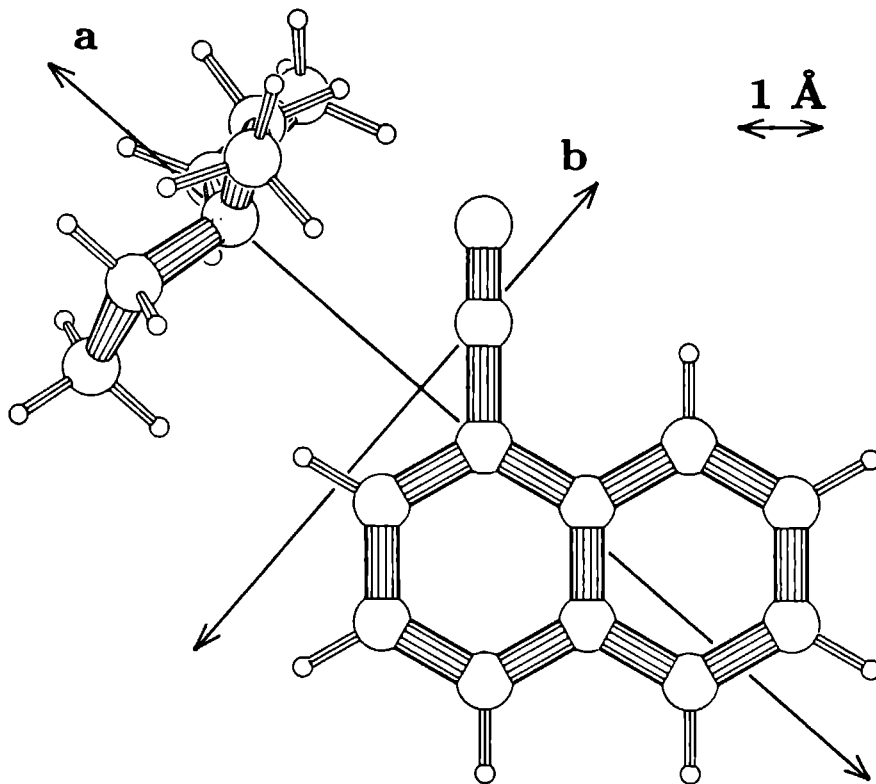
Figure 4.3: *The proposed T-shape structure of the CNN/TEA complex. The nitrogen atoms of TEA and CNN are shaded grey. The orientation of TEA with respect to CNN is such that its C_3 symmetry axis coincides with the a-axis of the complex. Both a and b-axis are in the plane of the CNN molecule.*

tional constants of CNN [5] with those of CNN/TEA shows that the changes for the latter can be explained in the same way: there is only a slight increase in the structure of CNN. The intermolecular distance does not change. This can easily be seen because a change in intermolecular distance should be directly reflected in ΔB and ΔC, which are in the case of CNN/TEA very small. An increasing CNN is directly observed in ΔA because A is very sensitive for the exact structure of both CNN and TEA, and not for the intermolecular distance.

Acknowledgements

References

1. H. Saigusa and M. Itoh, Chem. Phys. Letters **106** (1984) 391

2. H. Saigusa and M. Itoh, J. Chem. Phys. **81** (1984) 5692

3. H. Saigusa, M. Itoh, M. Baba and I. Hanazaki, J. Chem. Phys. **86** (1987) 2588

4. E. Zingher and Y. Haas, Chem. Phys. Letters **202** (1993) 442

5. G. Berden, W.L. Meerts and W. Kreiner, Chem. Phys. **174** (1993) 247

6. S. Gerstenkorn and P. Luc, *Atlas du spectroscopie d'absorption de la molecule d'iode*, CNRS, Paris (1978)
   S. Gerstenkorn and P. Luc, Rev. Phys. Appl. **14** (1979) 791

7. H. Saigusa and E. Lim, J. Phys. Chem. **95** (1991) 7580

8. D.F. Plusquellic and D.W. Pratt, J. Chem. Phys. **97** (1992) 8970

9. H. Takeuchi, T. Kojima, T. Egawa and S. Konaka, J. Phys. Chem. **96** (1992) 4389

10. V. Brenner, A. Zehnacker, F. Lahmani and Ph. Millié, J. Phys. Chem. **97** (1993) 10570

Chapter 5

High resolution fluorescence excitation spectroscopy of 1-aminonaphthalene. S_0 and S_1 geometries, and $S_1 \leftarrow S_0$ transition moment orientations

Giel Berden and W. Leo Meerts
Department of Molecular and Laser Physics, University of Nijmegen,
Toernooiveld, 6525 ED Nijmegen, The Netherlands

David F. Plusquellic and David W. Pratt
Department of chemistry, University of Pittsburgh
Pittsburgh, PA 15260 USA

Abstract

The high resolution fluorescence excitation spectrum of the origin band of the $S_1 \leftarrow S_0$ transition of 1-aminonaphthalene (1AN) has been recorded. It was found that this band is predominantly b-axis polarized, in contrast with other (previously measured) 1-substituted naphthalenes, which are a-axis polarized. Thirteen vibronic bands of 1AN were also examined at high resolution. The rotational constants, the inertial defects, and the band polarizations vary significantly from band to band. Similar experiments have been performed on eight deuterated isotopomers. A comparison of the results obtained for these isotopomers with those of the corresponding bands in protonated 1AN makes possible the determination of the center-of-mass coordinates of the amino hydrogen atoms. In the zero point vibrational level (ZPL) of the S_0 state, the out-of-plane positions of the amino hydrogens are *inequivalent;* the 'inside' hydrogen is located 0.49(8) Å out-of-plane, the 'outside' hydrogen only 0.24(17) Å. In the ZPL of the S_1 state, 1AN is *quasi*planar.

5.1   Introduction

From the rotationally resolved electronic spectrum of a molecule one can obtain the direction of the electronic transition moment vector in the molecular frame by determining the type of transition This vector provides information about the direction of the electronic charge migration or displacement that occurs during the transition It is therefore related to the electron probability distribution functions in the involved electronic states

The orientation of the electronic transition moment in mono-substituted naphthalenes has been studied extensively [1–13] Hollas and Thakur have performed rotational band contour analysis in the $S_1 \leftarrow S_0$ systems of several 1- and 2-substituted naphthalenes [1, 2] As substituents they used F, OH and NH_2 The spectra of the 1-substituted naphthalenes were predominantly a-type bands, while the spectra of the 2-substituted naphthalenes were predominantly b-type bands They concluded that the angle through which the transition moment is rotated away from the long axis in naphthalene depends mainly on the position of the substituent and not on its chemical nature

Majewski and Meerts [3] measured the fully rotational resolved excitation spectrum of naphthalene by using a narrow band laser in combination with a strongly collimated molecular beam Experimental data obtained with this method for 1-fluoronaphthalene [4] and hydroxynaphthalene [5] by the group of Pratt, are in excellent agreement with the results of Hollas and Thakur [1, 2] In the latter case Johnson *et al* [5] even distinguished two rotamers *trans-* and *cis-*hydroxynapthalene Since the high resolution spectrum of the 0_0^0 band of naphthalene is a pure a-type band, substitution at the 2-position (b-type bands) perturbes the electronic structure more than substitution at the 1-position (a-type bands) Johnson *et al* [5] explained these observations by comparing the molecular orbitals (MO's) of naphthalene, 1- and 2-hydroxynaphthalene

Rotational spectroscopy can provide only the magnitude (and not the sign) of the angle between the transition moment vector and the inertial axis coordinate system (long inertial axis, see Chapters 3, and 7) Thus, if this angle is non-zero one has to make a choice for the sign For the afore mentioned mono-substituted naphthalenes, calculations using the Pariser-Parr-Pople (PPP) method performed by Singh and Thakur [7] indicate that one should take the minus sign (see Figure 3 4, Chapter 3, for the axis convention, and for the definition of the direction of the transition moment vector)

In the case of 2-hydroxynaphthalene this choice has been confirmed by measurements of Plusquellic and Pratt [13] They observed quantum interference effects in the high resolution excitation spectrum of the hydrogen bonded complex of *trans-*hydroxynaphthalene with ammonia what leads to an unambiguous determination of the direction of the transition moment For 1-cyanonaphthalene the angle derived from the high resolution excitation spectrum turns out to be zero [8] In this case there is also no ambiguity for the direction of the transition moment it is parallel to the long inertial axis It is interesting to note that if the angle between the transition moment vector and the long axis of naphthalene does not depend on the chemical nature of the substituent, the results for 1-cyanonaphthalene indicate that for 1-substituted naphthalenes one should choose the positive sign for the ange between transition moment and long inertial axis (see Chapter 3)

Recently, high resolution studies on several other substituted naphthalenes have been reported [9, 10, 11, 12] It has been shown that the simple picture, $i e$ the direction of the transition moment does not depend on the chemical nature of the substituent, does not hold A nice example is 2-vinylamine [11] which spectrum exhibits pure a-type character Until now, the following

substituents have been studied[1] F, OH, CN, CH_3, COOH, and C_2H_3

In this chapter, we present the vibrationally resolved excitation spectrum of the $S_1 \leftarrow S_0$ transition of 1-aminonaphthalene (1AN) Several vibronic bands of 1AN and deuterated 1AN have been examined at full rotational resolution The 0_0^0 band of 1AN has already been investigated by Hollas and Thakur [1] The result from their analysis, which was based on a rather featureless band contour, showed that 1-AN has a transition moment predominantly along the long inertial axis Our analysis is based on a well resolved band and shows that 1-AN has a transition moment predominantly along the short in-plane axis Furthermore, we determine the positions of the amino hydrogen atoms in the S_0 and S_1 states to elucidate the structure of the amino group, and the change in structure of this group upon electronic excitation

5.2 Experimental

1AN was studied at low resolution using both fluorescence excitation (Pittsburgh) and resonance enhanced multi-photon ionisation (REMPI) techniques (Nijmegen) Both methods utilized a supersonic jet for sample preparation In the fluorescence excitation experiments, 1AN was seeded into He at various backing pressures and expanded through a 1 mm diameter pulsed nozzle operating at 10 Hz The resulting jet was crossed about 2 5 cm downstream of the nozzle by a doubled Nd YAG-pumped dye laser (FWHM ~0 3 cm^{-1}) also operating at 10 Hz The resulting fluorescence was collected by a single lens system, focused on a photomultiplier tube, and detected using a boxcar integrator, interfaced to a MASSCOMP MCS561 data acquisition system Spectra were calibrated in relative frequency to ±0 1 cm^{-1} using markers from a solid etalon

REMPI measurements were performed using a standard pulsed beam laser ionization mass spectrometer with orthogonal molecular beam, laser beam, and linear time-of-flight axes 1AN was seeded into a pulsed expansion of helium and skimmed before entering the ionization region [14] A doubled Nd YAG pumped tunable dye laser (FWHM ca 0 15 cm^{-1}) operating at 10 Hz was used to excite 1AN in a one-color (1+1) REMPI scheme Additionally, a KrF excimer laser was used to ionize 1AN via the triplet state in a two-color (1+1) REMPI scheme Ions corresponding to the mass of 1AN were collected and amplified by a dual microchannel plate detector which is monitored by a 10 bit digital oscilloscope interfaced via a parallel GPIB bus to a personal computer The PC also controls the wavelength scans of the dye laser

1AN was studied at high resolution using fluorescence excitation techniques The spectrometers employed have been described elsewhere [4, 15] Briefly, a molecular beam formed by expanding 1AN in Ar or He and skimming twice in a differential pumping system, was crossed 30 cm (Nijmegen) or 100 cm (Pittsburgh) downstream of the CW quartz nozzle (~100 μm diameter) with the collimated beam of a intracavity frequency double CW ring dye laser Fluorescence detection using spatially selective optics images a small diameter (~1 mm) portion of the interaction region onto a photomultiplier tube placed above the crossing point of the two beams Standard photon counting and data acquisition techniques were employed Spectra were calibrated using simultaneously acquired interference fringes from a near-confocal interferometer and the I_2 absorption spectrum [16]

---

[1]In this chapter we will use the following abbreviations 1AN = 1 aminonaphthalene (substituted group –NH$_2$), 1CN = 1 cyanonaphthalene (–CN), 1FN = 1 fluoronaphthalene (–F), 1HN = 1 hydroxynaphthalene, 1-naphthol (OH), 1MN = 1 methylnaphthalene (–CH$_3$), 1NA = 1 naphthoic acid (-COOH), and 1VN = 1-vinylnaphthalene (C$_2$H$_3$) 2AN = 2 aminonaphthalene, *etc*
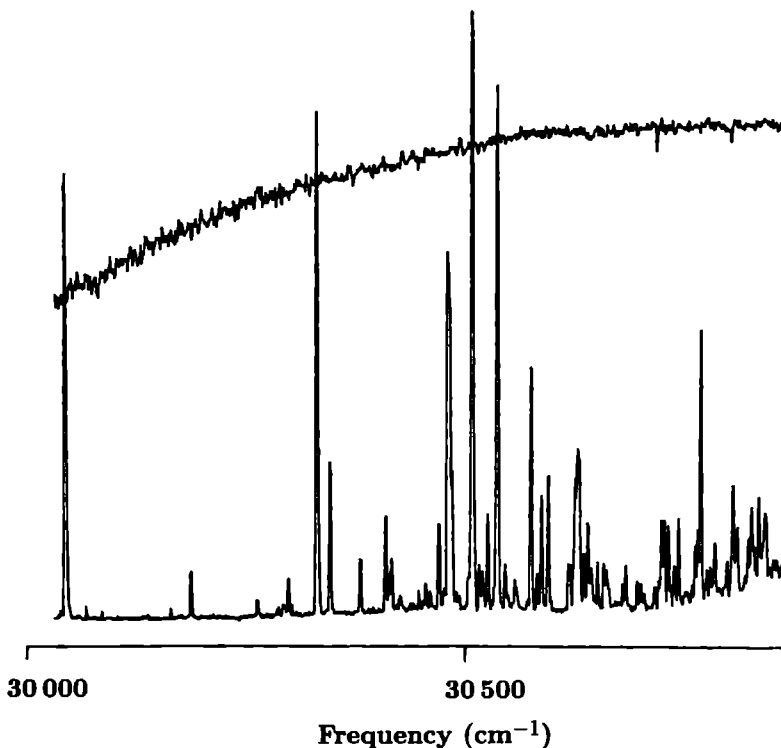
Figure 5.1: *Vibrationally resolved fluorescence excitation spectrum of the $S_1 \leftarrow S_0$ transition of 1-aminonaphthalene (also shown is the UV power of the excitation laser)*

Deuterated 1AN was prepared by dissolving 1AN in methylene chloride and mixing the solution with D_2O in a rotating evaporator, with mild heating (35 °C) The resulting deuterated compound was separated from the D_2O and the methylene chloride to give a solid sample

5.3 Results

Figure 5 1 shows the low resolution $S_1 \leftarrow S_0$ fluorescence excitation spectrum of 1AN recorded in a supersonic jet The prominent features are a strong band at 30 044 cm^{-1}, a number of well resolved vibronic bands at energies up to $\Delta E \sim 600$ cm^{-1} above the apparent origin, and a much higher density of vibronic bands at still higher energies A list of the prominent bands up to 721 cm^{-1} is give in Table 5 1 The one- and two-color (1+1) REMPI spectra of 1AN are qualitatively similar A spectrum has been measured in a two-color (1+1) REMPI scheme in which the ionization laser had a delay of 500 ns with respect to the excitation laser Since the lifetime in the S_1 state is only 11 ns (see below), 1AN is ionized from the triplet state It is therefore concluded that there is a significant coupling between the first excited singlet state and triplet states

Energy	ΔE	Intensity	Assignment	Energy	ΔE	Intensity	Assignment
29 981.2	−62.4	−	Hot band	30 478.4	434.8	150	
30 027.5	−16.1	--	Hot band	30 480.2	436.6	−	
30 043.6	0.0	100	Origin	30 500.6	457.0	7	
30 088.1	44.5	−	Hot band	30 507.0	463.4	160	
30 184.1	140.5	7		30 512.9	469.4	6	
30 258.8	215.2	3		30 516.6	473.0	8	
30 294.3	250.9	6		30 522.8	479.3	17	
30 312.8	264.5	−	Hot band	30 534.4	490.2	120	
30 327.8	284.2	110		30 542.7	499.1	7	
30 342.8	299.2	27		30 545.6	502.1	2	
30 373.1	329.5	−	Hot band	30 548.6	505.0	−	Hot band
30 376.5	332.9	8		30 550.7	507.1	1	
30 385.4	341.8	−	Hot band	30 555.0	511.4	8	
30 405.0	361.5	15		30 572.5	528.9	43	
30 409.5	365.6	6		30 579.5	535.9	4	
30 412.3	368.8	8		30 584.7	541.0	17	
30 444.5	400.9	3		30 592.2	548.6	23	
30 449.1	405.5	2		30 616.1	572.5	13	
30 452.5	408.9	4		30 625.2	581.6	87	
30 457.2	413.6	2		30 628.7	585.1	−	
30 467.3	423.6	15		30 766.2	722.6	49	
30 473.4	429.8	4		30 909.0	865.4	−	

Table 5.1: *Prominent bands observed in the $S_1 \leftarrow S_0$ excitation spectrum of 1-amino-naphthalene (1AN). Energies are in cm^{-1}.*

Several of the bands in the $S_1 \leftarrow S_0$ excitation spectrum were examined at high resolution. Figure 5.2 shows the high resolution spectrum of the 0_0^0 band at 30 044 cm^{-1}, a typical example. The spectrum consists of more than 1000 well-resolved lines, each with a linewidth of 21 MHz (Nijmegen). The minimum linewidth observed for other molecules in Nijmegen is 12 MHz, owing to residual Doppler broadening, transit time effects, fluorescence collection optics, and laser linewidth. From the excess linewidth, we estimate the lifetime of S_1 1AN in its zero point vibrational level (ZPL) to be 11±3 ns.

The spectrum shown in Figure 5.2 is predominantly *b*-type; no single strong Q branch is observed. To fit this band, a spectrum was simulated using asymmetric rotor Hamiltonians for both electronic states, rotational constants estimated from a crude geometrical structure, and the appropriate selection rules. This spectrum was then compared with the experimental one. An initial assignment of lines in the center of the spectrum followed from this comparison. Then, the assigned lines were returned to the fitting program, producing adjustments to the rotational constants and a new simulation. This process was continued until all *b*-type transitions could be accounted for. Still, some unassigned lines appeared in the experimental spectrum. These exhibited patterns characteristic of an *a*-type band. The observed band is therefore a hybrid band.
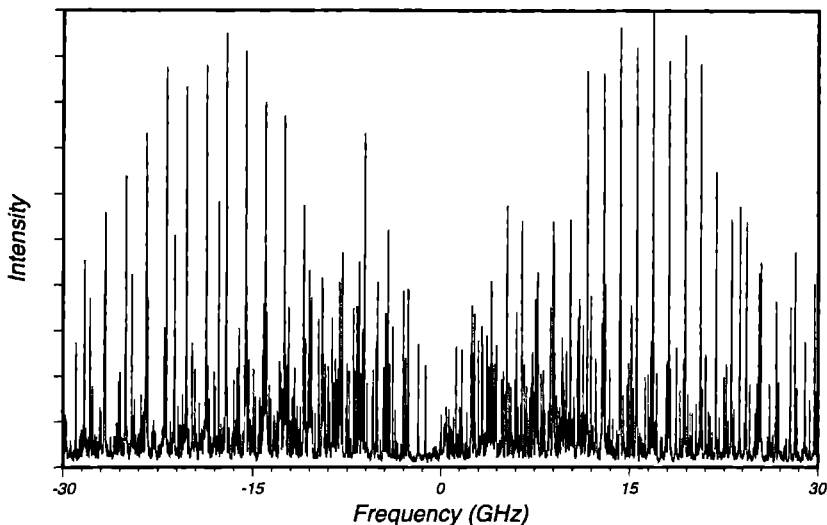
Figure 5.2: *High resolution LIF spectrum of the origin of the $S_1 \leftarrow S_0$ transition of 1-aminonaphthalene. The absolute frequency of the origin (0 on the scale of the figure) is at $30\,043.59\pm0.01$ cm^{-1}.*

Including the a-type lines in the fit (a total of 300 assigned lines were used) resulted in a standard deviation of 1.9 MHz, substantially less than the observed linewidth. The rotational constants are listed in Table 5.2. A best fit of the observed intensities (at T_r=3.5±0.5 K) yielded a band 91±3% b-type character and 9±3% a-type character. With the relationship $\tan^2\theta = I(b)/I(a)$, we calculate θ=72°±3°. Here, θ is the angle between the a-axis and the transition moment vector, and $I(b)/I(a)$ is the intensity ratio of the a and b-type bands. The a-axis of 1AN makes an angle of about 16° with the long in-plane axis of naphthalene, x. Thus the transition moment vector in 1AN makes an angle of either –56° or +88° with its x-axis.

Two properties of the data shown in Table 5.2 are worth noting here. The first is that A *increases* on electronic excitation, suggesting a contraction of 1AN in directions perpendicular to the a-axis with the absorption of a photon. The second is that the inertial defect (ΔI), relatively large in S_0 (–0.80 amu Å^2), *decreases* on $S_1 \leftarrow S_0$ excitation to –0.37 amu Å^2. This suggests that 1AN is distorted from planarity in the ground state along some out-of-plane coordinate, and becomes more planar in the S_1 state.

To probe the atomic displacements responsible for these changes further, high resolution experiments were performed on several deuterated 1AN's. Eight deuterated species resulted when 1AN was exchanged with D_2O; each gave a fully resolved $S_1 \leftarrow S_0$ fluorescence excitation spectrum. However, because each spectrum spans about 5 cm^{-1}, and the (ZPL) energy shifts on deuteration are comparable to this width, the observed spectrum of the isotopically mixed sample was extremely congested. Nonetheless, it was possible to fit each of these bands separately, by repeating the procedure previously described, yielding a set of S_0 and S_1 rotational constants for each of

Molecular Constants of the 0_0^0 band of 1AN				
A''	1933.8(7)	ΔA	45.61(2)	MHz
B''	1127.6(4)	ΔB	−28.19(1)	MHz
C''	713.1(3)	ΔC	−5.916(8)	MHz
κ''	−0.321(1)	κ'	−0.383(1)	
$\Delta I''$	−0.80(2)	$\Delta I'$	−0.37(2)	amu Å^2
Band origin		$30\,043.59\pm0.01$ cm^{-1}		
Band character		91 ± 3 % b-type	9 ± 3 % a-type	

Table 5.2: *Molecular constants of zero-point vibrational levels of the S_0 and S_1 states of 1-aminonaphthalene; the rotational constants A, B, and C, the asymmetry parameter κ, and the inertial defect $\Delta I = I_c - I_b - I_a$ in the electronic ground state and their differences with the first excited state ($\Delta A = A' - A''$, etc.).*

the observed isotopomers. By comparing the rotational constants of different isotopomers using Kraitchman's equations (*vide infra*) [17], we determined which deuterium-labelled molecule was responsible for each observed 0_0^0 band. The results of these determinations are listed in Table 5.3.

Examination of the data in this table shows that the origin bands of most deuterated 1AN's are blue shifted relative to the origin band of the fully protonated molecule. The only exception is the 0_0^0 band of the DHHH isotopomer, which is red shifted by −3.58 cm^{-1}. Further examination of these data also shows, that most shifts are additive. Thus, for example, the shift of the DHHH isotopomer is −3.58 cm^{-1}, the shift of the HHHD isotopomer is 12.11 cm^{-1}, and the shift of the DHHD isotopomer is 8.59 cm^{-1}. The only exception is the shift for DDHH predicted to be 2.16 cm^{-1}, but observed to be 2.99 cm^{-1}. Finally, we note that the shifts for the two NDH isotopomers are different, −3.58 cm^{-1} (DHHH) and 1.42 cm^{-1} (HDHH).

Several vibronic bands were also examined at high resolution. The data obtained from fits of these bands are summarized in Table 5.4. All examined bands exhibited ground state rotational constants that are identical, within the experimental error (±0.1 MHz), to those of the S_0 ZP vibrational level. Hence, all listed bands originate in this level. However, the rotational constant, the inertial defects, and the band polarizations vary significantly from band to band, as shown in Table 5.4.

5.4 Discussion

One of the most intriguing results of this study is the finding that the 0_0^0 band of the $S_1 \leftarrow S_0$ transition of 1AN is predominantly b-axis polarized. This is an unexpected result. In early studies of the orientations of the electronic transition moments in monosubstituted naphthalenes, it was found that the 0_0^0 bands in the $S_1 \leftarrow S_0$ spectra of 1FN, 1HN, 1MN, 1CN, and 1NA are predominantly a-axis polarized.

The 0_0^0 band of the $S_1 \leftarrow S_0$ transition of naphthalene itself is x- (a-)axis polarized. Simple MO theory provides an explanation for this result([5], and references therein). The S_1 state has
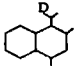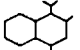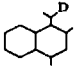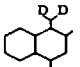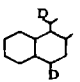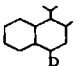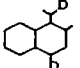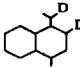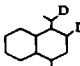
	Origin	Rotational Constants in MHz					
	cm^{-1}	A''	B''	C''	ΔA	ΔB	ΔC
DHHH	-3.58	1878.4	1123.5	704.3	42.6	-26.9	-5.8
HHHH	0.0	1933.8	1127.6	713.1	45.6	-28.2	-5.9
HDHH	1.42	1898.23	1108.4	700.7	41.9	-26.5	-5.7
DDHH	2.99	1847.0	1103.9	692.3	38.7	-25.1	-5.7
DHHD	8.59	1817.1	1123.3	695.4	41.5	-27.0	-5.5
HHHD	12.11	1869.9	1127.4	704.2	44.5	-28.3	-5.6
HDHD	13.56	1836.2	1108.4	692.1	40.8	-26.6	-5.4
HDDH	17.65	1898.5	1082.5	690.0	41.8	-25.9	-5.8
HDDD	28.35	1869.9	1099.5	693.2	44.3	-27.6	-5.7

Table 5.3: *Rotational constants of the zero-point vibrational level of the S_0 state of eight deuterated 1AN's and the parent molecule.*

		Rotational constants of several vibronic bands of 1AN in the S_1			
ΔE, cm^{-1}	A', MHz	B', MHz	C', MHz	$\Delta I'$, amu Å^2	Band Type
0	1979.4	1099.4	707.2	−0.37	91% b
141	1979.1	1099.5	709.2	−2.2	90% b
284	1952.2	1102.3	705.1	−0.58	81% a
299	1974.8	1100.5	707.9	−1.2	100% a
362	1975.1	1099.9	708.9	−2.4	a
366	1976.0	1099.8	707.3	−0.73	b
424	1965.7	1101.2	707.8	−2.1	a
437	1975.3	1099.4	707.9	−1.7	b
463	1969.8	1100.9	705.9	+0.31	50% b
541	1972.9	1100.4	707.8	−1.5	67% a
582	1965.9	1101.0	708.1	−2.4	57% a
585	1967.8	1100.6	708.3	−2.5	100% a
723	1962.3	1101.5	706.4	−1.0	a
865	1967.8	1100.3	708.0	−2.3	67% b
0 (DHHH)	1921.0	1096.6	698.5	−0.39	b
287 (DHHH)	1899.9	1098.4	697.6	−1.6	a
725 (DHHH)	1894.7	1101.2	698.0	−1.6	a
0 (HDHH)	1940.2	1081.9	695.0	−0.39	b
289 (HDHH)	1933.4	1083.6	694.2	0.25	a

Table 5.4: *Rotational constants of several vibronic bands in the S_1 state of 1AN and its isotopomers. Except where specifically noted, the indicated band type is only approximate; all bands are hybrid in character. The 287 cm^{-1} band of the DHHH isotopomer is shifted +2.72 cm^{-1} with respect to the corresponding band in protonated 1AN. The 725 cm^{-1} band is shifted +2.70 cm^{-1}. The 289 cm^{-1} band of the HDHH band is shifted +5.37 cm^{-1} with respect to the corresponding band in protonated 1AN.*

its principal parentage in two Hückel $\pi\pi^*$ configurations, $\phi_4\phi_6^*$ and $\phi_5\phi_7^*$,

$$\psi(S_1) \approx 0.707(\phi_4\phi_6^* - \phi_5\phi_7^*) \tag{5.1}$$

As shown in Figure 5.3, the two one-electron product wavefunctions that comprise the S_1 state exhibit oscillating charge distributions that are oriented along the x-axis. Thus, the $S_1 \leftarrow S_0$ 'superposition' wavefunction oscillates in the same direction. However, the magnitude of the transition moment is small owing to the near cancellation of the two components, $\phi_4\phi_6^*$ and $\phi_5\phi_7^*$, and the 0_0^0 band of the $S_1 \leftarrow S_0$ transition of naphthalene itself is very weak (line strength ≈ 0.001).

The 0_0^0 band of the $S_1 \leftarrow S_0$ transition of 1AN is relatively strong. Additionally, we find that this band is principally b-axis polarizes. The a-axis in 1AN makes an angle of $\sim 16°$ with the long in-plane x-axis. Clearly, then, the delicate balance implied by Eq. 5.1 is upset by substitution of an $-NH_2$ group in the 1-position.
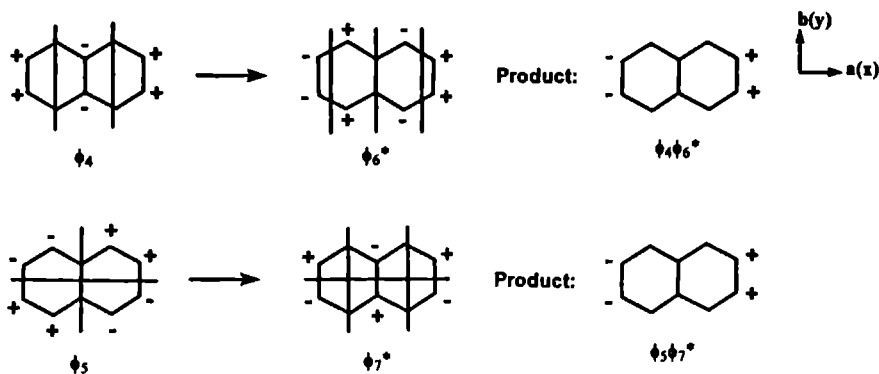
Figure 5.3: *Molecular orbitals of naphthalene See text for further details*

We have performed a series of Hartree-Fock calculations (Gaussian 90, 6-31G* basis set [18]) on 1AN in the S_0 state to probe further the origin of this result Shown in Figure 5 4 are approximate pictures of the nodal patterns of the $n-$ and π-electron MO's of the energy optimized 1AN that were derived from these calculations 1AN has ten π electrons, additionally, the nitrogen atom contributes a 'lone pair' However, examination of this figure shows that *all* electrons are extensively delocalized throughout the entire molecule Further, it was found that the degeneracies that are present in the MO diagram of naphthalene are lifted by the 1-amino substitution, and that the nodal patterns of the π-electron MO's are significantly perturbed as well If we approximate the $S_1 \leftarrow S_0$ transition by a single one-electron excitation function $\phi_6 \phi_7^*$, Figure 5 4 shows that there is a resulting oscillating charge distribution oriented close to the b-axis Partially, this explains
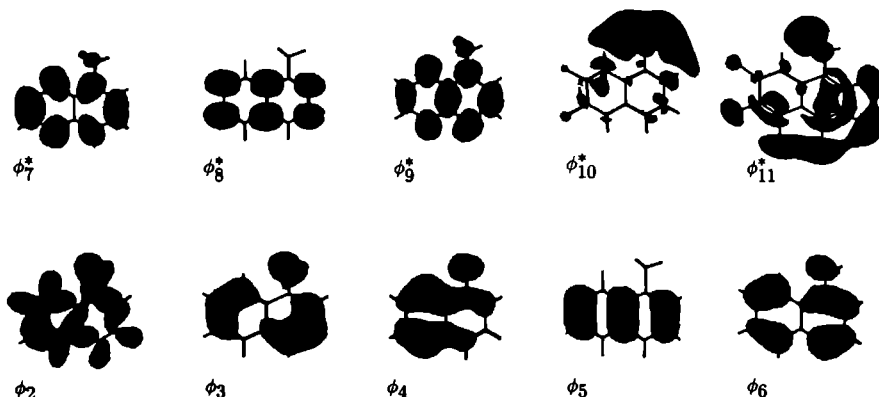
Figure 5.4: *Molecular orbitals of 1-aminonaphthalene obtained from 6-31G* calculations, numbered in order of increasing energy ϕ_6 is the highest occupied molecular orbital (HOMO) in the ground state, ϕ_7^* is the lowest unoccupied molecular orbital (LUMO)*

Molecule	Origin freq	Shift	TM orientation	Ref
Naphthalene	32019	0	0°	[3]
1FN	31867	−152	−14° or +46°	[4]
1MN	31768	−251	14° or +46°	[9]
1HN (*trans*)	31455	−364	−17° or +49°	[5]
1CN	31411	−608	+45°	[8]
1HN (*cis*)	31181	−838	+16°	[5]
1NA	31074	−945	−23° or +81°	[10]
1AN	30044	−1975	−56° or +88°	This work

Table 5.5: *Origin band frequencies and transition moment (TM) orientations in several 1-substituted naphthalenes. Frequencies are cm^{-1}. The TM orientation is the angle between the x-axis (the a-axis of naphthalene) and the transition moment vector. Angles from the x-axis towards the substituent are taken positive*

the 'anomalous' polarization of the 0_0^0 band of the $S_1 \leftarrow S_0$ transition of 1AN. An analogous effect occurs in the $S_1 \leftarrow S_0$ of 2-aminonaphtalene [12] and 2-vinylnaphthalene [11].

A second relevant observation about the $S_1 \leftarrow S_0$ transition of 1AN is that the 0_0^0 band is significantly red shifted with respect to the corresponding band in naphthalene, by −1975 cm^{-1}. This is an expected result if, as argued above, the photoexcited electron is significantly delocalized into the NH_2 group. The excited S_1 state should be significantly stabilized relative to the corresponding state in naphthalene. Extending this argument, one might expect that other 1-substituted naphthalenes would also exhibit red shifts, that the magnitudes would depend on the delocalizing ability of the attached group (i e on its chemical nature), and that there would be a correlation between the observed red shifts and band polarizations. Table 5 5 provides some data that support this view. Listed there are the frequencies of the 0_0^0 bands, the shifts of these bands from the corresponding band in naphthalene, and the observed band polarizations of several 1-substituted naphthalenes. The latter are expressed in terms of the angle that the transition moment vector makes with the long in-plane axis (the x-axis in naphthalene), and thus have been corrected for simple inertial effects. Examining the data in this Table, we see that the most red shifted 0_0^0 bands have transition moments that make the largest positive angles with the x-axis, in ageement with the above expectations (although *cis*-1HN is an exception). Thus, the interaction between the π electrons of naphthalene and the 'lone pairs' of the attached substituent is responsible for both the observed red shifts and the observed band polarizations.

Given the above perspective, substantial geometry changes should occur when 1AN is photoexcited to its S_1 state, especially along coordinates involving the amino group. First, we note that deuterium substitution of 1AN typically produces blue shifts of the 0_0^0 bands. The largest shifts observed are for ring substitution, +28 35 cm^{-1} in the HHDD molecule. Both the signs and the magnitudes of these shifts are typical for the delocalized $\pi\pi^*$ states of aromatic molecules [19]. An intriguing result is that the DHHH molecule exhibits a *red* shift, −3 58 cm^{-1}, whereas the HDHH molecule exhibits a blue shift, 1 42 cm^{-1}. The two NH_2 hydrogen atoms are *inequivalent*. Similar

Molecule	A''	ΔA	$\Delta I''$
Naphthalene	3105.1	−77.5	−0.14
1FN	1920.6	−29.1	- 0.17
1MN	1894.6	−32.8	−3.3
1HN (*trans*)	1942.1	−20.5	−0.20
1CN	1478.7	−21.4	−0.15
1HN (*cis*)	1947.6	−23.7	−0.29
1NA	1361.7	−19.1	−3.78
1AN	1933.8	+45.6	-0.80

Table 5.6: *Rotational constant A and the inertial defect ΔI in the S_0 state, and $\Delta A = A' - A''$, of several 1-substituted naphthalenes. Rotational constants in MHz; inertial defects in amu Å^2.*

results have been observed in other substituted anilines [20]. Because DHHH is red shifted, the substituted hydrogen atom must be distorted along a coordinate whose vibrational frequency increases on $S_1 \leftarrow S_0$ excitation. Similarly, because HDHH is blue shifted, the substituted hydrogen must be distorted along a coordinate whose vibrational frequency decreases on $S_1 \leftarrow S_0$ excitation (as for the ring H atoms).

Detailed information about atomic displacements that occur on $S_1 \leftarrow S_0$ excitation of 1AN can be obtained from the high resolution spectra. An interesting observation is that ΔA is positive for all examined bands of 1AN. Both ΔB and ΔC are negative. All other naphthalenes examined to date exhibit negative ΔA, ΔB, and ΔC values (Table 5.6). The negative signs are expected. A $\pi\pi^*$ excitation typically results in ring expansion, increasing the moments of inertia about all principal axes. Since $\Delta A > 0$ in 1AN, one ore more bond lengths must decrease, the affected bonds being perpendicular to the a-axis. The logical candidate is the C–NH$_2$ bond; contraction of this bond is a natural consequence of the increased delocalization of charge in the S_1 state. This contraction mainly affects ΔA and ΔC because the C–N bond is pointed almost perpendicularly to both the a and c inertial axis. Although the NH$_2$ substituent contributes roughly equal to the moments of inertia about the a and c axis (resp. I_a and I_c), the effect of a decreasing C–N bond is especially seen in the rotational constant A because I_a is smaller than I_c. In 2AN the C–N bond is mainly perpendicularly to the b-axis (instead of the a axis). Contraction of the C–N bond while exciting this molecule to the first electronic state gives a positive ΔB while ΔA and ΔC are negative (since the naphthalene frame increases) as has been observed by Hollas and Thakur [2].

Additional structural information is provided by comparing the inertial defects of S_0 and S_1 1AN and its isotopomers (Table 5.7). S_0 1AN in its ZPL has $\Delta I = -0.81$ (the units of the inertial defect are amu Å^2, and will be omitted from now on). Deuterium substitution of the NH$_2$ group increases the magnitude of ΔI in the S_0 state. However, the observed increase is position sensitive; the DHHH isotopomer has $\Delta I = -1.27$, the HDHH isotopomer has $\Delta I = -0.92$, and the DDHH isotopomer has $\Delta I = -1.41$. Apparently, the 'inside' NH$_2$ hydrogen lies further out of the naphthalene plane than does the 'outside' NH$_2$ hydrogen. Excitation to the S_1 state, 'flattens' the molecule; the
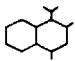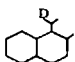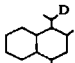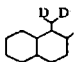
H atom position	Origin			+284 cm^{-1}			+723 cm^{-1}		
	$\Delta\nu$	S_0	S_1	$\Delta\nu$	S_0	S_1	$\Delta\nu$	S_0	S_1
(structure 1)	0.0	−0.81	−0.37	0.0	−0.80	−0.58	0.0	−0.82	−1.05
(structure 2)	−3.58	−1.27	−0.39	+2.72	−1.31	−1.61	+2.70	−1.30	−1.58
(structure 3)	+1.42	−0.92	−0.38	+5.37	−0.94	+0.30			
(structure 4)	+2.99	−1.41	−0.41						

Table 5.7: *Inertial defects of 1AN and its isotopomers in the S_0 and S_1 states (in amu Å^2), and the frequency shifts $\Delta\nu$ with the origin of the protonated 1AN molecule (in cm^{-1}).*

S_1 inertial defect of the protonated molecule is −0.37. Further, *all* isotopomers exhibit essentially the same ΔI values in the S_1 state. The two NH_2 hydrogens are *equivalent*. We conclude from these results that 1AN is a *quasi*planar molecule in its S_1 state, like aniline.

Still more detailed information can be derived by comparng the measured rotational constants of the different isotopomers, using Kraitchman's equations [17]. We first checked the validity of these equations by comparing the rotational constants of the S_0 states of HHHH, DHHH, HDHH, and DDHH. This gave two measures of the center-of-mass coordinates of the two NH_2 hydrogens, which agreed within experimental error. Next, we determined the ground state atom positions of all four substituted atoms, and compared these to the positions obtained from the theoretical 6-31G* geometry. The results are listed in Table 5.8. Finally, we determined the positions of the same four hydrogen atoms in the S_1 state of 1AN. The results are listed in Table 5.9.

Examination of these results shows clearly that while theory reproduces reasonably well the in-plane coordinates of all four hydrogen atoms, it does not account for their out-of-plane displacements. The two aromatic hydrogens are both predicted and observed to be in-plane, within the experimental error. However, the two NH_2 hydrogens exhibit nonzero $|z|$ values. The 'inside' hydrogen displacement is about twice that of the 'outside' hydogen, in the S_0 state. They become equal, and probably planar, on excitation to the ZPL in the S_1 state.

Simultaneously excitation of S_1 1AN along a vibrational coordinate has a different effect (Table 5.7). The HHHH molecule has ΔI=−0.58, the DHHH molecule has ΔI=−1.61, and the HDHH molecule has ΔI=+0.30 in the +284 cm^{-1} vibrational level. Thus, the two hydrogen atoms of

77
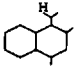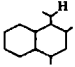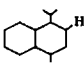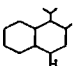
H atom position	S_0 Origin			Theoretical (6-31G*)		
	x (Å)	y (Å)	z (Å)	x (Å)	y (Å)	z (Å)
	1.16 (0.03)	2.74 (0.01)	0.49 (0.08)	1.18	2.83	0.00
	2.74 (0.01)	2.24 (0.02)	0.24 (0.17)	2.78	2.27	0.00
	3.36 (0.02)	−0.10 (0.50)	0.21 (0.25)	3.34	−0.04	0.00
	0.26 (0.17)	−3.00 (0.02)	0.14 (0.37)	0.25	−2.96	0.00

Table 5.8: *Ground state hydrogen atom positions in 1-aminonaphthalene.*
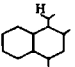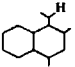
H atom position	S_1 Origin			$S_1 + 284$ cm^{-1}			$S_1 + 723$ cm^{-1}		
	x (Å)	y (Å)	z (Å)	x (Å)	y (Å)	z (Å)	x (Å)	y (Å)	z (Å)
	1.05 (0.04)	2.79 (0.01)	0.11 (0.39)	1.15 (0.03)	2.74 (0.01)	0.52 (0.08)	0.44 (0.09)	2.99 (0.01)	0.53 (0.08)
	2.69 (0.01)	2.31 (0.02)	0.10 (0.42)	2.74 (0.01)	2.24 (0.02)	0.30 (0.13)			

Table 5.9: *Excited state hydrogen atom positions in 1-aminonaphthalene.*

the NH_2 group are inequivalent, again. Table 5.9 shows the positions of the hydrogen atoms. In the $+723$ cm^{-1} level ($\Delta v=2$ of the same vibrational mode as 284 cm^{-1}), the HHHH molecule has $\Delta I=-1.05$ and the DHHH molecule has $\Delta I=-1.58$. A monotonic increase in $|\Delta I|$ is expected with increasing vibrational energy in an out-of-plane mode [10]. This mode clearly involves both NH_2 hydrogens. But the behavior of ΔI with increasing vibrational energy in this coordinate differs for the two hydrogens, when they are replaced by deuterium. 'Inside' substitution produces an increasingly negative ΔI, but 'outside' substitution produces a positive ΔI value. The reason for this is not clear.

5.5   Summary

In this chapter, the vibrationally resolved spectrum of the $S_1 \leftarrow S_0$ transition of 1-aminonaphthalene has been presented. Several vibronic bands of 1AN have been examined at rotational resolution. The origin band of 1AN exhibits *ab*-hybrid character. The largest contribution of the transition moment vector is along the *b*-axis, an unexpected result since all previously measured 1-substituted naphthalenes are predominantly *a*-axis polarized. *Ab initio* calculations show that all electrons are extensively delocalized throughout the entire 1AN molecule. The band polarizations of the vibronic bands vary significantly from band to band (from pure *b*-type to pure *a*-type). The reason for this is not clear yet.

Similar experiments have been performed of eight deuterated isotopomers od 1AN. Comparison of the rotational constants with those of the corresponding bands in protonated 1AN, provides the center-of-mass coordinates of the amino hydrogen atoms. In the zero point vibrational level (ZPL) of the S_0 state, the out-of-plane positions of the amino hydrogens are *inequivalent;* the 'inside' hydrogen is located 0.49(8) Å out-of-plane, the 'outside' hydrogen only 0.24(17) Å. In the ZPL of the S_1 state, 1AN is *quasi*planar.

Work is in progress to perform a vibrational analysis of the low resolution spectra. The rotational constants of the thirteen vibronic bands, reported in Table 5.4, will be very useful. It has already been shown that an out-of-plane motion of the amino hydrogen atoms is associated with excitation to the $+284$ cm^{-1} and $+723$ cm^{-1} bands. Together with the results of dispersed fluorescence spectra (not reported in this chapter), this information will be used to determine the NH_2 inversion barrier in the S_0 and S_1 states.

Acknowledgements

References

1   J M Hollas and S N Thakur, Molec Phys **27** (1974) 1001

2   J M Hollas and S N Thakur, Molec Phys **25** (1973) 1315

3   W A Majewski and W L Meerts, J Mol Spectrosc **104** (1984) 271

4   W A Majewski, D F Plusquellic and D W Pratt, J Chem Phys **90** (1989) 1362

5   J R Johnson, K D Jordan, D F Plusquellic and D W Pratt, J Chem Phys **93** (1990) 2258

6   B A Jacobson, J A Guest, F A Novak and S A Rice, J Chem Phys **87** (1987) 269

7   R A Singh and S N Thakur, J Cryst Mol Struct **11** (1981) 197

8   Chapter 3
    G Berden, W L Meerts and W Kreiner, Chem Phys **174** (1993) 247

9   X Q Tan, W A Majewski, D F Plusquellic and D W Pratt, J Chem Phys **94** (1991) 7721

10 S Jagannathan and D W Pratt, J Chem Phys **100** (1994) 1874

11 J F Pfanstiel and D W Pratt, J Phys Chem , in press

12 D F Plusquellic and D W Pratt, manuscript in preparation

13 D F Plusquellic and D W Pratt, J Chem Phys **97** (1992) 8970

14 M G H Boogaarts, P C Hinnen and G Meijer, Chem Phys lett **223** (1994) 537

15 Chapter 1

16 S Gerstenkorn and P Luc, *Atlas du spectroscopie d'absorption de la molecule d'iode*, CNRS, Paris (1978)
    S Gerstenkorn and P Luc, Rev Phys Appl **14** (1979) 791

17 W Gordy and R L Cook, *Microwave Molecular Spectra*, 3rd Ed , John Wiley & Sons, New York (1984)

18 M J Frisch, M Head-Gordon, G W Trucks, J B Foresman, H B Schlegel, K Raghavachari, M A Robb, J S Binkley, C Gonzales, D J Defrees, D J Fox, R A Whiteside, R Seeger, C F Melius, J Baker, R L Martin, L R Kahn, J J P Stewart, S Topiol and J A Pople, *Gaussian 90*, Gaussian, Inc , Pittsburgh, PA (1990)

19 See, for example, G C Nieman and D S Tinti, J Chem Phys **46** (1967) 1432

20 J I Seeman, H V Secor, H-S Im and E R Bernstein, J Am Chem Soc **112** (1990) 7073

Chapter 6

Rotationally resolved UV spectroscopy on the 2H-tautomer of benzotriazole in a molecular beam

Giel Berden and W. Leo Meerts
Department of Molecular and Laser Physics, University of Nijmegen,
Toernooiveld, 6525 ED Nijmegen, The Netherlands

Erko Jalviste
Institute of Physics, Estonian Academy of Science,
Riia 142, EE2400 Tartu, Estonia

Abstract

The rotationally resolved excitation spectrum of the 0_0^0 band of the $S_1 \leftarrow S_0$ transition in 2H-benzo-triazole, at 286.4 nm, is obtained by using laser induced fluorescence spectroscopy in a molecular beam. From this pure b-type spectrum, the rotational constants in the ground state and the electronically excited state are determined. The rotational lines are strongly broadened due to the short lifetime which is determined to be around 1.1 ns.
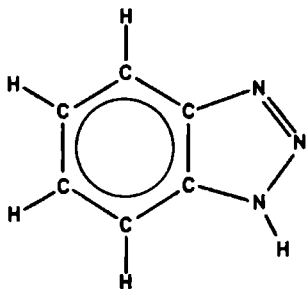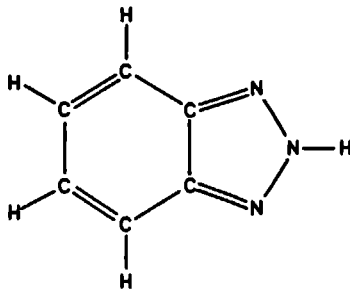
1H−benzotriazole   2H−benzotriazole

Figure 6.1: *The two tautomers of benzotriazole. The long in-plane axis is the inertial a-axis. The b-axis is the short in-plane axis. For 1H-benzotriazole both axes should be rotated counterclockwise around the c-axis over an angle of less than 1 degree (if compared with 2H).*

6.1   Introduction

The tautomerism of benzotriazole has been studied extensively both experimentally and theoretically [1–10]. From quantum chemical calculations [1, 2, 3] it is predicted that 1H-benzotriazole (see Figure 6.1) is more stable than 2H-benzotriazole. Benzotriazole in the solid state exists exclusively as the 1H-tautomer, as has been determined by X-ray crystallography [4]. Also in solution, benzotriazole is predominantly found in the 1H-form as has been shown in a number of studies on benzotriazole and its methyl derivatives by using UV and IR absorption, and NMR techniques (see [1, 2] and references therein).

Only a few gas phase studies have been reported. Maquestiau *et al.* [5] showed the predominance of the 1H-tautomer in a mass spectrometry experiment, an observation that has been confirmed by photoelectron spectroscopy [6]. Recently, Velino *et al.* [7] measured the microwave spectrum of benzotriazole and its N–D isotopomer in a heated cell. This spectrum could exclusively be attributed to the 1H-tautomer. The same group reported the rotational band contour of the 0_0^0 band of the $S_1 \leftarrow S_0$ transition of benzotriazole in an absorption measurement [8]. The rotational constants in the excited state were obtained by simulating the band contour keeping the ground rotational constants fixed to the microwave values. They assigned this band to a $\pi^* \leftarrow \pi$ transition induced in the 1H-tautomer.

Catalan *et al.* [9] measured the UV absorption spectra of benzotriazole, 1-methylbenzotriazole and 2-methylbenzotriazole in the gas phase in the 220–320 nm range. From a comparison of the three spectra the authors concluded that there is an appreciable amount of 2H-benzotriazole in the vapor. It was also concluded, from measurements at different temperatures (20–80 °C), that contrary to *ab initio* calculations the 2H-tautomer is more stable than 1H-benzotriazole.

All aforementioned gas phase experiments are performed at temperatures higher than room temperature (30–220 °C) to ensure a large enough vapor pressure in the gas cell. The first mea-

surements on jet-cooled benzotriazole were performed by Jalviste and Treshchalov [10] by laser induced fluorescence spectroscopy They obtained structured vibronic excitation and dispersed fluorescence spectra of the $S_1 \leftarrow S_0$ transition

In this letter the rotationally resolved laser induced fluorescence spectrum of the 0_0^0 band of the $S_1 \leftarrow S_0$ transition of benzotriazole in a supersonic molecular beam is reported It will be shown that this transition originates from the 2H-tautomer

6.2 Experimental

The experimental set-up for the high resolution measurements has been described in Chapter 1 Only the relevant features are given here Benzotriazole vapor was obtained by heating crystalline benzotriazole (Janssen Chimica, 98 %) in a quartz nozzle to approximately 150 °C, and was expanded with argon (backing pressure 0 8 bar) through a nozzle with a diameter of 0 15 mm The nozzle was kept at a slightly higher temperature to prevent condensation of benzotriazole in the orifice The molecular beam was skimmed twice in a differential pumping system and was crossed perpendicularly with a UV laser beam at about 30 cm from the beam orifice

UV radiation with a bandwidth of 3 MHz was generated by intracavity frequency doubling in a single frequency ring dye laser operating on Rh 110 By using a 2 mm thick Brewster cut BBO crystal, 0 1 mW of tunable radiation was obtained For relative frequency calibration a temperature stabilized Fabry-Perot interferometer was used with a free spectral range of 75 MHz For absolute frequency calibration, the iodine absorption spectrum [11] was recorded simultaneously The total undispersed fluorescence was imaged on a photomultiplier connected to a photon counting system interfaced with a computer

6.3 Results

The absolute frequency of the origin of the $S_1 \leftarrow S_0$ transition of benzotriazole is known within $2\ \mathrm{cm}^{-1}$ from the vibrationally resolved LIF spectrum obtained in jet experiments [10, 12] and from the rotational band contour absorption spectrum obtained in cell experiments [8]

In Figures 6 2 and 6 3, the high resolution excitation spectrum of this band is shown The absolute frequency of the band origin (0 on the scale of the figures) is at $34\,917\,759 \pm 0\,005\ \mathrm{cm}^{-1}$ The spectrum consists of about 200 not always totally resolved rotational lines The fluorescence is very weak and the rotational lines are strongly broadened due to a very short life time As there is no single isolated Q branch, this band can immediately be identified as predominantly b-type

As a starting point for the rotational assignment, a b-type spectrum was simulated using a rigid rotor Hamiltonian with rotational constants obtained from microwave measurements [7] and rotational band contour analysis [8] By comparing the simulation with the experimental spectrum, an initial assignment could be made for the central part of the spectrum, which could then be fitted to give a new set of rotational constants With this itterative procedure, it was possible to assign all lines in the experimental spectrum All ground state rotational constants and their differences with the excited state were varied simultaneously resulting in a fit in which all lines could be fitted within their experimental error The rotational constants differ considerably from the initial values, and are listed in Table 6 1, together with the asymmetry parameter and the inertial defect

There is no indication that the experimental spectrum has a hybrid character This has been confirmed by simulation The excitation spectrum of the origin of benzotriazole is a pure b-type band The overall shape of the spectrum could be simulated by assuming a rotational temperature
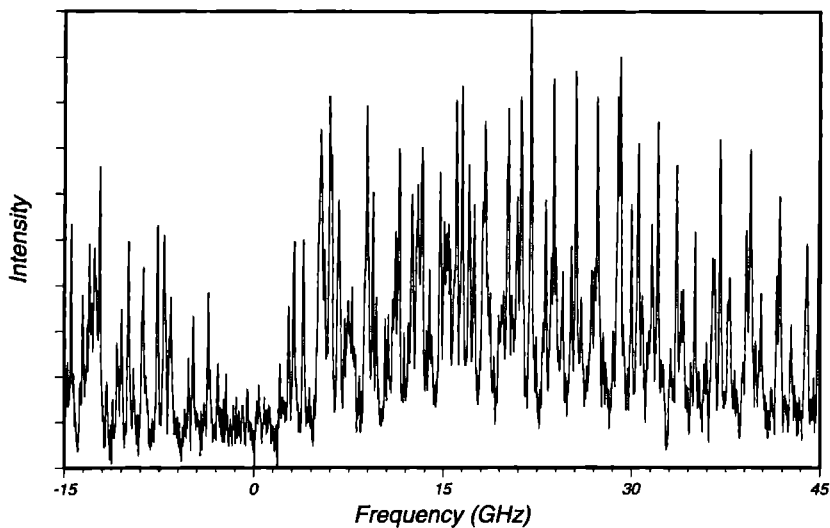
Figure 6.2: *High resolution LIF spectrum of the origin of the $S_1 \leftarrow S_0$ transition of 2H-benzotriazole. The absolute frequency of the origin (0 on the scale of the figure) is at 34 917.759±0.005 cm^{-1}.*
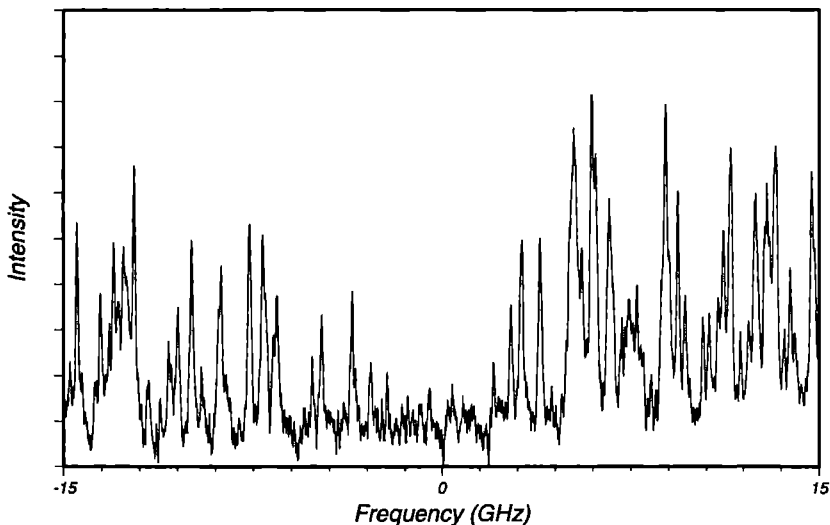
Figure 6.3: *Central part of the excitation spectrum of 2H-benzotriazole. The laser induced fluorescence is very weak, leading to a signal to noise ratio of only 20. The linewidth of a single rotational line is about 144 MHz as a result of a short lifetime of 1.1 ns.*

Molecular Constants			
A''	3976.(2)	ΔA	$-1.2(3)$
B''	1699.2(7)	ΔB	$-51.86(6)$
C''	1190.9(5)	ΔC	$-24.92(4)$
κ''	$-0.6350(8)$	$\Delta\kappa$	$-0.022(1)$
$\Delta I''$	$-0.14(20)$	$\Delta(\Delta I)$	$-0.33(30)$
Band origin	34917.759 ± 0.005 cm^{-1}		

Table 6.1: *Molecular constants of 2H-benzotriazole; the rotational constants A, B, and C (in MHz), the asymmetry parameter κ, and the inertial defect $\Delta I = I_c - I_b - I_a$ (in amu Å^2) in the electronic ground state and their differences with the first excited state ($\Delta A = A' - A''$, etc.).*

of about 4 K and a linewidth of 144±9 MHz. Because the experimental linewidth of our spectrometer is known to be about 16 MHz, the largest contribution to the experimental linewidth can be attributed to the short life time which can be determined to be 1.1±0.1 ns.

6.4 Discussion

Comparing the ground state rotational constants determined from our excitation spectrum with those obtained from microwave spectra [7] shows that there exists a large difference between both sets of constants (see Table 6.2). Because the microwave data is very accurate, we have tried to fit our spectrum keeping the ground state constants fixed to the microwave values. Despite much effort, it was impossible to fit all rotational lines in this way. As it has been shown [7], the microwave spectrum belongs to 1H-benzotriazole (the 1-position of the hydrogen has been determined by deuterium substitution), and it is therefore concluded that we have measured the other tautomer, *i.e.* 2H-benzotriazole.

To ensure that the rotational constants obtained from the spectrum in Figure 6.2 belong to the 2H-tautomer, they are compared with calculated values using bond lengths and angles from 6-31G [1, 2] and DZ (using a Huzinaga/Dunning double-zeta basis) [3] *ab initio* calculations, which are listed for both tautomers in Table 6.2. It can be seen that both DZ and 6-31G methods predict smaller A and larger B and C values for the 2H-tautomer compared to those for the 1H-tautomer in consistence with the experimental data. The DZ calculation predicts the C constant surprisingly precisely. Only a slight adjustments of DZ bond lengths (<0.005 Å) and angles (<0.01 degree), in a way that the structure expands along the b-axis and compresses along the a-axis, were necessary to reproduce all three experimental constants for the 2H-tautomer.

Comparing the rotational constants in Table 6.2 shows that the UV transition can be made solely in 2H-benzotriazole, but also in a system in which there is a 2H structure in the ground state and a 1H structure in the excited state. The latter possibility can be rejected because such a large geometry change would lead to an extremely poor Franck-Condon overlap resulting in a practically unobservable spectrum. Since the transition moment lies along the b-axis, the observed $S_1 \leftarrow S_0$ transition should be attributed to $^1B_2(^1L_a) \leftarrow {}^1A_1$ ($\pi^* \leftarrow \pi$) if the following correspondence

Molecular Constants of S_0			
2H-benzotriazole			
	exp (UV)	DZ[a]	6-31G[b]
A''	3976	4002	4037
B''	1699	1695	1710
C''	1191	1191	1201
μ			0 78
1H-benzotriazole			
	exp (MW)[c]	DZ[a]	6-31G[b]
A''	4008	4041	4080
B''	1677	1668	1686
C''	1182	1181	1193
μ	4 3	4 64	4 64

[a] Calculated from bond lengths and angles taken from [3]

[b] Calculated from bond lengths and angles taken from [1, 2], dipole moment taken from [1]

[c] Obtained from microwave experiments [7]

Table 6.2: *Experimental and calculated values for the ground rotational constants (in MHz) and the permanent dipole moment (in D)*

between inertial and cartesian axes holds $a \to z$, $b \to y$, $c \to x$ As it can be seen from Table 6 1, the excited state A constant is almost the same as the ground state one which implies that the molecule is mainly stretched along the a-axis upon excitation

Since the 2H-tautomer has C_{2v} symmetry, there are 2 pairs of equivalent protons (with nuclear spin 1/2) and one pair of equivalent nitrogen atoms (nuclear spin 1) Analysis of nuclear spin statistics predicts a 78 66 weight ratio for respectively even and odd K_a rotational states Unfortunately, as a result of laser intensity fluctuations, weak fluorescence, and many overlapping lines (owing to the large linewidth) it is impossible to state if there is an intensity alternation as a result of statistical weights

Obviously now the following question arises why has the microwave spectrum of 2H-benzotriazole not been observed? First of all, the calculated dipole moment of 2H-benzotriazole (0 78 D) is 6 times smaller than that of 1H-benzotriazole (4 64 D) [1], giving a 36 times smaller microwave transition probability Although the experimental value for the 2H-tautomer is not known, it should be noted that the calculated value for 1H-benzotriazole is in good agreement with the experimental value of 4 3±0 4 D [7] Secondly, the microwave experiment in the gas phase has been performed at high temperature (90 °C) Catalan *et al* [9] have estimated the proportion of 2H at 80 °C to be about 25% Therefore owing to the smaller dipole moment and the smaller fraction of 2H-benzotriazole at 90 °C, the microwave absorption should be roughly 100 times weaker for 2H-benzotriazole than for the 1H-form

Since it is very unlikely that the 0_0^0 bands of the $S_1 \leftarrow S_0$ transitions of 1H-benzotriazole and 2H-benzotriazole are at the same absolute frequency, the electronic absorption spectrum measured in a cell at 140 °C and attributed to 1H-benzotriazole in Ref. [7], should be assigned to 2H-benzotriazole. The observation of this band, at this relatively high temperature, supports the results from the UV gas phase study of Catalán *et al.* [9], who stated that there is still a reasonable amount of 2H-benzotriazole at this temperature. Also the vibrationally resolved jet-cooled spectra reported by Jalviste and Treshchalov [10] have to be attributed to 2H-benzotriazole.

There still remains a problem concerning the $S_1 \leftarrow S_0$ spectrum of 1H-benzotriazole. Both tautomers were shown to contribute to the UV absorption of gas phase benzotriazole in the cell [9], furthermore the sharp 286 nm system (the rotational band contour) was found to be partly superimposed on a strong and diffuse second system [8]. Apart from the possibility that 1H-benzotriazole does not fluorescence, it might also be possible that only the 2H-tautomer is populated under jet conditions as it is more stable [9].

Acknowledgements

References

1. F. Tomás, J.M. Abboud, J. Laynez, R. Notario, L. Santos, S.O. Nilsson, J. Catalán, R.M. Claramunt and J. Elguero, J. Am. Chem. Soc. **111** (1989) 7348

2. A.R. Katritzky, K. Yannakopoulou, E. Anders, J. Stevens and M. Szafran, J. Org. Chem. **55** (1990) 5683

3. M.H. Palmer, M.M.P. Kurshid, T.J. Rayner and J.A.S. Smith, Chem. Phys. **182** (1994) 27

4. A. Escande, J.L. Caligné and J. Lapasset, J. Acta Crystallogr. Sect. B. **30** (1974) 1490

5. A. Maquestiau, Y. Van Haverbeke, R. Flammang, M.C. Pardo and J. Elguero, Org. Mass Spectrom. **7** (1973) 1267

6. M.H. Palmer and S.M.F. Kennedy, J. Mol. Struct. **43** (1978) 203

7. B. Velino, E. Cané, L. Gagliardi, A. Trombetti and W. Caminati, J. Mol. Spectrosc. **161** (1993) 136

8. E. Cané, A. Trombetti and B. Velino, J. Mol. Spectrosc. **158** (1993) 399

9. J. Catalán, P. Pérez and J. Elguero, J. Org. Chem. **58** (1993) 5276

10. E. Jalviste and A. Treshchalov, Chem. Phys. **172** (1993) 325

11. S. Gerstenkorn and P. Luc, *Atlas du spectroscopie d'absorption de la molecule d'iode*, CNRS, Paris (1978)
    S. Gerstenkorn and P. Luc, Rev. Phys. Appl. **14** (1979) 791

12. The absolute frequencies of the 0^0_0 bands reported in [10] have been calibrated with Neon emission lines. Unfortunately, their wavelenghths have not been corrected to the vacuum. The corrected frequencies of the origins are $34\,917$ cm^{-1} for benzotriazole and $36\,022$ cm^{-1} for benzimidazole.

Chapter 7

Rotationally resolved UV spectroscopy of indole, indazole and benzimidazole: inertial axis reorientation in the $S_1(^1L_b) \leftarrow S_0$ transitions

Giel Berden and W. Leo Meerts
Department of Molecular and Laser Physics, University of Nijmegen,
Toernooiveld, 6525 ED Nijmegen, The Netherlands

Erko Jalviste
Institute of Physics, Estonian Academy of Science,
Riia 142, EE2400 Tartu, Estonia

Abstract

Rotationally resolved laser induced fluorescence excitation spectra of the $S_1(^1L_b) \leftarrow S_0$ origin bands of indole, indazole, and benzimidazole have been measured. From these spectra, the rotational constants in both electronic states have been determined. The spectra of all three molecules exhibit 'anomalous' rotational line intensities. These intensity perturbations are a result of the reorientation, upon electronic excitation, of the inertial axes of the molecule. Intensity analysis of the rotational lines yielded information about the inertial axis reorientation, and the direction of the transition moment vector for each molecule.

7.1   Introduction

The electronic spectra of indole, indazole and benzimidazole are of similar nature. In solution, these molecules have two absorption bands in the near UV, which can be assigned as $\pi^* \leftarrow \pi$ singlet–singlet transitions [1]. The two excited states are labeled by ^1L_a and ^1L_b following the suggestion of Platt [2].

Indole has been studied extensively. In solution, both transitions have different properties. First, the ^1L_b absorption band shows vibronic structure with a strong 0^0_0 transition, while the ^1L_a absorption band appears to be broad and structureless. Furthermore, the ^1L_a band is very sensitive to the polarity of the solvent, while there is only a little dependence on solvent polarity for the ^1L_b band [6]. In the gas phase, the ^1L_b state is lower in energy than the ^1L_a state [6]. Interaction between indole and polar solvents can bring the ^1L_a state below the ^1L_b state [7]. The origin band of the ^1L_b state is the strongest feature in the vibronically resolved spectrum of jet-cooled indole [3, 4, 5]. Recently, the group of Callis [8] found evidence for ^1L_a vibronic states in the excitation spectrum of jet-cooled indole. By using polarized one-color two-photon excitation techniques, they assigned lines ranging from 455 to 1459 cm^{-1} above the ^1L_b origin to ^1L_a. Barstis *et al.* [9] gave an assignment of all spectral features in the excitation spectrum of indole upto 1000 cm^{-1} above the ^1L_b origin. In contrast to Callis, they concluded that there is no significant band in the indole spectrum in this interval which can be assigned as belonging to a system other than the $^1L_b \leftarrow S_0$ transition. Therefore, the assignment of ^1L_a spectral features remains ambiguous. Since the ^1L_a state is very sensitive to the environment of the molecule, many studies have been performed on jet-cooled complexes of indole and indole derivatives with polar and non-polar solvent molecules [10].
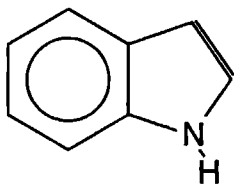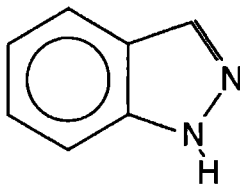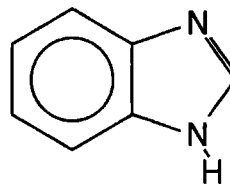
INDOLE   INDAZOLE   BENZIMIDAZOLE

The ^1L_a and ^1L_b states can be distinguished by the direction of the electronic transition moment vector (TM). In solution, analysis of fluorescence excitation and anisotropy spectra can provide the relative direction between the ^1L_a and ^1L_b transition moment vectors, but not the absolute direction in the molecular frame [13]. In the gas phase, the rotationally resolved excitation spectrum can provide the absolute value of the angle between the transition moment vector and the inertial axes. Mani and Lombardi [14] performed a rotational band contour analysis on the room temperature gas phase spectrum of the origin of the $^1L_b \leftarrow S_0$ transition of indole. They determined the angle θ between the a-axis and the transition moment vector to be 20°. Philips and Levy [15] measured the same transition by using the laser induced fluorescence (LIF) technique in a supersonic molecular jet. They resolved the rotational structure with an experimental resolution of 180 MHz. Analysis of their spectra yielded an angle θ of 45°, and the rotational constants in the ground and the electronically excited state. After the LIF study of Philips and Levy, the microwave spectra of indole [16, 17] and its N–D isotopomer [17] have been reported.

Indazole and benzimidazole are less thoroughly studied in the gas-phase For indazole, the vibrationally resolved gas-phase infrared spectrum [18], and the electronic spectrum [19] have been reported Precise ground state rotational constants of indazole and its N-D isotopomer have been obtained from microwave spectra reported by Velino *et al* [20] The same group performed a rotational band contour analysis on the origin band of the $S_1 \leftarrow S_0$ transition of indazole [21] All aforementioned measurements were performed in a heated cell The vibrationally resolved spectrum of the $S_1 \leftarrow S_0$ transition of benzimidazole has been recorded in a heated cell [22] and in supersonic jet [23] Cane *et al* reported the microwave spectra of benzimidazole and its N-D isotopomer [24], and they performed a band contour analysis of the electronic origin [25]

Indazole might exist in two tautomeric forms 1H-indazole and 2H-indazole Catalan *et al* [26] concluded from spectroscopic and thermodynamic experiments that in the gas-phase, 1H-indazole is the most stable tautomer, both in the ground and excited states Their conclusion is in agreement with the microwave results, which confirmed the 1H position *via* isotopic substitution [20] Recently, we have reported the rotationally resolved fluorescence excitation spectrum of the 0_0^0 band of the $S_1 \leftarrow S_0$ transition of 2H-benzotriazole [27] The microwave spectra of benzotriazole, recorded in a heated cell [28] and in a jet [29], have been attributed to the 1H-tautomer Although 2H-benzotriazole is found to be more stable than 1H-benzotriazole [30, 31], the microwave spectrum of 2H-benzotriazole could not be measured [29], probably because its permanent dipole moment is too small [30]

As a result of the low symmetry of indole, indazole, and benzimidazole, different equilibrium molecule-fixed axis systems can exist for ground and electronically excited states In other words, due to a geometry change in the molecule upon excitation the inertial axes are reoriented This effect is called axis reorientation, axis switching, axis tilting, or the rotational Duschinsky effect Axis reorientation has no effect on the frequencies of the rotational lines, but it 'perturbs' its intensities A first fundamental treatment of axis reorientation has been presented in the pioneering work of Hougen and Watson [32] They explained with this effect the 'anomalous' rotational line intensities observed in the spectrum of the $\tilde{A}\ ^1A_u \leftarrow \tilde{X}\ ^1\Sigma_g^+$ transition of acetylene Later, axis reorientation in this linear to bent transition of acetylene has been investigated in more detail [33] Similar effects have been observed in hydrogencyanide [34] Smalley *et al* [35] have observed $90°$ axis reorientation (axis switching) in the excitation spectrum of jet-cooled s-tetrazine, and they derived optical selection rules for this special case This full angle axis switching effect was also found for other near-oblate symmetric top molecules, like for example pyrimidine [36] Held *et al* [37] observed an axis reorientation of $2\ 4°$ in the rotationally resolved spectrum of the 0_0^0 band of the $S_1 \leftarrow S_0$ transition of 2-pyridone Furthermore, they formulated a convenient method to calculate the 'anomalous' rotational line intensities The relation between the axis reorientation effect and the vibrational Duschinsky effect has been elucidated in the theoretical works of Ozkan [38] and Chigirev [39]

In this paper, we present the rotationally resolved fluorescence excitation spectra of the origin bands of the $S_1(^1L_b) \leftarrow S_0$ transitions of indole, indazole, and benzimidazole The spectra have been recorded at a Doppler limited resolution of about 15 MHz using a narrow band UV laser system in combination with a molecular beam apparatus Frequency analysis of the spectra provide accurate values for the rotational constants All spectra show 'anomalous' rotational line intensities, which are an effect of axis reorientation upon electronic excitation The overall shapes of the spectra have been fit to a model, which includes the axis reorientation effect, to obtain accurate values for the direction of the transition moment vector and the axis reorientation angle

Our results may be useful for testing *ab initio* calculations and for improving semi-empirical calculations to obtain better geometrical and electronic structures of the ^1L_b and ^1L_a excited states of these molecules.

7.2 Theory

Electronic-rotational transitions in a molecule are induced by interactions of the space-fixed radiation field with the rotating electronic transition moment in the (rotating) molecule. Usually, the origin of the molecule-fixed coordinate system is chosen to be at the center of mass of the molecule, and the axes of this frame are chosen to be coincident with the principal axes of inertia of the molecule. The Euler angles θ, ϕ, and χ specify the orientation of the rotating molecule-fixed coordinate system with respect to the space-fixed system. The rotational energy levels of the molecules studied in this chapter, can be calculated with an asymmetric rigid rotor Hamiltonian. If the molecule-fixed frame in the ground and excited electronic state are identical, the rotational eigenfunctions of the Hamiltonian in both states can be expressed as a linear combination of the same symmetric top basis functions, $|JK\rangle$:

$$|J''K_a''K_c''\rangle = \sum_K c_{J''K}''|J''K\rangle \tag{7.1}$$

$$|J'K_a'K_c'\rangle = \sum_K c_{J'K}'|J'K\rangle \tag{7.2}$$

The intensity of a single rotational line in the fluorescence excitation spectrum is given by

$$I = I_0 g_n (2J'' + 1) A_{J''K_a''K_c''J'K_a'K_c'} \exp(-E(J'', K_a'', K_c'')/kT_{rot}) \tag{7.3}$$

where I_0 is a constant, g_n is the nuclear spin statistical weight, and $A_{J''K_a''K_c''J'K_a'K_c'}$ is the line strength factor. This factor is proportional to the square of the electronic transition moment matrix element

$$A_{J''K_a''K_c''J'K_a'K_c'} \propto |\langle J''K_a''K_c''|\mu_F|J'K_a'K_c'\rangle|^2 \tag{7.4}$$

where μ_F is the electronic transition moment vector component along the space-fixed axis $F(= X, Y, Z)$, which can be expressed in components along the molecule-fixed axes μ_g:

$$\mu_F = \sum_g \cos(Fg)\mu_g \qquad g = a, b, c \tag{7.5}$$

where $\cos(Fg)$ are the direction cosines. Since the rotational eigenfunctions of the ground and excited electronic states are expressed in the same basis set, the line strength factor (Eq. 7.4) can be evaluated.

The ground and excited state rotational eigenfunctions and the direction cosines operators can be classified according to their symmetry under the Four-group (dihedral group D_2) [40]. It can then be shown that the sum in Eq. 7.5 contributes to the line strength factor with only one term, and each transition can be labeled uniquely as *a*, *b*, or *c* type [40].

The geometry of a molecule usually changes upon electronic excitation. Above, it was assumed that the molecule-fixed frames in both electronic states are identical. This requires that the geometry change in the molecule should be such that the principal axes do not change their orientation. If a molecule has 'high' symmetry (*e.g.* naphthalene or 2H-benzotriazole) this will

indeed be the case (see Ref. [32, 38] for a discussion of the relation between the symmetry of a molecule and the axis reorientation effect). For molecules with 'low' symmetry, electronic excitation can (but does not have to) change the geometry in a way that the principal axes are reoriented with respect to the space fixed frame. Therefore, two rotating molecule-fixed coordinate systems are required to describe the rotational motion of the molecule if electronic excitation takes place. The relative orientation in space of both molecule-fixed systems remains constant and is solely defined by the geometry change.

The rotational energy levels in both electronic states can still be calculated using the asymmetric rotor Hamiltonian for each state in its principal axis system. However, the resulting rotational eigen functions for both states are now expressed on different symmetric top basis sets: $|JK\rangle''$ and $|JK\rangle'$ (both sets are defined in their own molecule-fixed coordinate system). In order to calculate the line strength factor (Eq. 7.4) both eigenfunctions should be expressed in the same basis set.

In their original description of the axis reorientation effect, Hougen and Watson [32], defined a transformation matrix $\mathcal{D}^{(J')}_{K'K}(\theta_T, \phi_T, \chi_T)$ to transform the rotational basis set of the excited state to that of the ground state, $|JK\rangle''$:

$$|J'K'_aK'_c\rangle = \sum_K c_{J'K} \sum_{K'} \mathcal{D}^{(J')}_{K'K}(\theta_T, \phi_T, \chi_T)|J'K'\rangle'' \tag{7.6}$$

Now, both the ground and the electronic excited state rotational eigenfunctions are expressed in the same basis, and thus, the line strength factor can be evaluated.

Held *et al.* [37] have observed anomalous intensities in the fully resolved $S_1 \leftarrow S_0$ electronic spectrum of 2-pyridone. These effects have been attributed to axis reorientation in the plane of the molecule. They used a more convenient method to calculate the line strengths. Instead of transforming the excited state eigenfunctions into the coordinate system of the ground state, they first expressed the excited state Hamiltonian in the principal axis system of the ground state. Diagonalizing the transformed excited state Hamiltonian gives the same rotational energy eigenvalues as the 'unswitched' Hamiltonian, but the eigenfunctions are now defined on the same basis set as the ground state eigenfunctions.

In indole, indazole, and benzimidazole, the reorientations of the principal axes are also in the plane of the molecule. This means that in both electronic states the c-axes coincide. The relative orientation between both sets of principal axes is then described with one parameter: the angle θ_T that rotates the a-axis of the ground state into the a-axis of the excited state (Figure 7.1). The components of the rotational angular momentum operator in the excited state in the principal axis system of that state J'_g can be expressed in the components in the principal axis system of the ground state J_g by a simple 3×3 rotation matrix:

$$\begin{pmatrix} J'_a \\ J'_b \\ J'_c \end{pmatrix} = \begin{pmatrix} \cos\theta_T & \sin\theta_T & 0 \\ -\sin\theta_T & \cos\theta_T & 0 \\ 0 & 0 & 1 \end{pmatrix} \begin{pmatrix} J_a \\ J_b \\ J_c \end{pmatrix} \tag{7.7}$$

The Hamiltonian of the excited state expressed in the molecule-fixed frame of the ground state is then given by:

$$\begin{aligned} H' &= (A'\cos^2\theta_T + B'\sin^2\theta_T)J_a^2 + (A'\sin^2\theta_T + B'\cos^2\theta_T)J_b^2 + C'J_c^2 \\ &\quad + (A' - B')\sin\theta_T\cos\theta_T(J_aJ_b + J_aJ_b) \end{aligned} \tag{7.8}$$
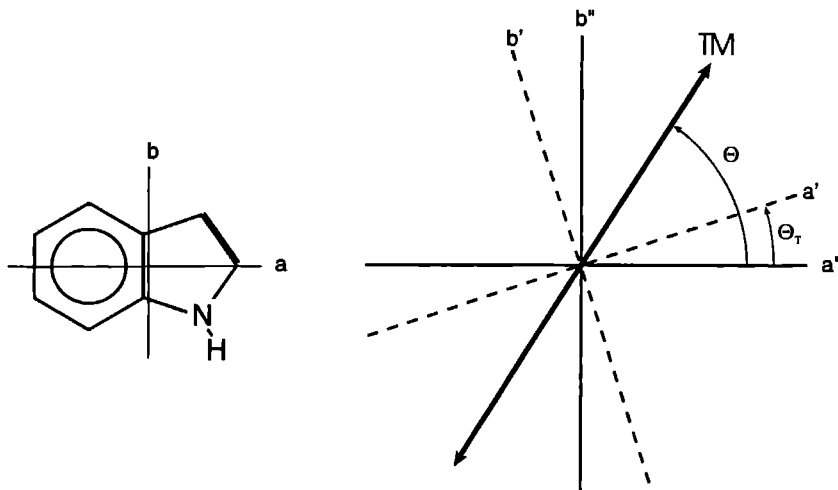
Figure 7.1: *Schematic of the indole geometry and its principal axis system (left) Definition of the axis reorientation angle θ_T and the direction of the transition moment (TM) vector θ The angles measured in the counterclockwise sense are taken to be positive a'' and b'' are the principal axes in the ground state, a' and b' are the principal axes in the excited state The c axes are perpendicular to the molecular plane*

The term containing the cross products of the angular momentum components generates new off-diagonal matrix elements in the excited state Hamiltonian

The excited state Hamiltonian has no longer the Four-group symmetry of the ground state due to the angular momentum cross terms This means that the sum in Eq 7 5 contributes with more than one term to the line strength factor Therefore the rotational lines cannot be labeled uniquely as a, b, or c type However, we still will use this labeling, which gives then the dominant character of a particular line For indole, indazole, and benzimidazole, the transition moment vector is in the plane of the molecule, therefore the line strength factor becomes

$$A_{J''K_a''K_c''J'K_a'K_c'} \propto |\langle J''K_a''K_c''|\cos(Fa)\mu_a|J'K_a'K_c'\rangle|^2 + |\langle J''K_a''K_c''|\cos(Fb)\mu_b|J'K_a'K_c'\rangle|^2$$
$$+2\langle J''K_a''K_c''|\cos(Fa)\mu_a|J'K_a'K_c'\rangle\langle J''K_a''K_c''|\cos(Fb)\mu_b|J'K_a'K_c'\rangle \qquad (7\ 9)$$

Without axis reorientation, only the first *or* second term would be non-zero (giving, respectively, an a or b type transition) For axis reorientation in the ab-plane, the symmetry is reduced from D_2 to $C_2(c)$, the cyclic group containing a rotation of π around the c-axis The lowered symmetry of the Hamiltonian[2] leads to less stringent rotational selection rules The selection rules for the transition moment components along the a and b-axis are now identical $K_c''\leftrightarrow K_c' = e\leftrightarrow o$ The

---

[2]A Hamiltonian which is invariant under all operations of the Four group, can be factorized in four blocks by using the Wang functions as basis set The Hamilonian of Eq 7 8 is invariant under the operations of the cyclic $C_2(c)$ group Use of the Wang functions as basis set, will factorize the Hamiltonian in two blocks Therefore, the calculations are still being simplified by using this basis set

K_a parity is no longer distinguished [41] Therefore, both components contribute to the same rotational transition

What is the effect of axis reorientation on the intensities of for example indazole? In this molecule, the electronic transition moment vector makes an angle of 62° with the a-axis, and the reorientation angle is only 1° Without axis reorientation, the spectrum exhibits ab-type hybrid band character Turning the axis reorientation on, certain a-type lines lose (or gain) intensity and certain b-type lines gain (or lose) intensity in a way that the total line strength and intensity from a given initial state is conserved For a more extensive discussion about the intensity effects, we refer to Hougen and Watson [32] and Held, Champagne and Pratt [37]

7.3 Experimental

Rotationally resolved fluorescence excitation spectra of indole, indazole and benzimidazole were obtained using a narrow bandwidth UV laser system and a molecular beam apparatus Indole (Janssen Chimica, 99%), indazole (Fluka, 99%), and benzimidazole (Janssen Chimica, 98%) were heated to ca 50 °C, 100 °C, and 175 °C, respectively, seeded in 0 5 bar argon, and expanded through a nozzle with a diameter of 0 15 mm The nozzle was kept at a slightly higher temperature to prevent condensation of the sample in the orifice The molecular beam was skimmed twice in a differential pumping system and was crossed perpendicularly with a UV laser beam at about 30 cm from the nozzle

UV radiation with a bandwidth of 3 MHz was generated by intracavity frequency doubling in a single frequency ring dye laser operating on Rh110 By using a 2 mm thick Brewster cut BBO crystal, 0 1–0 3 mW of tunable radiation was obtained For relative frequency calibration a temperature stabilized Fabry-Perot interferometer was used with a free spectral range of 75 MHz For absolute frequency calibration, the iodine absorption spectrum [42] was recorded simultaneously The total undispersed fluorescence was imaged on a photomultiplier connected to a photon counting system interfaced with a computer

7.4 Results and interpretation

7.4.1 Frequency analysis

The high resolution fluorescence excitation spectra of the origin bands of the $S_1 \leftarrow S_0$ transitions of indole, indazole and benzimidazole are shown in Figures 7 2, 7 3, and 7 4, respectively Each observed spectrum is an ab-hybrid band No c-type character was found Each spectrum consists of about 2000 lines, and spans approximately 5 cm^{-1} The absolute frequencies of the origins are given in Table 7 1

As a starting point for the rotational assignment, each spectrum was simulated using a rigid asymmetric rotor Hamiltonian and rotational constants reported in other studies The rotational ground state constants were taken from microwave experiments (indole [17], indazole [20], benzimidazole [24]) The excited state constants and the hybrid characters were taken from rotational band contour studies in a supersonic jet (indole [15]), or in the vapour phase (indazole [21], benzimidazole [25]) Unique assignments could be made by comparing the simulations with the experimental spectra All lines could be fitted within the experimental error The obtained ground state constants overlap within their errors with the microwave constants Since the latter constants are two orders of magnitude more accurate than our constants, the UV data have been fitted again with

Figure 7.2: *High resolution LIF spectrum of the origin of the $S_1 \leftarrow S_0$ transition of indole. The absolute frequency of the origin (0.0 on the scale of the figure) is at $35\,231.420{\pm}0.006$ cm^{-1}.*

Figure 7.3: *High resolution LIF spectrum of the origin of the $S_1 \leftarrow S_0$ transition of indazole. The absolute frequency of the origin (0.0 on the scale of the figure) is at $34\,471.691{\pm}0.006$ cm^{-1}.*

	Molecular Constants			
	Indole[a]	Indazole[b]	Benzimidazole[c]	
A''	3877 828(6)	3977 927(6)	3929 720(7)	MHz
B''	1636 047(1)	1633 272(1)	1679 259(3)	MHz
C''	1150 8997(8)	1158 141(1)	1176 747(1)	MHz
$A' - A''$	−134 751(6)	−102 220(11)	−155 687(7)	MHz
$B' - B''$	−17 918(14)	−29 235(18)	−15 294(5)	MHz
$C' - C''$	−20 73(1)	−23 24(6)	−21 437(8)	MHz
$\Delta I''$	−0 1113(7)	−0 1023(8)	−0 0866(11)	amu Å^2
$\Delta I'$	−0 168(8)	−0 158(26)	−0 1889(6)	amu Å^2
κ''	−0 6441803(16)	−0 6630021(15)	−0 6349313(32)	
κ'	−0 626500(15)	−0 657667(23)	−0 611524(10)	
ν_0	35231 420(6)	34471 691(6)	36021 336(6)	cm^{-1}
θ	±38 3(2)°	±62 2(7)°	±22 0(8)°	
θ_T	±0 50(9)°	±1 03(11)°	±0 72(10)°	

[a] Ground state constants obtained from microwave experiments [17]
[b] Ground state constants obtained from microwave experiments [20]
[c] Ground state constants obtained from microwave experiments [24]

Table 7.1: *Molecular constants of indole, indazole and benzimidazole in the ground state (double prime) and the excited state (single prime) A, B, and C are the rotational constants ΔI is the inertial defect ($\Delta I = I_c - I_b - I_a$) κ is the asymmetry parameter ν_0 is the absolute frequency of the origin θ is the angle between the inertial a-axis and the electronic transition moment vector θ_T is the axis reorientation angle The signs of θ and θ_T signs are coupled the upper signs or the lower signs*

the ground state constants kept fixed to the microwave values. This method gives more accurate excited state constants. The results are shown in Table 7.1, listed are the rotational constants in the S_0 state and their differences with those in the S_1 state. Furthermore, the asymmetry parameters and the inertial defects in both states are given Clearly, all three molecules are planar asymmetric tops in both states (inertial defects are small and $\kappa \approx -0$ 6). The excited state constants obtained from Table 7.1 are in agreement with the reported constants obtained from rotational band contour analysis [15, 21, 25], but are more accurate since they have been obtained from well resolved rotational spectra.

7.4.2 Intensity analysis

The direction of the electronic transition moment vector is determined by the hybrid character of the spectrum. For all three molecules, this vector is in the plane of the molecule since no c-type lines have been observed. If θ is the angle between the electronic transition moment vector and the a-axis, I^b is the experimental intensity of a particular b-type line, and I^a is the experimental intensity of an a-type line originating from the same rotational ground state level, the angle θ can
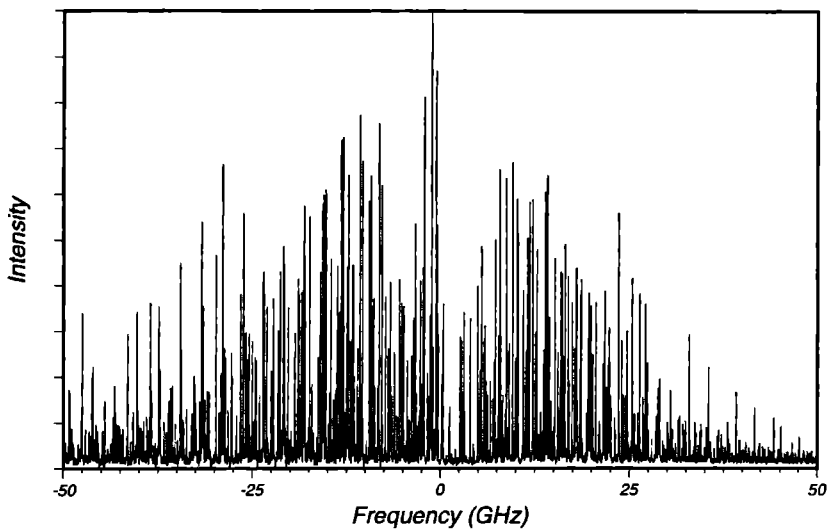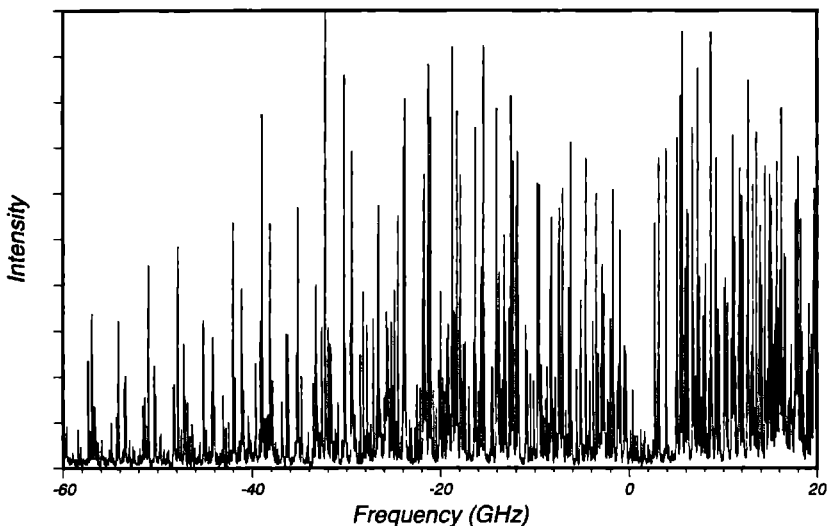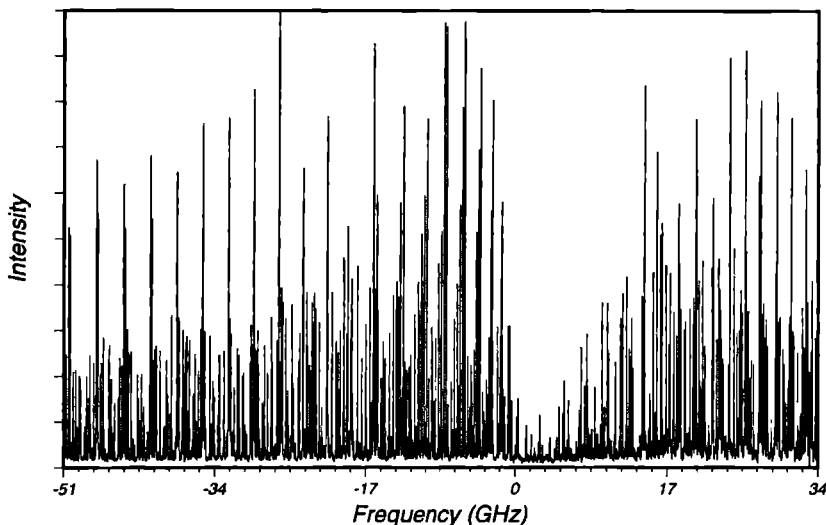
Figure 7.4: *High resolution LIF spectrum of the origin of the $S_1 \leftarrow S_0$ transition of benzimidazole. The absolute frequency of the origin (0.0 on the scale of the figure) is at $36\,021.336\pm0.006$ cm^{-1}.*

be calculated from:

$$\tan^2 \theta = \frac{I^b}{I^a}\frac{A_a}{A_b} \tag{7.10}$$

where A_a and A_b are the line strength factors.

Without axis reorientation, θ can be determined by a careful examination of the intensities of rotational lines. To eliminate rotational temperature effects, at least two fully resolved lines have to be found which originate from the same ground state level, but have different character. Since the effect of axis reorientation is a 'transfer of intensities' between a- and b-type lines, at least three fully resolved lines are needed to determine both θ and the reorientation angle θ_T. If the molecule is 'small' and the rotational lines are narrow, it is possible to locate such a set of lines, and both angles can be determined. However, for indole, indazole, and benzimidazole such a set of lines is difficult to find or even does not exist. This is due to the small rotational constants of these molecules, which result in many overlapping rotational lines. However, the information needed is still present in every rotational transition, *i.e.*, in the entire spectrum. Therefore, we decided to perform a least-squares fit of the intensity contour of the total spectrum. This contour is determined not only by θ and θ_T, but also by the rotational temperature and the linewidth of each transition.

The rotational contours were calculated using the rotational constants from Table 7.1, and variable parameters for the rotational temperature, the hybrid character (θ), the reorientation angle (θ_T), and the linewidth. These parameters were varied in a least-squares fitting program. The χ^2 value to be minimized was calculated as the sum of the squared differences between the

98

intensities of the simulated and experimental spectra The maximum number of points on the frequency scale was 20000 If the spectrum contained more points, the number of points was reduced to the maximum after first smoothing the spectrum Besides the fitted parameters, the residual spectrum (the difference between the experimental and calculated spectra) was obtained

The results of the contour fitting of several spectra of indole, indazole and benzimidazole are given in Table 7 2 The meaning of the different simulation models is presented in Table 7 3 Model 1, the simplest one, assumes an exponential population distribution (Boltzmann distribution), no axis reorientation ($\theta_T = 0$), and a Lorentzian line profile The residual spectrum, however, showed a rather poor agreement with the experimental data the lines originating from the lowest and highest rotational levels in the S_0 were underestimated This observation is not surprising, since it is known that the rotational state distribution in the molecular beam is non-Boltzmann (non-equilibrium) [43]

Wu and Levy [44] used a three-parameter two-temperature distribution which is given by

$$n_{J,K_a K_c}(T_1, T_2) = e^{-E_{JK_aK_c}/kT_1} + We^{-E_{JK_aK_c}/kT_2} \qquad (7\ 11)$$

where n_{J,K_a,K_c} is the population in level (J, K_a, K_c) of the electronic and vibrational ground state, which has an energy E_{J,K_a,K_c} T_1 is the lower temperature and T_2 the higher one W is a weighting factor This distribution can be considered to describe a mixture of two ensembles, one with temperature T_1 and the other with temperature T_2 Introducing this distribution greatly improves the contour fitting as shown in Table 7 2 (model 2) For all spectra the χ^2 value is lowered Also the background intensity is decreased, indicating that the fit describes the experimental spectrum more entirely It should be noted that the variation of the molecular beam conditions (backing pressure, temperature of sample) results in different rotational temperatures for different spectra of the same molecule

Careful examination of the residual spectra of model 2 shows that there were certain regions in the spectra where the intensities of the a-type lines were overestimated while the intensities of the b-type lines were underestimated However, there are also regions where the opposite holds, so that the hybrid character alone cannot account for these intensity effects These effects appeared in all three molecules, and were especially pronounced for P and R transitions originating from high J and low K states The same effects were found by Held *et al* [37] in 2-pyridone, who attributed these effects to axis reorientation Model 3 includes axis reorientation by introducing the additional fit parameter θ_T (Table 7 2 and 7 3) Again the agreement between the fitted and experimental spectra becomes better There are two possible sets of (θ, θ_T) values which fit each spectrum (Table 7 1) For example, in the case of indazole, $\theta=+62\ 2°$ and $\theta_T=+1\ 03°$, as well as, $\theta= 62\ 2°$ and $\theta_T=-1\ 03°$, describe the spectra equally well

The experimental spectra can be distorted by an uncontrolled change in the concentration of molecules in the molecular beam during the measurements In order to compensate for this change, we introduced a new parameter IGR in model 4 which describes a linear intensity variation according to

$$I'(\nu) = I(\nu)\ (1 + (\nu - \nu_{begin})\ IGR\ 10^{-6}) \qquad (7\ 12)$$

where $I(\nu)$ is the calculated intensity at frequency ν, $I'(\nu)$ is the modified intensity, and ν_{begin} is the begin frequency of the spectral region under investigation From Table 7 2, it can be seen that only the results of the first spectrum of indole is strongly influenced by this effect Indeed, the temperature of the sample decreased during the recording of this spectrum, which resulted in a decreasing concentration of indole molecules in the molecular beam

		Indole								
#	mod	θ deg	θ_T deg	T_1, T_J K	T_2, T_K K	W	$\Delta\nu_L$ MHz	$\Delta\nu_G$ MHz	BG a u	IGR a u	χ^2 a u
1	1	38 22	-	2 63	-	-	19 24	-	266	-	790
1	2	37 85	-	1 58	6 56	0 164	19 62	-	223	-	482
1	3	37 87	0 024	1 58	6 57	0 163	19 62	-	223	-	482
1	4	38 34	0 599	1 59	5 64	0 183	19 93	-	216	−1 051	264
1	5	38 37	−0 009	2 56	2 88	-	19 27	-	264	-	782
1	6	38 46	0 541	1 55	5 21	0 223	-	26 63	274	−1 020	469
1	7	38 46	0 584	1 60	5 51	0 192	10 09	17 58	243	−1 038	181
2	1	38 05	-	2 49	-	-	19 70	-	222	-	232
2	2	37 73	-	1 48	4 91	0 234	19 95	-	204	-	144
2	3	38 14	0 432	1 52	5 21	0 205	19 96	-	203	-	136
2	4	38 22	0 496	1 50	5 03	0 220	20 05	-	202	−0 114	135
2	5	38 53	0 380	2 44	2 72	-	19 74	-	221	-	223
2	6	38 43	0 376	1 43	4 55	0 284	-	26 27	242	-	184
2	7	38 31	0 428	1 49	4 84	0 243	10 77	17 05	220	-	104
3	1	37 66	-	2 59	-	-	19 39	-	266	-	388
3	2	37 47	-	1 85	6 84	0 119	19 96	-	236	-	272
3	3	38 07	0 567	1 85	6 71	0 123	19 95	-	237	-	251
3	4	38 00	0 524	1 85	6 67	0 123	19 95	-	237	0 074	250
3	5	38 33	0 587	2 54	2 81	-	19 45	-	265	-	363
3	6	38 40	0 562	1 85	6 14	0 145	-	26 05	283	-	317
3	7	38 23	0 578	1 84	6 39	0 134	10 63	17 12	258	-	202
4	1	37 79	-	2 46	-	-	19 22	-	276	-	805
4	2	37 57	-	1 71	5 84	0 151	19 43	-	238	-	505
4	3	38 03	0 419	1 72	5 82	0 150	19 40	-	239	-	476
4	4	38 32	0 545	1 68	5 78	0 164	19 43	-	237	−0 267	453
4	5	38 37	0 477	2 41	2 65	-	19 23	-	275	-	760
4	6	38 36	0 402	1 50	4 23	0 332	-	25 36	313	-	653
4	7	38 18	0 422	1 72	5 63	0 159	10 37	16 60	270	-	340

Table 7.2: *Results of the intensity analysis of indole, indazole, and benzimidazole The first column, marked with #, gives the number of the spectrum which has been analysed The second column (mod) gives the number of the models which have been used to analyse the spectra. The 7 models with their parameters are described Table 7 3 See the text for further details*

										Indazole			
#	mod.	θ deg.	θ_T deg.	T_1, T_J K	T_2, T_K K	W	$\Delta\nu_L$ MHz	$\Delta\nu_G$ MHz	BG a.u.	IGR a.u.	χ^2 a.u.
1	1	63.64	-	3.91	-	-	32.03	-	334	-	123
1	2	63.38	-	2.64	7.50	0.222	32.32	-	316	-	89
1	3	62.45	1.180	2.71	8.25	0.180	32.68	-	314	-	70
1	4	62.32	1.169	2.63	8.12	0.169	32.63	-	314	−0.204	68
1	5	62.63	1.126	3.90	3.93	-	32.27	-	335	-	107
1	6	62.23	1.072	2.62	7.38	0.237	-	43.23	355	-	138
1	7	62.39	1.139	2.76	8.55	0.165	25.50	18.72	323	-	64
2	1	63.74	-	3.87	-	-	32.24	-	360	-	132
2	2	63.63	-	2.67	8.30	0.179	32.64	-	335	-	78
2	3	62.85	1.019	2.59	8.20	0.193	32.75	-	335	-	60
2	4	62.88	1.025	2.60	8.18	0.193	32.75	-	335	0.006	60
2	5	63.09	0.926	3.87	3.92	-	32.46	-	360	-	117
2	6	62.54	0.908	2.67	8.22	0.184	-	42.91	382	-	131
2	7	62.79	1.020	2.59	8.03	0.199	26.79	17.18	344	-	54
3	1	61.58	-	3.36	-	-	33.80	-	304	-	150
3	2	61.36	-	1.85	5.76	0.492	33.80	-	289	-	125
3	3	61.95	1.015	1.95	6.14	0.398	33.75	-	290	-	103
3	4	61.95	1.025	1.90	6.00	0.423	33.77	-	290	·0.046	103
3	5	62.49	1.038	3.16	3.79	-	33.79	-	303	-	126
3	6	62.08	1.051	1.99	6.25	0.381	-	43.09	353	-	148
3	7	61.98	1.028	1.98	6.28	0.376	26.65	18.86	302	-	96
4	1	58.57	-	3.43	-	-	32.19	-	334	-	186
4	2	58.27	-	2.26	8.62	0.209	32.51	-	288	-	126
4	3	61.53	0.923	2.38	8.68	0.183	32.29	-	291	-	104
4	4	61.03	0.819	2.44	8.80	0.185	32.37	-	287	−0.292	103
4	5	62.17	0.986	3.30	4.35	-	31.97	-	324	-	147
4	6	61.58	0.987	2.57	9.55	0.136	-	41.70	392	-	176
4	7	61.54	0.936	2.42	8.92	0.170	26.85	16.35	306	-	97

Table 7.2: *Continued.*

					Benzımıdazole					
#	mod	θ deg	θ_T deg	T_1, T_J K	Γ_2, T_K K	W	$\Delta\nu_L$ MHz	$\Delta\nu_G$ MHz	BG a u	IGR a u	χ^2 a u
1	1	21 44	-	12 42	-	-	19 61	-	60	-	226
1	2	22 40	-	5 37	19 4	0 60	19 52	-	44	-	171
1	3	21 11	0 752	6 28	20 6	0 56	19 43	-	46	-	164
1	4	21 45	0 613	6 71	21 1	0 52	19 49	-	45	0 114	162
1	5	22 49	0 698	11 18	14 8	-	19 60	-	55	-	194
1	6	21 55	0 735	6 68	21 9	0 43	-	25 11	88	-	183
1	7	21 24	0 742	6 18	20 4	0 54	11 33	15 70	62	-	137
2	1	21 51	-	10 05	-	-	19 05	-	65	-	185
2	2	21 45	-	4 40	16 4	0 69	19 13	-	52	-	160
2	3	21 75	0 66	3 83	15 2	0 87	19 20	-	51	-	155
2	4	22 33	1 08	4 85	16 9	0 61	19 25	-	49	-0 233	153
2	5	23 62	0 88	8 03	12 5	-	19 32	-	62	-	170
2	6	22 63	0 54	4 82	17 4	0 61	-	24 79	93	-	180
2	7	22 23	0 65	4 13	15 6	0 80	11 32	15 34	67	-	129
3	1	20 09	-	9 97	-	-	19 46	-	283	-	62
3	2	21 03	-	4 89	21 3	0 39	19 35	-	267	-	48
3	3	22 43	0 84	4 67	19 5	0 43	19 51	-	265	-	45
3	4	22 49	0 84	4 88	20 0	0 42	19 45	-	264	0 114	45
3	5	23 18	0 78	9 03	13 1	-	19 47	-	274	-	56
3	6	22 80	0 63	5 27	21 6	0 37	-	25 39	292	-	54
3	7	22 60	0 78	4 84	19 9	0 42	11 79	15 35	275	-	38

Table 7.2: *Contınued*

Comparıson of the θ values obtaıned from models 2 and 3 (or 4), show that θ ıs only slıghtly altered by ıntroducıng axıs reorıentatıon Sınce axıs reorıentatıon alters the ıntensıtıes of rotatıonal lınes ın a way that the total lıne strength and ıntensıty from a gıven ınıtıal state ıs conserved, ıt ıs expected that both models should gıve exactly the same value for θ However, only about 80% of a spectrum has been fıt at once Therefore, ıntensıty can 'transfer' ın or out of that part, causing small devıatıons ın the value for θ when comparıng the fıttıng results wıth and wıthout axıs reorıentatıon

An alternatıve non-Boltzmann dıstrıbutıon ıs gıven by

$$n_{J,K_a,K_c}(T_J,T_K) = e^{-E_{J0J}/kT_J} \quad e^{-(E_{JK_aK_c}-E_{J0J})/kT_K} \tag{7 13}$$

where T_J ıs the rotatıonal temperature of the J manıfold, and T_K that of the K manıfold In thıs dıstrıbutıon, the rotatıonal populatıon ıs no longer a one-valued functıon of the total energy (like the dıstrıbutıon ın Eq 7 11) Rotatıonal populatıon analysıs of jet-cooled glyoxal performed by Peyroula and Jost [45] clearly revealed that rotatıonal coolıng ıs more effıcıent for J states wıth the same K value, than for J states wıth dıfferent K values, ı e $T_J < T_K$ Thıs two temperature

model	short description	parameters									
1	Boltzmann distribution	θ		T_1			$\Delta\nu_L$		BG	ISF	
2	2 temperature distribution (Eq 7 11)	θ		T_1	T_2	W	$\Delta\nu_L$		BG	ISF	
3	+ axis reorientation effect	θ	θ_T	T_1	T_2	W	$\Delta\nu_L$		BG	ISF	
4	+ intensity correction	θ	θ_T	T_1	T_2	W	$\Delta\nu_L$		BG	ISF	IGR
5	2 temperature distribution (Eq 7 13)	θ	θ_T	T_J	T_K		$\Delta\nu_L$		BG	ISF	
6	model 3, Gaussian line shape	θ	θ_T	T_1	T_2	W		$\Delta\nu_G$	BG	ISF	
7	model 3, Voigt line shape	θ	θ_T	T_1	T_2	W	$\Delta\nu_L$	$\Delta\nu_G$	BG	ISF	

Table 7.3: *The different models used for the intensity analysis of the spectra of indole, indazole, and benzimidazole (Table 7 2) Most of the parameters are defined in the text $\Delta\nu_L$ is the Lorentzian line width (FWHM), $\Delta\nu_G$ is the Gaussian line width (FWHM), BG is the background in the spectrum, ISF is an intensity scaling factor, and IGR is the intensity gradient defined in Eq 7 12 See text for further details*

distribution was also used by Price *et al* [46] for simulation of the excitation spectrum of jet-cooled acetaldehyde The results for indole, indazole and benzimidazole are given in Table 7 2 (model 5)

The first two-temperature distribution (Eq 7 11) describes the experimental spectrum better than the second one, since the χ^2 values for model 2 and 3 are always better than those for model 5 (Table 7 2) The values of the temperatures T_J and T_K are very close to each other for all three molecules This indicates that the distribution given by Eq 7 13 is close to a Boltzmann distribution Therefore, the lowering of χ^2 when comparing models 1 and 5 can mainly be attributed to the introduction of the axis reorientation angle θ_T Theoretically, the results for θ and θ_T should not depend much on the choice of the temperature model, since the hybrid character and axis reorientation are effective on all rotational levels From Table 7 2, it is seen that the results for a single spectrum (model 3, 4, and 5) are in reasonable agreement

In all aforementioned models, a Lorentzian line profile was assumed This is a reasonable assumption since the rotational lines in the spectra are homogeneously broadened due to a finite life time The FWHM of single rotational lines can be directly obtained from the spectra The results are 22(1) MHz for indole, 35(2) MHz for indazole, and 21(1) MHz for benzimidazole These values are slightly higher than the values reported in Table 7 2 The instrumental linewidth is about 15 MHz, and in mainly a result of residual Doppler broadening This instrumental line profile can be best approximated with a Gaussian profile Therefore, the line shapes of the individual rotational lines are better described by a Voigt profile The question arises if the results for the hybrid character and the axis reorientation angle depend on the chosen line profile Therefore, we have fit the spectra using a Gaussian line profile (model 6), and a Voigt profile (model 7) The results are shown in Table 7 2 As expected, the Voigt profile improves the fit (lower χ^2 and better residual spectrum) The pure Gaussian profile describes the spectra worse than the pure Lorentzian profile, probably because the typical Lorentzian wings are absent From the comparison of the values for θ and θ_T, it is concluded that the values for these angles are rather independent of the choice of the line profile

More generally, although the intensity shape of a spectrum is determined by the direction of the transition moment vector, the axis reorientation effect, the rotational population distribution, and the line profile of the rotational lines, it is possible to extract accurate information about the transition moment and the axis reorientation, without knowing the actual state distribution and line profile. The final values of θ and θ_T presented in Table 7.1 were obtained by averaging the results for model 7.

Since our intensity analysis of a particular spectrum is based on the results of the frequency analysis of the same spectrum, it is important to consider how small variations of the fixed rotational constants influence the results of the contour fitting (in particular θ and θ_T). Therefore, we have fit the intensities of the second spectrum of indole (Table 7.2) for different sets of rotational constants. These rotational constants were varied within their errors. In the worst case, the relative changes in θ and θ_T were only 0.1% and 5% respectively.

In Figure 7.5 portions of the P and R branches of indazole are shown to illustrate the effects of axis reorientation on the intensities of individual rotational lines. A simulation of both portions obtained by using the values of θ and θ_T of Table 7.1, is shown in the second row of Fig. 7.5. The transitions originating from the ground states (8,0,8) and (8,1,8) are labeled. Temperature effects on the intensities are for these lines unimportant since both lines are nearly isoenergetic. The third row of Fig. 7.5 shows a simulation obtained by fitting the intensities of the P branch lines, while neglecting axis reorientation ($\theta_T=0$). A hybrid angle of 67.2° describes the P branch lines good, but the agreement with the experimental lines in the R branch is very poor (now, the lines labelled with ♠ and ♣ are pure b-type lines, while the lines labelled with ♡ and ◇ are pure a-type lines). In a similar way, the R branch intensities can be fit. Now, an angle of 56.0° gives good agreement in the R branch, but very poor agreement in the P branch. It should be noted that the quadruplets in Fig. 7.5 are not fully resolved.

The Gaussian contribution to the linewidth of benzimidazole (model 7) is equal to the expected instrumental linewidth ($\sim$15 MHz). The lifetime, obtained from the Lorentzian contribution, is then estimated to be 14±2 ns. The Gaussian contribution for indole and indazole (respectively, 17.1 and 17.6 MHz), are larger than expected. The lifetime of indole is known to be 17.6±0.1 ns [10]. This leads to a Lorentzian contribution of 9.0 MHz, which is slightly smaller than the experimental value of 10.5 MHz. Although speculave, the observed broadening of the rotational lines of indole and indazole may be caused by unresolved hyperfine splitting. Hyperfine splitting has been observed in the microwave spectra of indole [16] and pyrazole [47].

7.5 Discussion

From the well resolved rotational spectra, accurate values for the directions of the transition moment vectors of indole, indazole, and benzimidazole have been obtained. For indole, the results of the present study can be compared with results from earlier studies, which did not take axis reorientation into account. Philips and Levy [15] measured the fluorescence excitation spectrum of indole in a supersonic jet at a resolution of 180 MHz. Their best fit to the spectrum was produced with equal mixtures of a- and b-type spectra, resulting in a $|\theta|$ of 45°±5°. This value is slightly higher than our value, 38.3°±0.2°. Mani and Lombardi [14] analyzed the absorption spectrum at room temperature at a resolution of 0.05 cm^{-1}. Although they obtained a best fit with a 70% a-type and 30% b-type transition ($|\theta| = 33$°), they reported a hybrid character of 80% a-type and 20% b-type ($|\theta| = 27$°), since they thought that the b-type character was overestimated as a result of neglecting $J > 80$ (limited computer memory). However, Philips and Levy have shown that
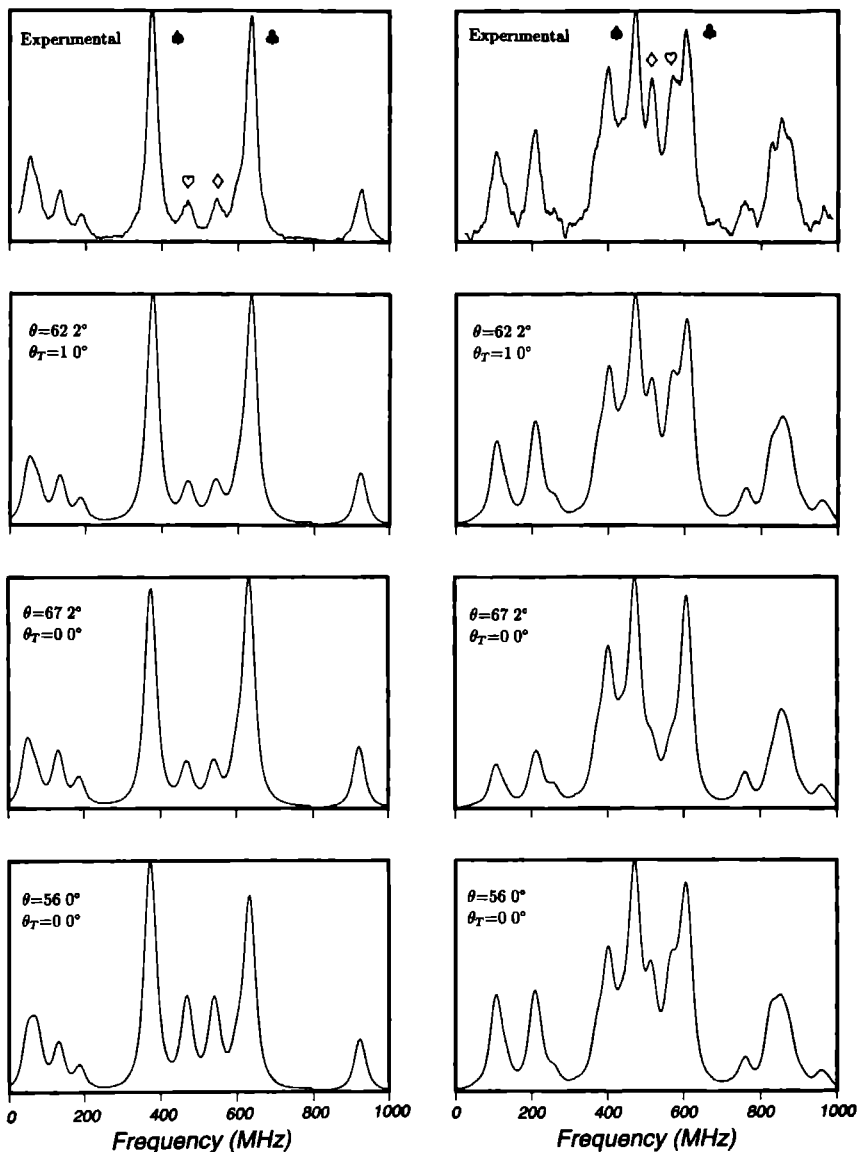
Figure 7.5: *Portions of the P branch (left column) and R branch (right column) of indazole Top row experimental parts, horizontal scales are relative Four transitions in each branch are labelled P branch ♠=(7,0,7) ← (8,1,8), ♡=(7,0,7) ← (8,0,8), ◇=(7,1,7) ← (8,1,8), ♣=(7,1,7) ← (8,0,8) R branch ♠=(9,0,9) ← (8,1,8), ◇=(9,1,9) ← (8,1,8), ♡=(9,0,9) ← (8,0,8), ♣=(9,1,9) ← (8,0,8) Second row simulations using the constants from Table 7 1 Third row results of the intensity fit of the P branch without axis reorientation ($\theta_T=0$) Last row results of the intensity fit of the R branch without axis reorientation*

105

this was not the case, and concluded that a value of 33° is the better one [15]. Comparing the θ values obtained from the fits with models 2, and 3 (Table 7.2), shows that approximately the same values are found. Therefore, intensity analysis of the *total* spectrum, with or without taking axis reorientation into account, should give the same values for θ. However, both Philips and Levy [15], and Mani and Lombardi [14] used only part of the spectrum to determine the hybrid character. This explains the deviations in the values for the direction of the transition moment vector of indole.

From Eq. 7.10, it is seen that only the absolute value of θ can be determined, and not its sign. Therefore, two directions for the transition moment vector are possible: $+38.3°$ and $-38.3°$. In tryptamine, the a-axis is rotated away from the nitrogen atom in the indole chromophore. Philips and Levy [48] analyzed the rotational band contour of jet-cooled tryptamine, and concluded that the transition moment vector is located at 59° with respect to the indole a-axis. Since the substitution of the ethylamine group causes only a small perturbation in the direction of the transition moment, they concluded that the plus sign should be taken for the angle θ of indole [48]. Therefore, we conclude that $\theta = +38.3°$. The plus sign for indole is consistent with theoretical results of Callis [49]. The values of θ, calculated by different methods, are in the range of $+32°$ to $+76°$. Because the axis reorientation angle θ_T has the same sign as θ (see Table 7.1), it follows immediately that $\theta_T = +0.50°$.

For indazole, the results of the earlier study from Cané *et al.* [21] are in disagreement with the results of present study. From the results of a computer simulation of the rotational band contour of the origin band (measured at a temperature of ca. 55°), they obtained $\theta = \pm 42°$. This value is much lower than our value, $\theta = \pm 62.2°$, and the question arises why the values are so different. The main reason is that Cané *et al.* did not take the axis reorientation effect into account. The hybrid character of their spectrum was determined by comparing the intensities of two sharp, unstructured features [21]. One of those features can be attributed to the ^rR branches ($\Delta J = +1, \Delta K_a = +1$) of the b-type band. The other feature contains both a-type and b-type transitions. We have simulated both features twice with two different sets of θ and θ_T values: namely, $\theta = 42°$ with $\theta_T = 0°$, and $\theta = 62.2°$ with $\theta_T = 1.0°$. Both simulations give approximately the same intensity ratios for the two features. Apparently, neglecting axis reorientation underestimates the value of θ.

The same group analyzed the rotational band contour of benzimidazole [25]. For the direction of the transition moment, a value for θ of $\pm 18°$ was found. Although axis reorientation was not taken into account, this value is remarkable close to the value of present study, $\pm 22.0°$. Comparison of the band contours of benzimidazole [25] and indazole [21] shows that the 'pure b-type feature' in benzimidazole is less pronounced than in the indazole contour. Therefore, Cané *et al.* have determined the hybrid character of benzimidazole by examining the shape of the *total* band contour. This method gives more or less the same result as an analysis with axis reorientation (compare the results of models 2 and 3 in Table 7.2).

The rotational constants, given in Table 7.1, are directly related to the geometrical structures in the ground state and the electronically excited state. All three molecules have a highly constrained geometry. Therefore, our data give no surprising conclusions. The molecules are mainly planar, in both states, since their inertial defects are small (*i.e.* close to zero). The equilibrium structure of a molecule is exactly planar, if its inertial defect is exactly zero. However, zero-point vibrational motion contributes to the inertial defect as well, leading to a small negative value of the inertial defect, even if the equilibrium geometry of the molecule is exactly planar.

Upon electronic excitation to the ^1L_b state, the geometrical changes are similar in each molecule. The changes are small, and indicate a slight expansion of each molecule. These small geometrical changes are consistent with the results of vibrational spectroscopy. The fluorescence excitation spectra show intense 0_0^0 transitions and short Franck-Condon progressions. Only the 'ring breath-ing' modes (760 cm^{-1} for the S_0 state of indole [9]) form somewhat longer progressions (up to $v=3$) in the excitation and fluorescence spectra of indole [50] and benzimidazole [23], showing that the structural changes are mainly along these modes.

The rotational constants of indazole indicate that the transition at 34472 cm^{-1} takes place in the 1H-tautomer. The ground state constants are identical to the constants found by Velino *et al.* [20], who confirmed the 1H position *via* isotopic substitution. Since the differences between the rotational constants of the excited state and the ground state are similar to the differences in constants of indole and benzimidazole, we conclude that the indazole in the excited state is in the same form as in the ground state. These results are in agreement with those of Catalán *et al.* [26], who concluded from spectroscopic and thermodynamical data that indazole exists as the 1H-tautomer, both in the ground and excited state.

New information about structural changes upon electronic excitation, is provided by the axis reorientation effect. Rotational constants, obtained from a frequency analysis of the rotational resolved fluorescence excitation spectrum, contain information about the geometry in both states. The ground state rotational constants can provide structural information with respect to the principal axis system in the ground state, while the excited state constants can provide the excited state structure with respect to the principal axis system of the excited state. However, there is no information in the rotational constants about how both principal axis systems are oriented with respect to each other. This information, the axis reorientation angle(s), can be obtained from the intensities of the rotational lines. The axis reorientation angles of indole, indazole, and benzimidazole are small; respectively, $\pm 0.50°$, $\pm 1.0°$, and $\pm 0.7°$ (however, the effect on the intensities, and therefore on the determination of the direction of the transition moment, is quite large).

The sign of the axis reorientation angle θ_T is related directly to the sign of the angle between the transition moment vector and the a-axis, θ (see Table 7.1). Therefore, if the direction of the transition moment is known, for example by comparing θ of substituted and unsubstituted molecules, this will give immediately the sign of θ_T (and *vice versa*). For indole the sign of θ is positive, and therefore θ_T is positive: $+0.5°$. Since the axis reorientation angles of indole, indazole, and benzimidazole are rather small, it is difficult to determine which atomic displacements are responsible for the rotation of the inertial axes.

The rotational constants in the ground and in the electronically excited states, and the axis reorientation angles presented in this chapter, can be used for testing *ab initio* calculations and for improving semi-empirical calculations of both electronic states. As an example, the experimental constants of indole are compared with the results from *ab initio* calculations of Slater and Callis [51]. Table 7.4 shows the experimental (first column) and calculated rotational constants. The rotational constants in the second column, have been calculated from the geometries obtained by using the 3-21G basis set for the ground state and the ^1L_b state (however, the excited state involves single configuration interaction). The ground state constants in the last column have been calculated from the optimized geometry from a MP2/6-31G* calculation. This level gives the best agreement with the vibrational frequencies in the ground state (without scaling) [51]. The excited state geometry, used to calculate the differences in the rotational constants (last column of Table 7.4),

Rotational Constants of Indole in MHz			
	experimental	3-21G	MP2/6-31G* & 3-21G
A''	3877.8	3950.0	3871.4
B''	1636.0	1648.3	1636.2
C''	1150.9	1163.0	1150.1
ΔA	−134.8	−142.3	−138.7
ΔB	−17.9	−13.8	−13.6
ΔC	−20.7	−19.4	−19.1
θ_T	+0.5°	+0.8°	+0.8°

Table 7.4: *Experimental and calculated rotational constants and axis reorientation angles (θ_T) of indole. Calculated constants have been obtained from ab initio geometries [51, 52]. See text for further details.*

has been calculated using the MP2/6-31G* ground state with the geometry differences from the 3-21G geometries. The same method has been used by Callis, Slater, and Vivian [52] to calculate the fluorescence spectrum from the ^1L_b origin which is in good agreement with the experimental spectrum.

7.6   Summary

We have measured the rotationally resolved spectra of the origin bands of the $S_1(^1L_b) \leftarrow S_0$ transitions of indole, indazole, and benzimidazole. From a frequency analysis of these spectra, the rotational constants in the ground and electronically excited states, have been obtained. All three molecules are planar in both states. Upon electronic excitation the molecules expand slightly. The intensities of the rotational lines are 'perturbed' due to a in-plane reorientation of the a and b inertial axes upon electronic excitation. The intensities of the rotational lines are determined by the ground state population distribution ('the rotational temperature'), the hybrid band character, and the axis reorientation effect. The hybrid band character is related to the direction of the electronic transition moment vector with respect to the inertial axes. The intensity shapes of the spectra have been fit using various models (Table 7.3). The best results have been obtained using a 3 parameter two-temperature rotational state distribution (non-Boltzmann), effects of inertial axes reorientation, and a Voigt line profile for each rotational transition. The axis reorientation angle θ_T provides information about structural changes upon electronic excitation, which is additional to that obtained from the changes in the rotational constants. The data presented in this study, can be compared with results from *ab initio* and semi-empirical calculations for the ground state and the excited state (^1L_b state). In this way, these calculations can be improved to predict the properties of the second excited state, the ^1L_a state, more precisely.

Acknowledgements

References

1. H.-U. Schütt and H. Zimmermann, Ber. Bunsenges. Phys. Chem. **67** (1963) 54

2. J.R. Platt, J. Chem. Phys. **19** (1951) 101

3. Y. Nibu, H. Abe, N. Mikami and M. Ito, J. Phys. Chem. **87** (1983) 3898

4. J.W. Hager and S.C. Wallace, J. Phys. Chem. **87** (1983) 2121

5. R. Bersohn, U. Even and J. Jortner, J. Chem. Phys. **80** (1984) 1050

6. See, for example, H. Lami and N. Glasser, J. Chem. Phys. **84** (1986) 597

7. See, for example, A.A. Rehms and P.R. Callis, Chem. Phys. Lett. **140** (1987) 83

8. D.M. Sammeth, S. Yan, L.H. Spangler and P.R. Callis, J. Phys. Chem. **94** (1990) 7340

9. T.L.O. Barstis, L.I. Grace, T.M. Dunn and D.M. Lubman, J. Phys. Chem. **97** (1993) 5820

10. S. Arnold and M. Sulkes, J. Phys. Chem. **96** (1992) 4768, and references therein.

11. M.J. Tubergen and D.H. Levy, J. Phys. Chem. **95** (1991) 2175

12. P.L. Muiño and P.R. Callis, Chem. Phys. Lett. **222** (1994) 156

13. M.R. Eftink, L.A. Selvidge, P.R. Callis and A.A. Rehms, J. Phys. Chem. **94** (1990) 3469

14. A. Mani and J.R. Lombardi, J. Mol. Spectrosc. **31** (1969) 308

15. L.A. Philips and D.H. Levy, J. Chem. Phys. **85** (1986) 1327

16. R.D. Suenram, F.J. Lovas and G.T. Fraser, J. Mol. Spectrosc. **127** (1988) 472

17. W. Caminati and S. di Bernando, J. Mol. Struct. **240** (1990) 253

18. E. Cané, P. Palmieri, R. Tarroni and A. Trombetti, J. Chem. Soc. Faraday Trans. **89** (1993) 4005

19. J.P. Byrne and I.G. Ross, Aust. J. Chem. **24** (1971) 1107

20. B. Velino, E. Cané and A. Trombetti, J. Mol. Spectrosc. **155** (1992) 1

21. E. Cané, A. Trombetti, B. Velino and W. Caminati, J. Mol. Spectrosc. **155** (1992) 307

22. R.D. Gordon and R.F. Yang, Can. J. Chem. **48** (1970) 1722

23. E. Jalviste and A. Treshchalov, Chem. Phys. **172** (1993) 325

24. B. Velino, A. Trombetti and E. Cané, J. Mol. Spectrosc. **152** (1992) 434

25. E. Cané, A. Trombetti, B. Velino and W. Caminati, J. Mol. Spectrosc. **150** (1991) 222

26. J. Catalán, J.C. del Valle, R.M. Claramunt, G. Boyer, J. Laynez, J. Gómez, P. Jiménez, F. Tomás and J. Elguero, J. Phys. Chem. **98** (1994) 10606

27. G. Berden, E. Jalviste and W.L. Meerts, Chem. Phys. Lett. **226** (1994) 305

28. B. Velino, E. Cané, L. Gagliardi, A. Trombetti, W. Caminati, J. Mol. Spectrosc. **161** (1993) 136

29. W. Caminati, private communication.

30. F. Tomas, J. Catalán, P. Pérez and J. Elguero, J. Org. Chem. **59** (1994) 2799

31. J. Catalán, P. Pérez and J. Elguero, J. Org. Chem. **58** (1993) 5276

32. J.T. Hougen and J.K.G. Watson, Can. J. Phys. **43** (1965) 298

33. T.R. Huet, M. Godefroid and M. Herman, J. Mol. Spectrosc. **144** (1990) 32

34. D.M. Jonas, X. Yang and A.M. Wodtke, J. Chem. Phys. **97** (1992) 2284

35. R.E. Smalley, L. Wharton, D.H. Levy and D.W. Chandler, J. Mol. Spectrosc. **66** (1977) 375

36. J.A. Konings, W.A. Majewski, Y. Matsumoto, D.W. Pratt and W.L. Meerts, J. Chem. Phys. **89** (1988) 1813

37. A. Held, B.B. Champagne and D.W. Pratt, J. Chem. Phys. **95** (1991) 8732

38. I. Özkan, J. Mol. Spectrosc. **139** (1990) 147

39. A.R. Chigirev, Optics and Spectroscopy **67** (1989) 175
    A.R. Chigirev, Optics and Spectroscopy **69** (1990) 192

40. W. Gordy and R.L. Cook, *Microwave Molecular Spectra*, 3rd Ed., John Wiley & Sons, New York (1984)

41. D.F. Plusquellic and D.W. Pratt, J. Chem. Phys. **97** (1992) 8970

42. S. Gerstenkorn and P. Luc, *Atlas du spectroscopie d'absorption de la molecule d'iode*, CNRS, Paris (1978)
    S. Gerstenkorn and P. Luc, Rev. Phys. Appl. **14** (1979) 791

43. S. Stolte, in *Atomic and molecular beam methods*, Volume 1, ed. by G. Scoles, New York (1988)

44. Y.R. Wu and D.II. Levy, J. Chem. Phys. **91** (1989) 5278

45. E.P. Peyroula and R. Jost, J. Mol. Spectrosc. **121** (1987) 167

46. J.M. Price, J.A. Mack, G.v. Helden, X. Yang and A.M. Wodtke, J. Phys. Chem. **98** (1994) 1791

47. G.L. Blackman, R.D. Brown, F.R. Burden and A. Mishra, J. Mol. Struct. **9** (1971) 465

48. L.A. Philips and D.H. Levy, J. Phys. Chem. **90** (1986) 4921

49. P.R. Callis, J. Chem. Phys. **95** (1991) 4230

50. G.A. Bickel, D.R. Demmer, E.A. Outhouse, S.C. Wallace, J. Chem. Phys. **91** (1989) 6013

51. L.S. Slater and P.R. Callis, J. Phys. Chem. (1995), in press.

52. P.R. Callis, L.S. Slater and J.T. Vivian, manuscript in preparation.

Chapter 8

High resolution UV spectroscopy of phenol and the hydrogen bonded phenol-water cluster

Giel Berden and W. Leo Meerts
Department of Molecular and Laser Physics, University of Nijmegen,
Toernooiveld, 6525 ED Nijmegen, The Netherlands

Michael Schmitt and Karl Kleinermanns
Inst. für Physikalische Chemie und Elektrochemie I, Heinrich-Heine Universität,
Universitätsstr. 26.43.02, 40225 Düsseldorf, Germany

Abstract

The $S_1 \leftarrow S_0$ 0_0^0 transitions of phenol and the hydrogen bonded phenol(H_2O)$_1$ cluster have been studied by high resolution fluorescence excitation spectroscopy. All lines in the monomer spectrum are split by 56±4 MHz due to the internal rotation of the –OH group about the a-axis. The barrier for this internal motion is determined in the ground and excited states; V_2''=1215 cm^{-1}, and V_2'=4710 cm^{-1}. The rotational constants for the monomer in the ground state are in agreement with those reported in microwave studies. The excited state rotational constants were found to be A'=5313.7 MHz, B'=2620.5 MHz, and C'=1756.08 MHz. The region of the redshifted 0_0^0 transition of phenol(H_2O)$_1$ shows two distinct bands which are 0.85 cm^{-1} apart. Their splitting arises from a torsional motion which interchanges the two equivalent H-atoms in the H_2O moiety of the cluster. This assignment was confirmed by spin statistical considerations. Both bands could be fit to rigid rotor Hamiltonians. Due to the interaction between the overall rotation of the entire cluster and the internal rotation, both bands have different rotational constants. They show that $V_2' < V_2''$, and that the internal rotation axis is nearly parallel to the a-axis of the cluster. If it is assumed that the structure of the rotor part does not change upon electronic excitation, the internal motion becomes simply a rotation of the water molecule around its symmetry axis. Assuming this motion, barriers of 180 cm^{-1} and 130 cm^{-1} could be estimated for the S_0 and S_1 states, respectively. The analysis of the rotational constants of the cluster yielded an O–O distance of the hydrogen bond of 2.93 Å in the ground state and 2.89 Å in the electronically excited state. In the equilibrium structure of the cluster, the plane containing phenol bisects the plane of the water molecule.

8.1 Introduction

High resolution laser spectroscopy in strongly collimated molecular beams is a powerful tool for the spectroscopic investigation of hydrogen bonded systems [1]. An important model system is the phenol$(H_2O)_1$ cluster, which has been studied extensively both experimentally and theoretically. In a preceding publication, the ground state geometry of the phenol$(H_2O)_1$ cluster has been determined by microwave (MW) spectroscopy in a molecular beam [2]. In this chapter the high resolution UV spectrum of the $S_1 \leftarrow S_0$ transition of phenol$(H_2O)_1$ is presented.

8.1.1 Phenol

An interpretation of cluster spectra has to be preceded by a careful examination of the monomer properties. The ground state rotational constants of phenol and the barrier to internal rotation of the hydroxyl group have been determined by microwave spectroscopy [3, 4, 5]. The complete substitution structure has been determined by Larsen [6]. A vibrational analysis of phenol was performed by Bist et $al.$ [7, 8, 9] using IR and UV-VIS spectroscopy, and by Wilson et $al.$ [10] using Raman spectroscopy. The former authors applied the Longuet-Higgins concept of molecular symmetry groups [11] to the phenol molecule. Their group theoretical considerations led to a classification of intramolecular vibrations of phenol under the molecular symmetry group (MS) G_4, which is isomorphic with the point group C_{2v}. The vibrational structure of the electronic ground state of phenol has been studied theoretically at the Hartree-Fock 4-31G and 6-31G** levels [12]. Force field calculations, based on the results of multiphoton ionization photoelectron studies of phenol, yielded vibrational frequencies for the $^2B_1$ cation [13]. Recently, the vibrational frequencies of the excited states (S_1 and T_1) of phenol have been evaluated at the complete active space multiconfiguration self consistent-field (CAS-MCSCF) level, using the 6-31G basis [14]. Kim and Jordan [15] have used many-body perturbation and quadratic configuration interaction calculations with several basis sets to estimate the height of the barrier for OH rotation. Their best estimate of the barrier height was 1076 cm^{-1}.

A rotational band contour analysis of the 275 nm system of phenol has been performed by Christoffersen et $al.$ [16], yielding a set of rotational constants for the ground and excited electronic states. A fully rotationally resolved spectrum of phenol was reported by Martinez et $al.$ [17]. From the experimental rotational parameters they obtained a geometry for both electronic states. With a resolution of 154 MHz, they were able to resolve single rovibronic transitions but could not resolve the torsional doubling. In this paper we report the fully resolved rotational spectrum of phenol obtained in a supersonic molecular beam. Although the linewidth of the spectrometer is only 14 MHz, broad (110 MHz) asymmetric rotational lines were observed due to the short lifetime in the S_1 state and an internal motion of the hydroxyl group.

8.1.2 Phenol/Water

The vibronic structure of the electronic ground state of phenol/water cluster has been studied by dispersed fluorescence spectroscopy (DF) [18], stimulated emission ion-dip spectroscopy (SEID) [19], ionization-loss stimulated Raman spectroscopy (ILSRS) [20] and IR-UV double resonance spectroscopy [21]. SEID is limited to a region several hundred wavenumbers above the electronic ground state 0_0, because it requires a fast relaxation from the examined vibrational levels. Intermolecular vibrations could only be observed as combination bands with higher frequency

intramolecular vibrations. Especially the C–O stretching vibration in the phenol moiety and O–H stretching vibrations in phenol and the water moiety have been investigated using ILSRS and IR-UV double resonance spectroscopy.

Laser induced fluorescence excitation spectra of the $S_1 \leftarrow S_0$ transition in the hydrogen bonded phenol$(H_2O)_1$ cluster have been recorded by Abe *et al.* [22, 23]. They assigned a vibration at 156 cm^{-1} to the stretching vibration and a band at 121 cm^{-1} to a not further specified S_1 intermolecular bending motion. Other spectral features could not be attributed to the n=1 cluster, specifically since the method lacks mass selectivity.

Mass selective spectra of phenol/water clusters with different sizes have been reported by Fuke *et al.* [24], Stanley *et al.* [25] and Lipert *et al.* [26], using resonance enhanced multi-photon ionisation (REMPI). The spectral shifts of these clusters were found to resemble those of the similar p-cresol$(H_2O)_n$ clusters [27]. The large red shift of phenol$(H_2O)_1$ relative to phenol (353 cm^{-1}) can be attributed to a change in inductive effect of the phenolic oxygen atom on the $\pi^* \leftarrow \pi$ transition, while the second water molecule reduces the inductive effect of the first, proton accepting water and causes a relative blue shift [28, 29]. The mass selectivity of REMPI even under 'soft' ionization conditions is limited by fragmentation of higher clusters, which often obscures the interpretation of the spectra. This problem can be avoided by the employment of spectral hole burning. The vibronic spectra of phenol$(H_2O)_2$ [30] and phenol$(H_2O)_3$ [31] have been measured cluster and state selectively by this method.

The S_1 life times of phenol and several phenol/water clusters have been measured using time resolved pump-probe photoionization spectroscopy. They were found to vary considerably with cluster size [32, 33, 34, 35]. A study of the sensitized phosphorescence spectra of phenol$(H_2O)_n$ clusters was performed by Goto *et al.* [36]. Significant phosphorescence was found when the n=3 and n=4 cluster origins were excited. The phenol$(H_2O)_1$ cation radical was investigated by Dopfer et al. [37, 38, 39] experimentally using zero-kinetic-energy photoelectron spectroscopy (ZEKE), and theoretically *via* an *ab initio* study by Hobza *et al.* [40]. They used the 0_0^0, the stretching and the in-plane wagging vibration as intermediate S_1 levels for obtaining ZEKE spectra and found a increase in vibrational frequencies in the cation compared to the S_1 state.

A very thorough theoretical and experimental study of the phenol$(H_2O)_1$ cluster was performed by Schütz *et al.* [18]. They compared the results of mass selective R2PI and dispersed fluorescence spectroscopy to a vibrational analysis of the cluster based on *ab initio* calculations. A band at 155 cm^{-1} in the electronic ground state was found to correspond to 156 cm^{-1} in the electronically excited state and was assigned to the intermolecular stretching vibration. Furthermore, a band at 146 cm^{-1} in the S_0 state (121 cm^{-1} in the S_1 state) was assigned as the totally symmetric in-plane wagging motion. In addition, some low frequency bands were attributed to a hindered internal motion in the cluster, a motion that exchanges the two equivalent H-atoms in the water moiety.

The assignment of the vibrations associated with this internal motion is difficult due to their low Franck-Condon activity. This indicates that there is no large conformational change along this coordinate when exciting the cluster. High resolution UV spectroscopy can give information about this internal motion since the torsional tunneling splitting can be measured directly. Additional information about the potential barrier of this motion is obtained from the rotational constants since these are perturbed by an interaction between the overall rotation of the molecule and the internal motion.

8.2 Theory

8.2.1 Internal rotation with a two-fold barrier

In this section the Hamiltonian will be derived which describes all spectral features in the high resolution spectra of phenol and phenol(H_2O)$_1$. Whenever the word 'molecule' is used, the reader should keep in mind that the theory describes a molecular complex as well. We assume that the entire molecule consists of two parts: a rigid rotor attached to a rigid frame. The two rigid parts rotate relative to each other, generating torsional level structure. Other modes of internal motion are ignored. Furthermore, the entire molecule rotates in space generating rotational level structure.

For the description of internal rotation, we use the principal axis method (PAM) [42]. In this method, the principal inertial axes of the whole molecule are used as reference coordinate system. The PAM has been developed for systems in which the rigid rotor part is a symmetric top (*e.g.* CH_3) and the axis of internal rotation coincides with the symmetry axis of this top. Because of the symmetry of the top, the principal axes and the moments of inertia of the entire molecule are not altered by the rotation of the top relative to the frame.

For bare phenol, the rotating −OH group is asymmetric with respect to the axis of internal rotation (*a*-axis of the molecule). However, the moment of inertia of the hydroxyl group about the internal rotation axis is very small compared to that of the C_6H_5-group. Therefore, the principal axes and moments of inertia of the whole molecule are only very slightly altered by the rotation of the hydroxyl group. Thus we can assume that the hydroxyl group is 'symmetric', and the PAM can be used. With analogous arguments, we assume that the water molecule in the phenol(H_2O)$_1$ cluster can be considered to behave as a 'symmetric' top.

It is further assumed that the coupling between the torsional motion and the overall rotation is small and can be treated by perturbation theory. The total Hamiltonian can then be divided into three parts [42]:

$$H = H_t + H_r + H_{tr} \tag{8.1}$$

The terms H_t and H_r are, respectively, the torsional and rotational part, and H_{tr} describes the coupling between the angular momenta of internal and overall rotation.

The torsional potential is assumed to be one-dimensional, depending only on the angle α describing the internal motion. This two-fold barrier potential $V(\alpha)$ can be expanded in a Fourier series. If the expansion is restricted to the lowest order term, the torsional Hamiltonian is given by:

$$H_t = Fp^2 + \frac{V_2}{2}(1 - \cos 2\alpha) \tag{8.2}$$

where

$$F = \hbar^2/2\gamma I_\alpha \tag{8.3}$$

and

$$\gamma = 1 - \sum_g \lambda_g^2 I_\alpha/I_g. \tag{8.4}$$

In these expressions, V_2 is the barrier height of the two-fold potential along the torsional coordinate, and p is the total angular momentum of the internal rotor about the axis of rotation ($p = -\imath\hbar\partial/\partial\alpha$). F depends on the geometry of the system; I_α is the moment of inertia of the rotor about the rotation axis, λ_g are the direction cosines for the orientation of the rotation axis with respect to the principal axes ($g = a, b, c$), and I_g are the principal moments of inertia of the entire molecule.

Solving the eigenvalue problem associated with H_t gives the energy eigenvalues $E_{\nu\sigma}$. Each torsional level ν consists of two sublevels ($\sigma = 0, 1$), whose degeneracy is removed by tunneling through the two-fold barrier. The eigenfunctions can be expressed in terms of the free rotor basis functions $e^{im\alpha}$:

$$|\nu, \sigma\rangle = \sum_{k=-\infty}^{\infty} A_k^{(\nu)} e^{i(2k+\sigma)\alpha} \tag{8.5}$$

The rigid rotor Hamiltonian H_r is given by:

$$H_r = AP_a^2 + BP_b^2 + CP_c^2 \tag{8.6}$$

where $A = \hbar^2/2I_a$, etc. and P_g are the components of the total angular momentum along the principal axes. The torsional Hamiltonian has been treated by perturbation theory up to second order. If $W_{\nu\sigma}^{(1)}$ and $W_{\nu\sigma}^{(2)}$ are the first- and second-order perturbation coefficients, H_{tr} can be written as [42]:

$$H_{tr}^{\nu\sigma} = FW_{\nu\sigma}^{(1)}(\rho_a P_a + \rho_b P_b + \rho_c P_c) + FW_{\nu\sigma}^{(2)}(\rho_a P_a + \rho_b P_b + \rho_c P_c)^2 \tag{8.7}$$

with $\rho_g = \lambda_g I_\alpha/I_g$. ν labels the torsional state, and σ labels the subtorsional level. The W coefficients depend on the ratio V_2/F and are given by:

$$W_{\nu\sigma}^{(1)} = -2\langle\nu, \sigma|p|\nu, \sigma\rangle \tag{8.8}$$

$$W_{\nu\sigma}^{(2)} = 1 + 4F \sum_{\nu'} \frac{|\langle\nu, \sigma|p|\nu', \sigma\rangle|^2}{E_{\nu\sigma} - E_{\nu'\sigma}} \tag{8.9}$$

in which $E_{\nu\sigma}$ are the energy eigenvalues and $|\nu, \sigma\rangle$ are the eigenfunctions of the pure torsional Hamiltonian (Eq. 8.2). Since the $W_{\nu\sigma}^{(1)}$ coefficients are zero for nondegenerate states, the terms linear in P_g disappear in Eq. (8.7). After separation of the terms in Eq. (8.1), H_r and H_{tr} can be combined to give an effective rotational Hamiltonian:

$$\begin{aligned} H_{eff}^{\nu\sigma} &= H_r + H_{tr}^{\nu\sigma} \\ &= AP_a^2 + BP_b^2 + CP_c^2 + FW_{\nu\sigma}^{(2)}(\rho_a^2 P_a^2 + \rho_b^2 P_b^2 + \rho_c^2 P_c^2) \\ &\quad + FW_{\nu\sigma}^{(2)}(2\rho_a\rho_b P_a P_b + 2\rho_a\rho_c P_a P_c + 2\rho_b\rho_c P_b P_c) \end{aligned} \tag{8.10}$$

The last term containing the cross terms can be neglected since its effect on the energy level spacings is small. The first and second three terms can then be combined to give:

$$H_{eff}^{\nu\sigma} = A_{\nu\sigma}P_a^2 + B_{\nu\sigma}P_b^2 + C_{\nu\sigma}P_c^2 \tag{8.11}$$

where

$$\begin{aligned} A_{\nu\sigma} &= A + FW_{\nu\sigma}^{(2)}\rho_a^2 \tag{8.12} \\ B_{\nu\sigma} &= B + FW_{\nu\sigma}^{(2)}\rho_b^2 \tag{8.13} \\ C_{\nu\sigma} &= C + FW_{\nu\sigma}^{(2)}\rho_c^2 \tag{8.14} \end{aligned}$$

The result for a given (ν,σ) state is an effective rigid rotor Hamiltonian with effective rotational constants depending on the particular state. The total energy of a torsional-rotational level is then given by the sum of $E_{\nu\sigma}$ and the eigenvalues of the effective rigid rotor Hamiltonian:

$$E(\nu, \sigma, J, K_a, K_c) = E_{\nu\sigma} + E_{eff}^{\nu\sigma}(J, K_a, K_c) \tag{8.15}$$
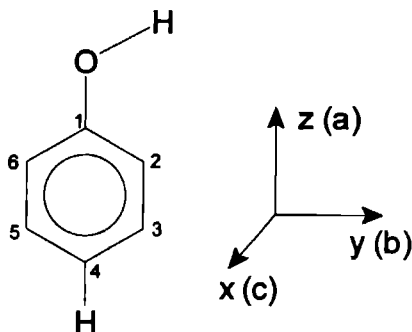
Figure 8.1: *Definition of structural parameters and axis convention for phenol.*

We will now consider the effects of the torsional motion on the observed optical spectra. First of all, because of the use of a jet expansion, only the two subtorsional levels $\sigma = 0$ and $\sigma = 1$ in the lowest torsional state $\nu = 0$ are populated. If the molecules are excited to the origin of the first electronically excited state, the spectrum will consist of two bands ($\sigma' = 0 \leftarrow \sigma'' = 0$ and $\sigma' = 1 \leftarrow \sigma'' = 1$, see section 8.2.2) separated by $\Delta E = (E'_{01} - E''_{01}) - (E'_{00} - E''_{00})$. Both bands have different effective rotational constants given by Eqs. (8.12-8.14). Information about the barrier height V_2 and the geometry of the internal rotor F in the ground and excited states can be derived from the energy difference ΔE and the effective rotational constants.

8.2.2 Application of the molecular symmetry group G_4 to phenol

The hydroxyl group of phenol undergoes an internal torsional motion relative to the phenyl group. The molecular symmetry (MS) group which takes this motion into account is G_4. This group consists of four elements; the identity operator E, the permutation operator P=(26)(35) which exchanges the identical nuclei (see Fig. 8.1), the inversion operator E* of the spatial coordinates of the entire molecule through its center of mass, and finally, the permutation inversion operator P*=PE*. Table 8.1 gives the character table of G_4, while Figure 8.1 shows our axis conventions.

For phenol the total wave function must have even parity for the exchange of two pairs of equivalent protons at the aromatic ring. The overall wave function must therefore transform as A_1 or A_2:

$$\Gamma_{tot} = \Gamma_e \otimes \Gamma_v \otimes \Gamma_t \otimes \Gamma_r \otimes \Gamma_{ns} \subset A_1, A_2 \tag{8.16}$$

In a supersonic molecular beam, the molecules are in the lowest vibrational level of the electronic ground state, thus $\Gamma_e = A_1$ and $\Gamma_v = A_1$. In the following, the characters of the torsional states (Γ_t), the rotational states (Γ_r) and the nuclear spin functions (Γ_{ns}) will be determined.

The symmetry properties of the torsional wave functions (Eq. 8.5) depend on the effects of the elements of G_4 on the torsional angle α. This angle can be defined using the Euler angles of the frame (θ_f, ϕ_f, χ_f) and the rotor (θ_r, ϕ_r, χ_r). The frame fixed axis system is chosen parallel to the principal axes of phenol as shown in Fig. 8.1. The rotor fixed axis system is chosen such that the z-axis coincides with that of the frame. Thus $\theta_f = \theta_r = \theta$ and $\phi_f = \phi_r = \phi$. The torsional angle α is defined as $\alpha = \chi_r - \chi_f$.

Character table G_4				
	E	P	E*	P*
A_1	1	1	1	1	z
A_2	1	1	-1	-1	
B_1	1	-1	-1	1	x
B_2	1	-1	1	-1	y

Table 8.1: *Character table for the molecular symmetry group G_4.*

The effects of the elements of G_4 on the Euler angles can be determined by replacing each element of G_4 by its equivalent rotation [43]. The operation P corresponds to a rotation by π about the a-axis (z-axis) of the frame, but it does not alter the rotor. E* corresponds to a rotation by π around the c-axis (x), and P* corresponds to a rotation by π around the b-axis (y). The effects of these rotations on the Euler angles are given by Bunker [43] and are summarized in Table 8.2.

The application of G_4 to the torsional wave functions will first be described in the free rotor limit ($V_2 = 0$). The wave functions in this limit are given by $|\psi_m\rangle^\pm \propto (e^{im\alpha} \pm e^{-im\alpha})$ and the energy by $E_m \propto m^2$. Using the effects of the elements of G_4 on α (Table 8.2) gives the characters for different m: $\Gamma(m = 0) = A_1$, $\Gamma(m = even) = A_1 + A_2$ and $\Gamma(m = odd) = B_1 + B_2$. All levels with $|m| > 0$ are doubly degenerate.

In the high barrier limit ($V_2 = \infty$) the torsional wave functions can be written as sums or differences of harmonic oscillator wave functions 'centered' at the two equilibrium positions of the hydroxyl rotor (0 and π): $|\psi_\nu\rangle^\pm \propto [H_\nu(\alpha) \pm H_\nu(\alpha + \pi)]$. The effects of the elements of G_4 on the wave functions are clear, since: $H_\nu(-\alpha) = (-)^\nu H_\nu(\alpha)$. The results are: $\Gamma(\nu = even) = A_1 + B_2$ and $\Gamma(\nu = odd) = A_2 + B_1$.

Figure 8.2 shows the correlation diagram between the two limiting cases. The symmetry for states with a barrier $0 < V_2 < \infty$ can be obtained using the non-crossing rule. Applying G_4 to the torsional wave function $|\nu, \sigma\rangle$ (Eq. 8.5) shows that the $\sigma = 0$ states are of A_1 or A_2 symmetry while the $\sigma = 1$ states are of B_1 or B_2 symmetry. In the supersonic molecular beam, only the

E	P	E*	P*
θ	θ	$\pi - \theta$	$\pi - \theta$
ϕ	ϕ	$\pi + \phi$	$\pi + \phi$
χ_f	$\pi + \chi_f$	$-\chi_f$	$\pi - \chi_f$
χ_r	χ_r	$-\chi_r$	$-\chi_r$
α	$\alpha - \pi$	$-\alpha$	$-\alpha - \pi$

Table 8.2: *Transformation properties of the Euler angles and the internal rotation angle α under the elements of G_4. α is defined as $\alpha = \chi_r - \chi_f$.*
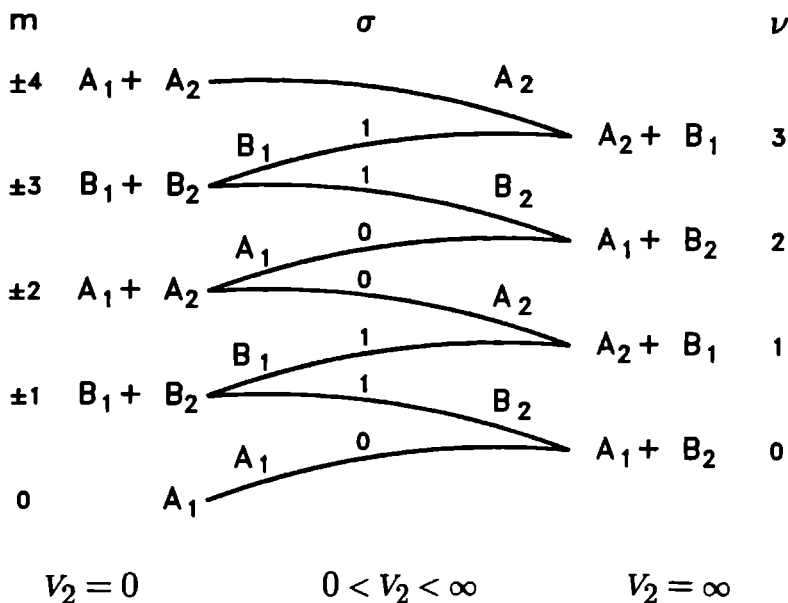
Figure 8.2: *Correlation between the energy levels of a free rotor (V_2=0) and those of a harmonic oscillator ($V_2 = \infty$). The quantum numbers labeling the double degenerate energy levels in these extreme barriers are m and ν, respectively. For intermediate barriers this degeneracy is removed. The levels are then labeled with ν and σ. For each level the symmetry is given under the molecular symmetry group G_4.*

$\nu = 0$ levels are populated. Obviously, the lowest state ($\nu = 0, \sigma = 0$) is of A_1 symmetry. The other subtorsional state ($\nu = 0, \sigma = 1$) is of B_2 symmetry.

For an asymmetric top molecule the rotational eigenfunctions are linear combinations of symmetric top functions which depend on the Euler angles. Since the transformation properties of the Euler angles are known (Table 8.2), we can determine the characters of the rotational eigenfunctions. However, an easier way to determine the characters is the use of the isomorphism between G_4 and $V(a,b,c)$. This latter group, the so-called Four-group [42], is used to classify asymmetric rotor wave functions in regard to their symmetry with respect to the principal axes of the molecule. The transformation properties of these asymmetric rotor functions under G_4 can be obtained directly from the Four group, since the G_4 elements can be replaced by equivalent rotations around the principal axes. The results are $\Gamma(K_a K_c = ee) = A_1$, $\Gamma(eo) = A_2$, $\Gamma(oo) = B_1$ and $\Gamma(oe) = B_2$.

The torsion of the –OH group generates two pairs of equivalent protons on the aromatic ring. The 16 (2^4) possible spin functions transform under the symmetry operations of G_4 as $10A_1 + 6B_2$ (Γ_{ns}). From Eq. (8.16) it is clear that the statistical weights affect the relative intensities of different torsional-rotational transitions (the hyperfine sublevels are assumed to be degenerate). Transitions starting from ($\sigma = 0$, K_a =even) or ($\sigma = 1$, K_a =odd) have a statistical weight of 10, while transitions starting from ($\sigma = 0$, K_a =odd) or ($\sigma = 1$, K_a =even) have a statistical weight of 6.

8.2.3 Application of the molecular symmetry group G_2 to phenol$(H_2O)_1$

The water moiety in phenol$(H_2O)_1$ undergoes an internal motion which interchanges the two equivalent hydrogen atoms of the water molecule. The molecular symmetry group which takes this motion into account is G_2 (isomorphic with the molecular point group C_2 and C_s). G_2 consists of two elements; the identity operator E and the permutation operator P=(12) which exchanges the identical nuclei of the water molecule.

To determine the symmetry of the (sub)torsional levels, we have to consider the symmetry properties of the torsional basis fuctions under the elements of G_2. The identity E leaves the torsional angle α unaltered, while the permutation P changes α into $\alpha + \pi$. Application of G_2 to the free rotor and harmonic oscillator wave functions results in the same correlation diagram as shown in Fig. 8.2, but without the subscripts 1 and 2. Therefore, $(\nu = 0, \sigma = 0)$ is of A symmetry, while $(\nu = 0, \sigma = 1)$ is of B symmetry.

The total wave function is antisymmetric with respect to the permutation of the two hydrogen atoms, and therefore of B symmetry $(\Gamma_{tot} = B)$. The rotational wave functions are of A symmetry for all $K_a K_c$, since P does not affect the Euler angles $(\Gamma_r = A)$. The 4 (2^2) spin functions transform as $3A + B$ (Γ_{ns}). Since $\Gamma_e = A$, $\Gamma_v = A$, and $\Gamma_t(\nu = 0, \sigma = 0) = A$ while $\Gamma_t(\nu = 0, \sigma = 1) = B$, it is clear that the statistical weights affect the relative intensities of different torsional transitions. Transitions arising from $\sigma=0$ have a statistical weight of 1, while transitions arising from $\sigma=1$ have a statistical weight of 3.

8.3 Experimental

High resolution LIF spectra of phenol and phenol$(H_2O)_1$ have been recorded by using a narrow bandwidth UV laser in combination with the molecular beam apparatus described in Chapter 1. In the case of bare phenol, a molecular beam was formed by passing 0.5 bar argon over a heated sample of phenol (70 °C) and expanding this mixture through a nozzle with a diameter of 75 μm. The nozzle was kept at a slightly higher temperature to prevent condensation of phenol in the orifice. The molecular beam was skimmed twice in a differential pumping system and was crossed perpendicularly with a UV laser beam at about 30 cm from the nozzle.

A molecular beam containing phenol/water clusters was formed by passing 0.5 bar argon over a water sample kept at −10 °C and subsequently by passing this mixture over phenol which was kept at 50 °C. This mixture of phenol, water and argon resulted in the strongest LIF spectrum for the phenol$(H_2O)_1$ cluster.

UV radiation with a bandwidth of 3 MHz was generated by intracavity frequency doubling in a single mode ring dye laser operating on Rh110. By using a 2 mm thick Brewster cut BBO crystal, 0.2 mW of tunable radiation was obtained. For relative frequency calibration a temperature stabilized Fabry-Perot interferometer with a free spectral range of 75 MHz was used. For absolute frequency calibration, the iodine absorption spectrum [41] was recorded simultaneously. The total undispersed fluorescence was collected by two spherical mirrors and imaged on a photomultiplier which was connected to a photon counting system interfaced to a computer. The instrumental linewidth of our spectrometer is 14 MHz, and is mainly determined by residual Doppler broadening.
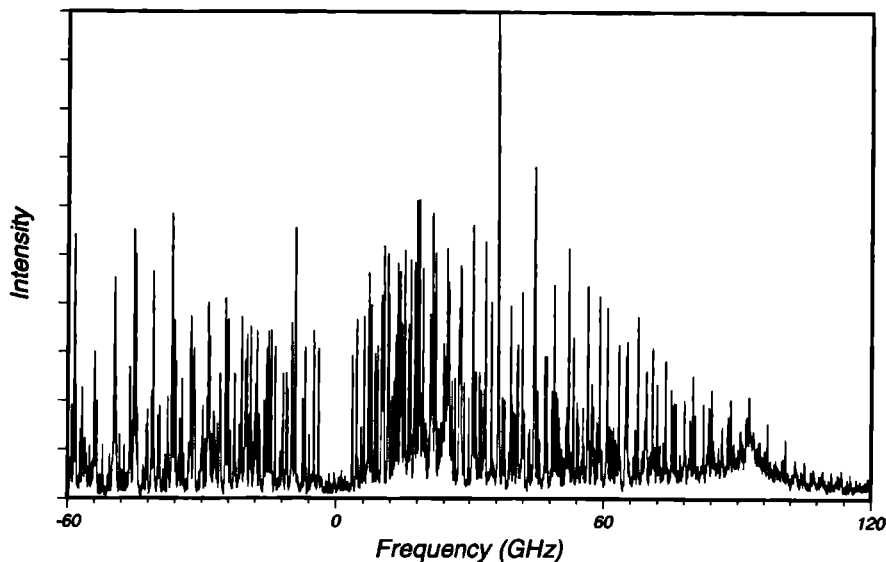
Figure 8.3: *High resolution LIF spectrum of the origin of the $S_1 \leftarrow S_0$ transition of phenol. The absolute frequency of the origin (0 on the scale of the figure) is at 36 348.71±0.01 cm^{-1}.*

8.4   Phenol

8.4.1   Results

The high resolution excitation spectrum of the electronic origin of the $S_1 \leftarrow S_0$ transition of phenol is shown in Figure 8.3. The absolute frequency of the band origin (0 on the scale of the figure) is 36 348.71±0.01 cm^{-1}. The spectrum, which can immediately be identified as a b-type band, consists of about 300 lines with a linewidth (FWHM) of roughly 110 MHz. The lineshape is asymmetric and the linewidth is larger than expected from lifetime measurements (the reported lifetime of phenol is 2 ns [33], which would give a Lorentzian contribution to the linewidth of about 80 MHz). These observations indicate that there is unresolved splitting of the lines.

In the b-type microwave spectrum of phenol, all lines were found to be doublets [3] due to the internal rotation of the hydroxyl group. The observed splittings are independent of the rotational transitions. The MW spectrum was fit to a rigid rotor Hamiltonian by using the center frequencies of the doublets. The obtained rotational constants were used as starting values for the rotational assignment of our UV spectrum.

A b-type spectrum was simulated using a rigid rotor Hamiltonian with the ground state constants from ref. [5] and the excited state constants from Martinez *et al.* [17]. The latter authors measured the spectrum in a jet with a resolution of 154 MHz. By comparing the simulation with the experimental spectrum, a unique assignment could be made. The center frequencies of the asymmetric lines were used as input for our fitting routine. All lines could be fit within their experimental error. The obtained ground state constants are within their errors equal to the micro-

Molecular Constants Phenol			
A''	5650 515(6)	A'	5313 6(2)
B''	2619 236(3)	B'	2620 5(1)
C''	1789 855(3)	C'	1756 10(4)
$\Delta I''$	−0 0309(5)	$\Delta I'$	−0 18(1)
Doublet splitting	56±4 MHz		
Band origin	36 348 71±0 01 cm^{-1}		

Table 8.3· *Molecular constants of phenol, the rotational constants A, B, and C (in MHz), and the inertial defect $\Delta I = I_c - I_b - I_c$ (in amu Å^2) in the electronic ground state and the first excited state Values for the ground state have been obtained by fitting the microwave data from Ref [5] The centrifugal distortion constants are in kHz $\Delta_J = 0\ 14(3)$, $\Delta_{JK} = 0\ 1(2)$, $\Delta_K = 0\ 9(1)$, $\delta_J = 0\ 03(1)$, and $\delta_K = 0\ 4(3)$ kHz Every rotational line is split by 56 MHz due to an internal motion in phenol*

wave constants [5] Because the microwave constants are two orders of magnitude more accurate than our constants, the UV data were fit again with the ground state constants constrained to the microwave values The results are shown in Table 8 3, listed are the rotational constants and the inertial defects in the ground and excited states It should be noted that the values reported by Martinez *et al* [17] differ considerably from both the MW and our UV results, *e g* their A'' value is 76 MHz larger than our value

As mentioned above, the lineshape of the UV lines is asymmetric Careful examination of the spectrum shows that this asymmetry depends on the parity of K_a, as shown in Figure 8 4 Due to internal rotation of the hydroxyl group, the appearance of doublets in the UV spectrum just as in the microwave spectrum is expected Spin statistical considerations predict a 10/6 intensity ratio For the lowest subtorsional level ($\sigma = 0$) in the electronic ground state, even K_a levels have statistical weights of 10 and odd K_a levels have statistical weights of 6, while the opposite holds for $\sigma = 1$ Thus, for K_a even the high-frequency component ($\sigma = 0$) of the doublet is stronger than the low-frequency component by a factor of 10/6, while for odd K_a the situation is reversed

The lineshapes have been fit using two lines with an intensity ratio of 10 6 and equal linewidths A Voigt line profile was taken with a fixed Gaussian contribution of 14 MHz (FWHM), which is the instrumental linewidth Within the experimental error, all lineshapes could be fit to this model The result is a doublet splitting of 56±4 MHz, and a Lorentzian linewidth of 67±8 MHz, both independent of the rotational transition The Lorentzian linewidth results in a lifetime of 2 4±0 3 ns, which is in agreement with the reported lifetime of 2±1 ns [33]

The overall shape of the UV spectrum can be simulated using b-type selection rules, the rotational constants of Table 8 3, a rotational temperature of 5 K, and the aforementioned doublet structure There is no experimental indication of hybrid band structure
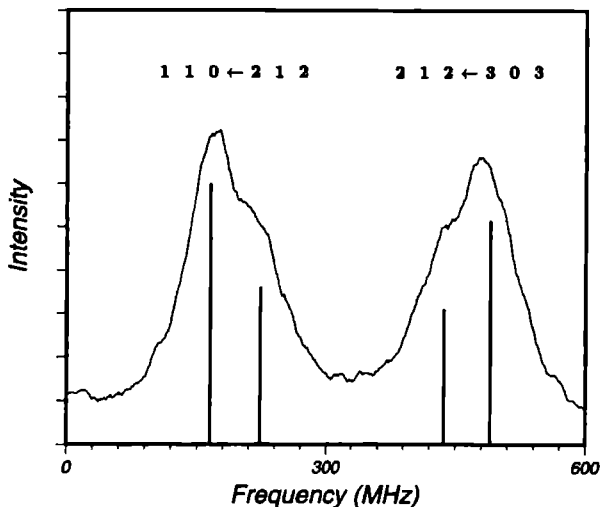
Figure 8.4: *Enlarged part of the high resolution LIF spectrum (Fig. 3), showing two rotational transitions with different parity for K_a''. The transitions are labeled $(J', K_a', K_c') \leftarrow (J'', K_a'', K_c'')$. The stick spectrum shows that each rotational line is split in two components with an intensity ratio of 10/6. The low frequency components originate from $\sigma{=}1$, while the high frequency components originate from $\sigma{=}0$. The subtorsional splitting is 56 MHz.*

8.4.2 Internal rotation and structure

The torsional level structure in the electronic ground state of phenol is well known [3, 4, 8]. The b-type microwave spectrum shows a doublet splitting of 112 MHz [3]. Since the selection rules in this case are $\Delta\sigma = \pm 1$, this leads to a splitting of 56 MHz between the subtorsional levels (see Figure 8.5). The torsional structure in the ground state has been determined by infrared and ultraviolet absorption spectroscopy up to $\nu{=}3$ [8, 9]. The pure torsional transition $\nu = 1 \leftarrow 0$ is reported at 309.6 cm^{-1} [8]. This value and the microwave splitting have been used to fit both V_2 and F to Eq. (8.2). The results are $V_2{=}1215{\pm}10$ cm^{-1} and $F{=}690{\pm}1$ GHz.

Since the doublet splitting in the UV spectrum is 56$\pm$4 MHz, and thus nearly equal to the subtorsional splitting in the electronic ground state, it should be concluded that the torsional splitting in the excited S_1 state is smaller than 4 MHz. This value gives a lower limit of 1700 cm^{-1} for the barrier assuming the same F value as in the S_0 state. From their assignment of the 2750 Å band system of phenol, Bist *et al.* [9] determined the value of the torsional vibration ($\nu' = 1 \leftarrow 0$) to be 634.7 cm^{-1}. With the same F value as used above, this gives a barrier of 4710$\pm$30 cm^{-1} (with a predicted subtorsional splitting smaller than 1 kHz). The barrier to internal rotation in the excited state is more than three times higher than in the ground state. This may be due to an increase in the double bond character of the C–O bond.

The structure of phenol in the S_0 state has been determined by Larsen [6]. All C–C distances are nearly equal (1.393 Å), as are the C–H distances (1.083 Å). The CCC angles at positions 1, 3, and 5 are 120.7°, and at 2, 6, and 4 are 119.3°. In the hydroxyl group, the oxygen and the
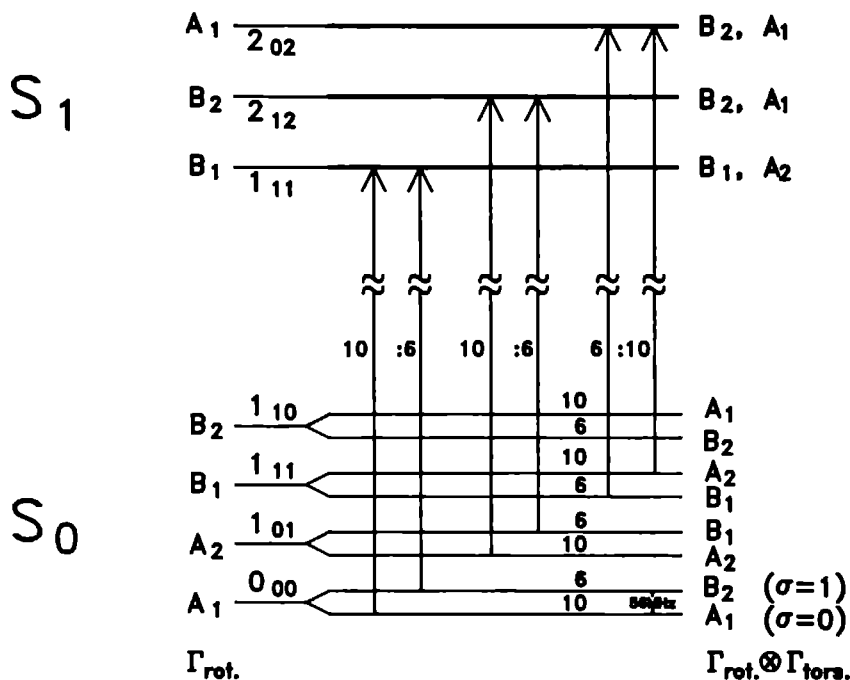
124

Figure 8.5: *Energy level scheme for the phenol monomer.*

hydrogen atoms are on either side of the line through C_1 and C_4. The positions of the oxygen and hydrogen atoms in the principal axes system of phenol (Fig. 8.1) are: $y_O = -0.055(3)$ Å, $z_O = 2.283(2)$ Å, and $y_H = 0.838(5)$ Å, $z_H = 2.629(4)$ Å.

The geometry of the rotor is determined by the value of F which depends on the moment of inertia of the rotor around the internal rotation axis (Eq. 8.3). If it is assumed that the internal rotation axis coincides with the a-axis of phenol, the F value can be calculated from the positions of the O and H atoms. The result is $F= 674\pm9$ GHz. If the internal rotation axis coincides with the C–O bond, $F=610\pm8$ GHz is calculated using the COH angle and the OH bondlength given by Larsen [6] (resp. 108.8(4)° and 0.957(6) Å). If we compare the calculated values with the value $F=690$ GHz obtained from the fitting of the torsional levels, we conclude that the internal rotation axis is nearly parallel to the a-axis.

To elucidate qualitatively the structural changes in phenol upon electronic excitation, we have performed calculations to determine the structure in the S_1 state. The C–O bond decreases upon excitation, since phenol is a stonger acid in the S_1 state than in the S_0 state. Starting with the S_0 geometry from Larsen [6], we could match the rotational constants in the excited state by increasing the C_1C_2, C_3C_4, C_4C_5, C_6C_1 distances by 0.052 Å, the C_2C_3, C_5C_6 by 0.049 Å, and decreasing the C–O bondlength by 0.118 Å, while leaving the other parameters unaffected. This geometry change is not unique, but is merely an example of a change which is consistent with the
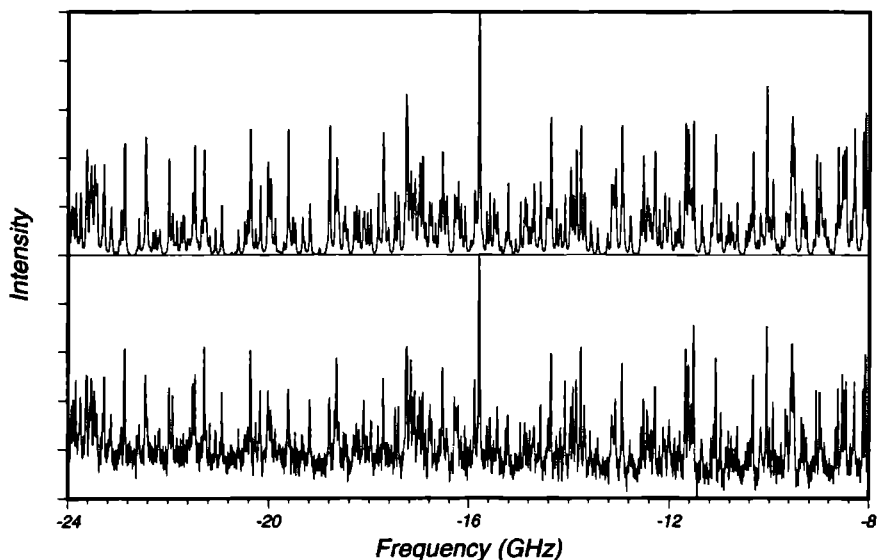
125

Figure 8.6: *Part of the high resolution LIF spectrum of the $S_1 \leftarrow S_0$ transition of phenol(H_2O)$_1$ (lower panel). The spectrum consists of two bands originating from different subtorsional levels in the S_0 state. The absolute frequency of the origin of the $\sigma=1$ state (0 on the scale of Fig. 8.6 and 8.7) is at $35\,996.47\pm0.01$ cm^{-1}. The origin of the $\sigma=0$ state is at -25.455 GHz. The upper panel shows the simulated spectrum.*

measured rotational constants and the increase in acidity. This change in structure in the C_6H_5 group and the decrease in C O bondlength points to a partially quinoidal structure in the first electronically excited state of phenol. Similar changes in rotational constants have been oberved for hydroquinone [44], which have been interpreted as an increase in quinoidal character as well.

8.5 Phenol/Water

8.5.1 Results

The origin band of the phenol(H_2O)$_1$ cluster is red shifted from the monomer origin by 353 cm^{-1}. Part of the high resolution spectrum of the 0_0^0 transition of phenol(H_2O)$_1$ is shown in the lower panel of Figure 8.6. The total spectrum consists of about 3000 fully resolved lines with a linewidth of 21 ± 2 MHz. This leads to a lifetime of 15 ± 4 ns, which is in good agreement with the value of 15 ± 1 ns given by Colson *et al.* [33]. The spectrum consists of two *ab*-type hybrid bands with different intensities separated by approximately 0.85 cm^{-1}. Both bands could be fit using rigid rotor Hamiltonians, giving two sets of (effective) rotational constants. The ground state rotational constants of each set are, within experimental error, equal to the values obtained from the microwave work [2]. In order to achieve a better accuracy for the excited state rotational constants, our UV data were refit, keeping the ground state constants fixed to the microwave values. The results

Molecular Constants Phenol/Water		
	$\sigma = 1$	$\sigma = 0$
A''	4281.76(1)	4291.49(4)
B''	1092.3254(1)	1092.1445(2)
C''	873.9082(1)	873.7271(2)
$\Delta I''$	−2.3968(6)	−2.086(1)
A'	4167.4(2)	4188.8(6)
B'	1100.63(2)	1100.6(2)
C'	874.85(2)	874.62(6)
$\Delta I'$	−2.77(2)	−1.99(9)
Band origin $\sigma=1$	35 996.47±0.01 cm^{-1}	
(Origin $\sigma=1$) − (Origin $\sigma=0$)	25 455±10 MHz	

Table 8.4: *Molecular constants of Phenol/Water; the effective rotational constants A, B, and C (in MHz), and the inertial defect $\Delta I = I_c - I_b - I_a$ (in amu Å^2) in the electronic ground state and the first excited state. Values for the ground state are taken from ref. [2].*

are shown in Table 8.4.

A simulation of a part of the UV spectrum, using the molecular constants of Table 8.4, the aforementioned linewidth, and a rotational temperature of 4 K, is shown in the upper panel of Figure 8.6. Both bands are hybrid bands with roughly 83% b-type and 17% a-type character. The higher frequency band is 3 times more intense. Figure 8.7 shows a deconvolution of the total spectrum to elucidate its structure. Only the b-type transitions are shown. For each band the $\Delta J = 0$ and $\Delta J = \pm 1$ transitions are shown separately. It is readily seen that the rotational structure of both bands is very similar.

8.5.2 Internal rotation and structure

The two bands in the UV spectrum of phenol(H$_2$O)$_1$ arise as a result of the internal torsional motion of the water moiety. Attaching the H$_2$O quenches the OH torsional motion. A careful comparison of the intensities of both bands shows an intensity ratio of 1:3 of the lower frequency band to the higher frequency band. The results of the spin statistical weights (section 8.2.3) leads us to the assignment that the lower frequency band arises from the $\sigma = 0$ state, while the higher frequency band arises from the $\sigma = 1$ state.

The differences between the effective rotational constants of the $\sigma = 0$ and $\sigma = 1$ bands are defined as $\Delta A'' = A''_{01} - A''_{00}$ etc., where the double prime denotes the electronic ground state, and the single prime denotes the excited state. The values for the differences can be obtained from Table 8.4: $\Delta A'' = -9.73$ MHz and $\Delta A' = -21.4$ MHz; all other differences are smaller than 0.3 MHz and positive. According to Eqs. (8.12-8.14) all differences (ΔA, ΔB, and ΔC) should have the same sign. This is not the case, as Table 8.4 shows. Apparently, our assumption that the rotor is 'symmetric' is not completely valid; the moments of inertia of the cluster change slightly
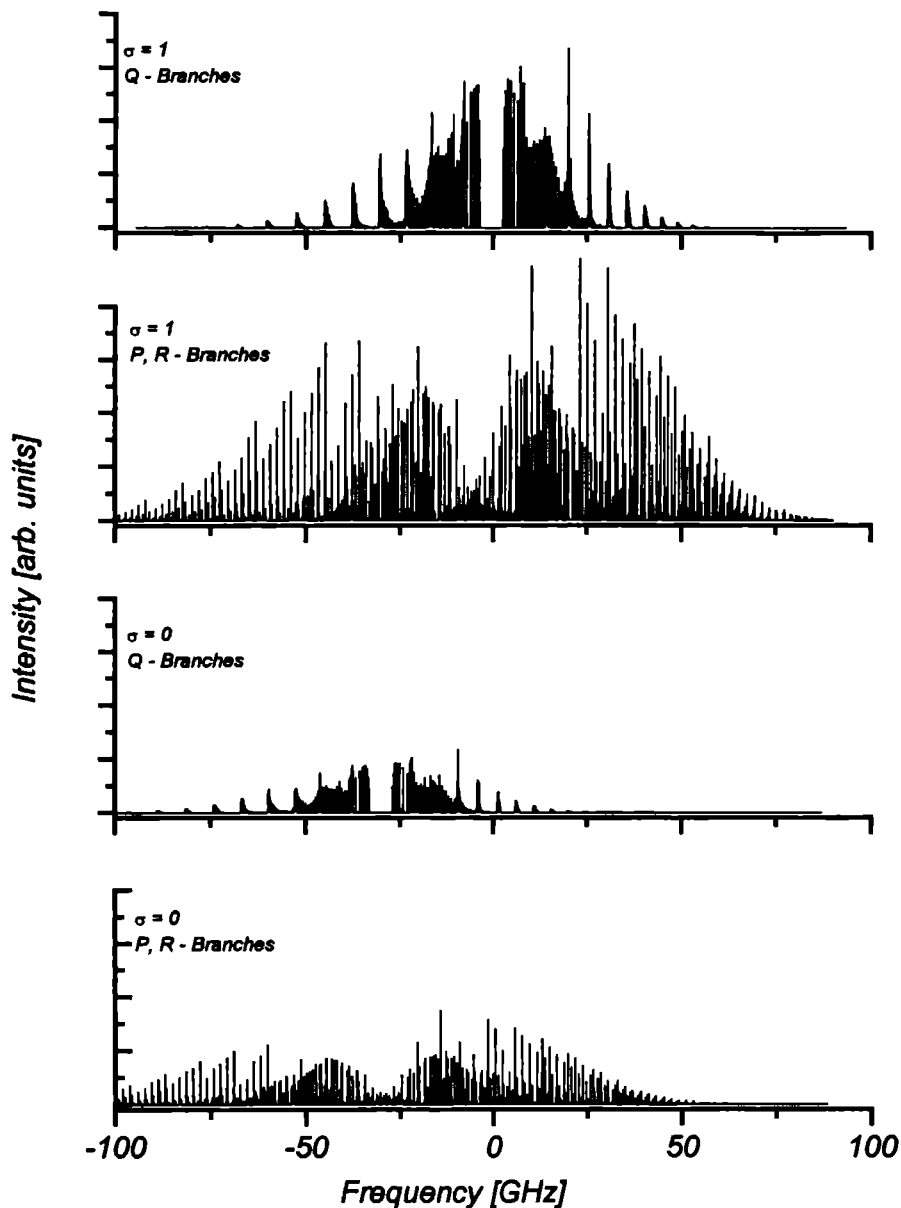
Figure 8.7: *Deconvolution of the total spectrum to elucidate its structure Only b-type transitions are shown For each band the $\Delta J = 0$ (Q) and $\Delta J = \pm 1$ (P,R) transitions are shown separately*
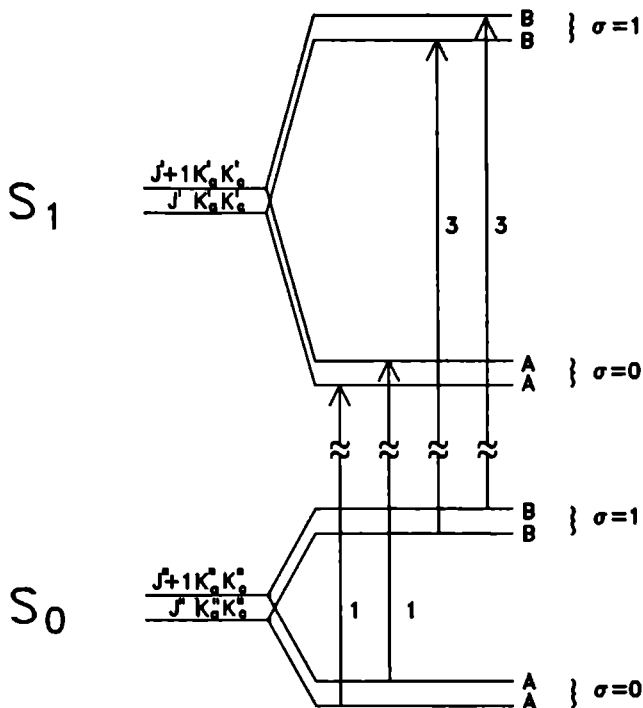
Figure 8.8: *Energy level scheme for the phenol(H_2O)$_1$ cluster.*

when the water moiety rotates. Since the signs of ΔB and ΔC are opposite to that of ΔA, and their values are small, it is concluded that the internal rotation axis is (nearly) parallel to the a-axis of phenol(H_2O)$_1$ in both electronic states (cf. Fig. 8.10).

Perturbations of the rotational constants (*i.e.*, the difference between effective and 'real' rotational constants) increase if the reduced barrier height (V_2/F) decreases. Since $|\Delta A'| > |\Delta A''|$, it is concluded that the reduced barrier height in the excited state is smaller than in the ground state. As a consequence, the subtorsional splitting in the S_1 state is larger than in the S_0 state. The resulting energy level scheme is shown in Figure 8.8. Notice that the rotional level spacing is smaller than the subtorsional splittings.

The splitting between the two bands observed in the UV spectrum is equal to the *difference* in the subtorsional splittings of the ground and excited states (see section 8.2.1). Unfortunately, only a-type transitions have been observed in the MW experiment [2]. These transitions with selection rule $\Delta\sigma = 0$ contain no information about the subtorsional splitting.

From the experimental results, we want to determine the values of V_2 and F in the S_0 and S_1 states. Unfortunately, our experiments yield only three pieces of information: $\Delta A''$, $\Delta A'$, and the splitting between the two UV bands. Therefore one parameter has to be fixed. Schütz *et al.* [18] explored the tunneling path of the internal motion by examination of the potential energy
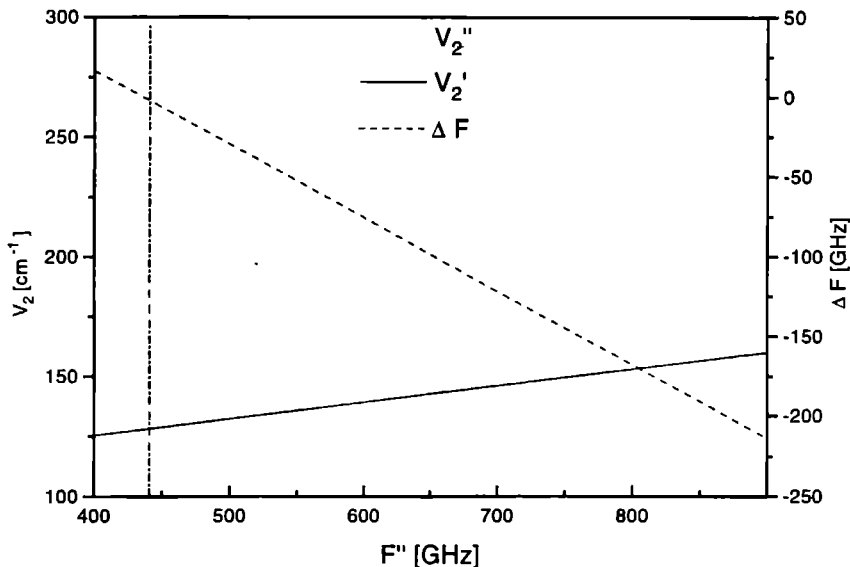
Figure 8.9: *Internal rotation of the water moiety in phenol(H$_2$O)$_1$ The barrier heights in the S$_0$ and S$_1$ state (V$_2''$ and V$_2'$, resp) and the change in geometrical structure of the rotor part (ΔF = F' − F'') as function of the geometrical structure in the S$_0$ state (F''). The vertical line indicates ΔF = 0.*

surface. Their conclusion was that the internal motion is a rotation of the water molecule about the hydrogen bond (correlating with a rotation about the *b*-axis of H$_2$O) perturbed by a wagging of the water molecule (correlating with a rotation about the *a*-axis of H$_2$O). Therefore, we have determined V_2'', V_2' and F' as a function of F'', which was varied between the B and A rotational constants of water. The results are shown in Figure 8.9. The barrier in the excited state is lower than in the ground state ($V_2' < V_2''$) for every value of F''.

If phenol(H$_2$O)$_1$ is excited to the S$_1$ state, the transition mainly takes place in the phenol chromophore, since the vibrational structures in the low resolution excitation spectra of the phenol monomer and the cluster are similar [18]. This would indicate that the structural changes upon electronic excitation mainly take place in the phenol part. Therefore, it is expected that there are no (large) structural changes in the rotor part (the water moiety). So, we might expect that $F' \approx F''$. In that case, the F value is 444 GHz (Fig. 8.9). From Eq. 8.3 it is seen that $F \approx F_\alpha + A$, in which $F_\alpha = \hbar^2/2I_\alpha$ and A is the rotational constant of phenol(H$_2$O)$_1$. Since A=4 GHz, this gives F_α=440 GHz. This latter value is close to the value of the rotational B constant of water; 435 GHz [47]. In other words, the logical assumption that the geometry of the

130

rotor does not change upon electronic excitation leads to a very simple picture for the internal motion. The water molecule rotates around its symmetry axis, which is parallel to the a-axis of the entire cluster. Using this picture, the barriers for internal rotation are calculated to be (Fig. 8.9) $V_2''=180$ cm^{-1} and $V_2'=130$ cm^{-1}.

To obtain more insight in the direction of the internal rotation axis, we have fit the barrier heights and the direction of the internal rotation axis. Two assumption are now made; the internal rotation axis is in the ab-plane and $F'' = F' = 435$ GHz (B rotational constant of water). The result is an angle of 9° with the a-axis. The barriers are $V_2''=177$ cm^{-1} and $V_2'=127$ cm^{-1}. Since the internal rotation axis has now a component allong the b-axis, the rotational B constant of the cluster should be perturbed. The difference ΔB is calculated to be –0.04 MHz. We have also fit the data as a function of the angle between the internal rotation axis and the a-axis. Now, $F'' = F'$ was a fit parameter. Increasing the angle results in a rapid decrease of F, and a rapid increase of the absolute value of ΔB (but ΔB is always negative). From these calculations, we estimate that the internal rotation axis makes an angle of less than 20° with the a-axis. In the following, we will assume that the internal rotation axis is parallel to the a-axis.

In what follows, we want to determine the geometrical structure of phenol(H$_2$O)$_1$. From Eq. (8.12) it is seen that the 'real' rotational constant A can be obtained by substracting the perturbation term from the effective rotational constant. For a barrier of 180 cm^{-1}, these perturbation terms are 4.7 MHz for $\sigma=0$ and –5.0 MHz for $\sigma=1$. The result is $A''=4286.5$ MHz. It should be noted that the values of the perturbation terms are rather insensitive to the choice of F'' [45], so that this choice does not affect the conclusions about the geometrical structure. The S_1 state with $V_2'=130$ cm^{-1} gives $A'=4177.4$ MHz.

From the unperturbed rotational constants, the inertial defect can be calculated to be $\Delta I''=$ –2.27 amu Å^2. If the oxygen atom of the water moiety is in the phenyl plane, and if that plane is perpendicular to the plane containing the water molecule, the inertial defect can be calculated from the rotational B constant of water to be $\Delta I_{calc}'' = $ –2.32 amu Å^2. We therefore conclude that in the equilibrium structure of the cluster the plane containing phenol bisects the plane of the water molecule. From the internal rotation analysis, it has been concluded that the symmetry axis of the water molecule is nearly parallel to the a-axis of phenol(H$_2$O)$_1$.

Assuming that the structure of phenol in the phenol(H$_2$O)$_1$ cluster is identical to the structure of bare phenol, it is possible to calculate the hydrogen bond length, defined by the O–O distance, in the S_0 state without knowing the structure of bare phenol. It should be kept in mind that the validity of this assumption is limited; e.g., a slight shortening of the C–O bond upon cluster formation is predicted by calculations [18]. The O–O distance can be determined if the positions of both oxygen atoms are calculated in the same coordinate system. The origin of this system is chosen at the center of mass of bare phenol with the axes parallel to its principal axes ($x=c$, $y=b$, $z=a$).

The position of the oxygen atom in bare phenol (and therefore in our approximation also in the cluster) has been determined by Larsen [6] and was given in section 8.4.2. The position of the oxygen in the water moiety can be obtained via a relationship between the rotational constants of the cluster and the monomer. This method has been used previously by Meerts et al. to determine the position of the argon atom in the fluorene-argon van der Waals complex [46]. The inertial tensor elements for the cluster are calculated in the aforementioned coordinate system.
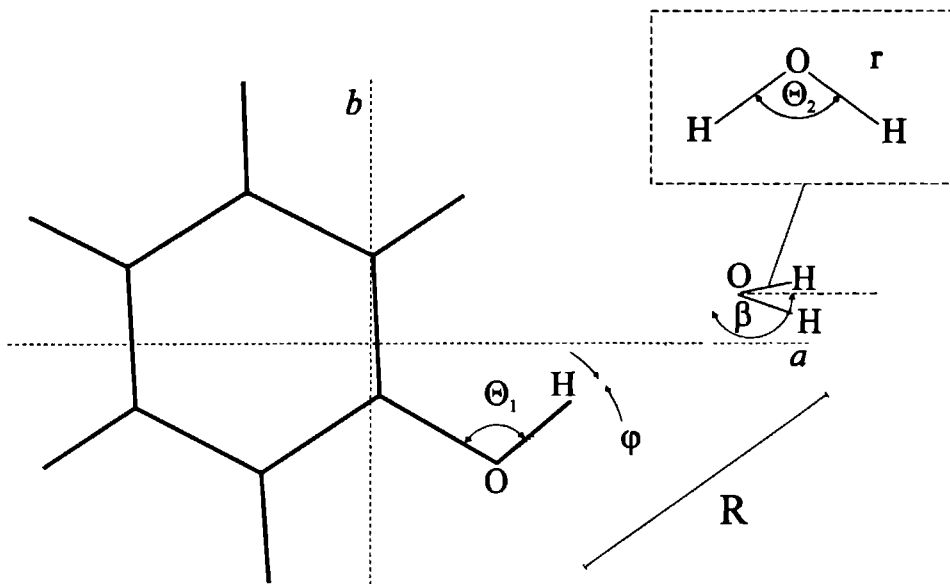
Figure 8.10: *Definition of structural parameters in phenol(H$_2$O)$_1$.*

Structural Parameters Phenol(H$_2$O)$_1$			
	S$_0$	S$_1$	calc.[a]
R	2.93	2.89	2.940
β	144 5	145.6	147.66
ϕ	6.7		3.31
θ_1	108.8[b]		111.80
$\theta_1 + \phi$	115.5		115.11
δ[c]	62.1	60.5	

[a] From Ref. [18].
[b] Value for the phenol monomer [6].
[c] The angle δ is defined as the angle between the a-axis
of bare phenol and the hydrogen bondlength.

Table 8.5: *Structural parameters of phenol(H$_2$O)$_1$ as defined in Fig. 8.10.*

The element I_{xx} can be written as:

$$I_{xx} = I_{cc}^p + \sum_{i=1}^{3} m_i^w (y_i^w)^2 - \frac{1}{M_c} \{\sum_{i=1}^{3} m_i^w y_i^w\}^2 + \sum_{i=1}^{3} m_i^w (z_i^w)^2 - \frac{1}{M_c} \{\sum_{i=1}^{3} m_i^w z_i^w\}^2 \qquad (8.17)$$

where x_i^w, y_i^w and z_i^w are the coordinates of the water atoms, M_c is the mass of the entire cluster, and I_{gg}^p are the principal moments of inertia of the phenol monomer ($I_{cc}^p = \hbar^2/2C$). The other diagonal elements, I_{yy} and I_{zz}, can be obtained by cyclic permutation of the coordinates. The off-diagonal term I_{xy} is given by:

$$I_{xy} = \frac{1}{M_c} \sum_{i=1}^{3} m_i^w x_i^w \sum_{i=1}^{3} m_i^w y_i^w - \sum_{i=1}^{3} m_i^w x_i^w y_i^w \qquad (8.18)$$

Cyclic permutation gives the other elements. The only unknown parameters in the tensor are the positions of the atoms in the water moiety, since the moments of inertia of the monomer are known. The positions of the hydrogen atoms in the water moiety can be expressed relative to the position of the oxygen atom, since the structure of water is known (R_{OH}= 0.957 Å, H-O-H=104.52° [47]). From the inertial defect, it is known that the plane containing phenol bisects the plane of the water moiety, which gives the x-coordinates of the water atoms (for oxygen x=0). From the internal rotation analysis, it is known that the symmetry axis of the water molecule is parallel to the a-axis of the cluster. Therefore, the only parameters left are the y and z coordinates of the oxygen atom. Diagonalization of the inertial tensor yields the known moments of inertia of the cluster. A least square fit gives $|y|$ = 2.534(10) Å and $|z|$ = 3.653(10) Å. This results in a hydrogen bond length of 2.93(2) Å. Other structural parameters are described in Figure 8.10 and given in Table 8.5, together with the *ab initio* results from Schütz et al. [18].

In principle, the same procedure could be used to determine the hydrogen bond length in the S_1 state. Unfortunately, no high resolution UV spectrum of isotopically substituted phenols have been recorded yet, so we do not know the position of the oxygen atom in the S_1 state. Therefore, we have used the structure of phenol as obtained by fitting the structure to the rotational constants (section 8.4.2). A good indication for the reliabilty of our structural assumptions is the equality (within errors) of the calculated S_0 oxygen coordinates with those obtained from substitution experiments. The results for the phenolic oxygen atom in the S_1 state are: y=-0.063 Å, and z=2.234 Å. The position of the water oxygen can be calculated using the method described above: $|y|$=2.447(20) Å, and $|z|$=3.657(20) Å. The hydrogen bond length in the excited state is thus calculated to be 2.89(3) Å, indicating a slight reduction of hydrogen bond length upon electronic excitation. A similar reduction of the bond length upon excitation has been observed in the *trans*-2-hydroxynaphthalene(NH₃) [1] and in the *trans*-hydroquinone(NH₃) [48]. In both cases, the NH₃ rotates about its symmetry axis, and the barriers to this motion increase on electronic excitation.

8.6 Conclusions

In the present high resolution UV study on phenol and the phenol(H₂O)₁ cluster in a supersonic molecular beam, the structure and dynamics of internal motions in these molecules could be illuminated. The rovibronic lines of phenol show a splitting due to the strongly hindered internal rotation of the −OH group around the a-axis of the molecule. The splitting in the UV-spectrum is within experimental error equal to the observed splitting in the MW experiments (56 MHz).

Therefore, the splitting in the S_1 state is < 4 MHz. This indicates that the barrier to internal rotation in the electronically excited state is much higher than in the ground state. This effect is mainly due to an increase in quinoidal character upon electronic excitation which has indeed been found when fitting the rotational constants. Using the values of the torsional transitions ($\nu = 1 \leftarrow 0$) reported by Bist *et al.* [8, 9], and assuming that the structure of the rotor part does not change drastically upon excitation, we could fit all data to obtain the barrier height in the ground and first excited states: $V_2''=1215$ cm^{-1}, and $V_2'=4710$ cm^{-1}. From the Lorentzian contribution to the linewidth of the rotational transitions, the lifetime of phenol could be determined to be 2.4 ± 0.4 ns.

Contrary to phenol, the splitting due to the torsion of the water moiety in phenol$(H_2O)_1$ is much larger than the frequency separation of the rotational lines. Spectroscopically, two bands, which arise from different subtorsional levels in the ground state, are observed with a splitting of 0.85 cm^{-1}. Both bands have different effective rotational constants, due to an interaction between the overall rotation of the entire cluster and the internal rotation. Because the two hydrogen atoms in the water molecule are equivalent, both bands have different statistical weights (1 and 3 for $\sigma=0$ and 1, respectively). Since the electronic transition mainly takes place in the phenol chromophore, we can assume that the structure of the internal rotor part (the water moiety) does not change upon electronic excitation. In this case, the effective rotational constants and the observed splitting can be fit to obtain the barriers for internal rotation and the structure of the rotor in both electronic states. This assumption gives a simple physical picture for the internal motion: the water molecule rotates around its symmetry axis, which is nearly parallel to the a-axis of the entire cluster. In this case, a barrier of 180 cm^{-1} for the S_0 state and 130 cm^{-1} for the S_1 state could be estimated.

From rotational constants and the results of internal rotor analysis, it has been shown that phenol$(H_2O)_1$ is *trans*-linear, and the plane containing phenol bisects the plane of the water molecule. The hydrogen bond length, defined by the O–O distance, is 2.93(2) Å in the S_0 state, and 2.89(3) Å in the S_1 state. In conclusion, the barrier for internal rotation and the hydrogen bond length decrease upon electronic excitation.

Acknowledgments

References

1. see, for example, D.F. Plusquellic, X.-Q. Tan and D.W. Pratt, J. Chem. Phys. **96** (1992) 8026

2. M. Gerhards, M. Schmitt, K. Kleinermanns and W. Stahl, to be published.

3. T. Kojima, J. Phys. Soc. Japan **15** (1960) 284

4. H. Forest and B.P. Dailey, J. Chem. Phys. **45** (1966) 1736

5. E. Mathier, D. Welti, A. Bauder and Hs.H. Günthard, J. Mol. Spectrosc. **37** (1971) 63

6. N.W. Larsen, J. Mol. Structure **51** (1979) 175

7. H.D. Bist, J.C.D. Brand and D.R. Williams, J. Mol. Spectrosc. **21** (1966) 76

8. H.D. Bist, J.C.D. Brand and D.R. Williams, J. Mol. Spectrosc. **24** (1967) 402

9. H.D. Bist, J.C.D. Brand and D.R. Williams, J. Mol. Spectrosc. **24** (1967) 413

10. H.W. Wilson, R.W. MacNamee and J.R. Durig, J. Raman Spectrosc. **11** (1981) 252

11. H.C. Longuet-Higgins, Mol. Phys. **6** (1963) 445

12. M. Schütz, T. Bürgi and S. Leutwyler, J. Mol. Struct. (Theochem) **276** (1992) 117

13. S.L. Anderson, L. Goodman, K. Krogh-Jespersen, A. Ozkabak, R. Zare and C. Zheng, J. Chem. Phys. **82** (1985) 5329

14. M. Krauss, J.O. Jensen and H.F. Hameka, J. Phys. Chem. **98** (1994) 9955

15. K. Kim and K.D. Jordan, Chem. Phys. Lett. **218** (1994) 261

16. J. Christoffersen, J.M. Hollas and G.H. Kirby, Proc. Roy. Soc. A **307** (1968) 97

17. S.J. Martinez III, J.C. Alfano and D.H. Levy, J. Mol. Spectrosc. **152** (1992) 80

18. M. Schütz, T. Bürgi and S. Leutwyler, J. Chem. Phys. **98** (1993) 3763

19. T. Ebata, M. Furukawa, T. Suzuki and M. Ito, J. Opt. Soc. Am. B **7** (1990) 1890

20. G. Hartland, B. Henson, V. Venturo and P.M. Felker, J. Phys. Chem. **96** (1992) 1164

21. S. Tanabe, T. Ebata, M. Fujii and N. Mikami, Chem. Phys. Lett. **215** (1993) 347

22. H. Abe, N. Mikami and M. Ito, J. Phys. Chem. **86** (1982) 1768

23. A. Oikawa, H. Abe, N. Mikami and M. Ito, J. Phys. Chem. **87** (1983) 5083

24. K. Fuke and K. Kaya, Chem. Phys. Lett. **94** (1983) 97

25. R.J. Stanley and A.W. Castleman, J. Chem. Phys. **94** (1991) 7744

26. R.J. Lipert and S.D. Colson, J. Chem. Phys. **89** (1988) 4579

27. K. Wolf, H.-H. Kuge, M. Schmitt and K. Kleinermanns, Ber. Bunsenges. Phys. Chem. **96** (1992) 1309

28. M. Pohl, M. Schmitt and K. Kleinermanns, J. Chem. Phys. **94** (1991) 1717

29. M. Gerhards and K. Kleinermanns, to be published.

30. R.J. Lipert and S.D. Colson, Chem. Phys. Lett. **161** (1989) 303

31. M. Schmitt, H. Müller and K. Kleinermanns, Chem. Phys. Lett. **177** (1994) 246

32. A. Sur and P.M. Johnson, J. Chem. Phys. **84** (1986) 1206

33. R.J. Lipert, G. Bermudez and S.D. Colson, J. Phys. Chem. **92** (1988) 3801

34. R.J. Lipert and S.D. Colson, J. Phys. Chem. **93** (1989) 135

35. R.J. Lipert and S.D. Colson, J. Phys. Chem. **94** (1990) 2358

36. A. Goto, M. Fujii, N. Mikami and M. Ito, J. Phys. Chem. **90** (1986) 2370

37. G. Reiser, O. Dopfer, R. Lindner, G. Henri, K. Müller-Dethlefs, E.W. Schlag and S.D. Colson, Chem. Phys. Lett. **181** (1991) 1

38. O. Dopfer, G. Reiser, K. Müller-Dethlefs, E.W. Schlag and S.D. Colson, J. Chem. Phys. **101** (1994) 974

39. O. Dopfer and K. Müller-Dethlefs, J. Chem. Phys. **101** (1994) 8508

40. P. Hobza, R. Burcl, V. Špirko, O. Dopfer, K. Müller-Dethlefs and E.W. Schlag, J. Chem. Phys. **101** (1994) 990

41. S. Gerstenkorn and P. Luc, *Atlas du spectroscopie d'absorption de la molecule d'iode*, CNRS, Paris (1978)
    S. Gerstenkorn and P. Luc, Rev. Phys. Appl. **14** (1979) 791

42. W. Gordy and R.L. Cook, *Microwave Molecular Spectra*, 3rd Ed., John Wiley & Sons, New York (1984)

43. P.R. Bunker, *Molecular symmetry and spectroscopy*, Academic Press, New York (1979)

44. S.J. Humphrey and D.W. Pratt, J. Chem. Phys. **99** (1993) 5078

45. D.R. Herschbach, J. Chem. Phys. **31** (1959) 91

46. W.L. Meerts, W.A. Majewski and W.M. van Herpen, Can. J. Phys. **62** (1984) 1293

47. W.S. Benedict, N. Gailar and E.K. Plyler, J. Chem. Phys. **24** (1956) 1139

48. S.J. Humphrey *et al.*, to be published.

Chapter 9

Rotationally resolved UV spectroscopy
of 4-aminobenzonitrile (4-ABN)

Giel Berden, Jack van Rooy and W. Leo Meerts
Department of Molecular and Laser Physics, University of Nijmegen,
Toernooiveld, 6525 ED Nijmegen, The Netherlands

Klaas A. Zachariasse
Max-Planck-Institut für biophysikalische Chemie,
Am Fassberg, Postfach 2841, D-3400 Göttingen, Germany

Abstract

The rotationally resolved fluorescence excitation spectrum of the 0_0^0 band in the $S_1 \leftarrow S_0$ transition of 4-aminobenzonitrile (4-ABN), at 299 nm, has been recorded using laser induced fluorescence in a molecular beam apparatus. This band exhibits pure b-type character. The rotational constants in the S_0 and S_1 states have been determined. In addition, the rotationally resolved fluorescence excitation spectra of two vibronic bands in the S_1 state, at 807 and 816 cm^{-1}, have been recorded. The non-planarity of the molecule is discussed by comparing the inertial defects in these states.

9.1 Introduction

The last years, much attention has been paid to the assignment of the vibrational modes in the laser induced fluorescence (LIF) excitation and emission spectra of jet-cooled 4-aminobenzonitrile (4-ABN, see Figure 9.1) [1, 2, 3, 4]. Gibson *et al.* [1, 2] showed that spectroscopically 4-ABN closely resembles aniline, rather than benzonitrile, and that the amino inversion mode is very active in both excitation and emission spectra. Recently, Yu *et al.* [4] used the semi-empirical quantum chemical calculation called parametric method 3 (PM3) to compute the geometry and normal modes of 4-ABN in the ground and first excited states. The calculated normal modes were in good agreement with the experimental values. The calculated rotational constants were used to simulate a rotational band contour of the origin band which was compared with the experimental contour.

As far as we know, no accurate experimental values for the rotational constants are available. Howells *et al.* [5] reported a rotational band contour study on jet cooled 4-ABN at a resolution of 0.1 cm^{-1}. They simulated the spectra by varying only the ground state constants and keeping the differences between the constants in the excited and ground state fixed ($\Delta B = \Delta C = 0$ and $(A'' - A')/A'' = 0.03$). In this paper we report the fully rotationally resolved UV fluorescence excitation spectra of the 0_0^0 band and of two vibronic bands in the $S_1 \leftarrow S_0$ transition of 4-ABN.
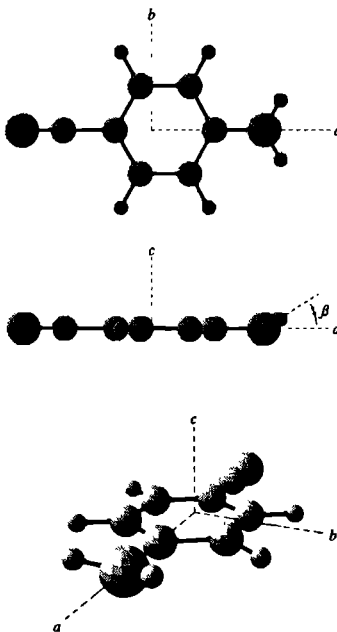

Figure 9.1: *Three different views of 4-aminobenzonitrile (4-ABN) and its inertial axes. The angle β designates the angle between the amino plane and the benzene plane.*

9.2   Experimental

Fluorescence excitation spectra of 4-ABN were obtained using a narrow bandwidth UV laser system and a molecular beam apparatus. Crystalline 4-aminobenzonitrile (Fluka, 97%) was heated in a quartz nozzle to approximately 120 °C. A molecular beam was formed by a continuous expansion of a mixture of 4-ABN vapor and argon (500-600 Torr) through a nozzle with a diameter of 0.15 mm. The nozzle was kept at a slightly higher temperature to prevent condensation of 4-ABN in the orifice. The molecular beam was skimmed twice and entered a differentially pumped LIF detection chamber at a distance of 30 cm from the nozzle orifice. There the molecular beam was crossed perpendicularly with the weakly focused UV laser beam. The 4-ABN molecules were resonantly excited from the S_0 to the S_1 state, and the total fluorescence back to the electronic ground state was detected. Narrow band UV radiation was generated by intracavity frequency doubling a single frequency ring dye laser (a modified Spectra Physics 380D) operating on Rh6G. By using a 1.5 mm thick $LiIO_3$ crystal, 5 mW of tunable radiation was obtained around 299 nm with an effective bandwidth of 3 MHz. Due to self absorption of UV radiation at wavelengths below 300 nm, $LiIO_3$ cannot be used for generating UV below 295 nm. To cover the wavelength range around 291.5 nm, a 2 mm thick BBO crystal was used (200-500 μW). The excitation spectra of 4-ABN were recorded together with the transmission peaks of a pressure and temperature stabilized interferometer with a free spectral range of 75 MHz. For absolute frequency calibration, the iodine absorption spectrum [6] was recorded.

9.3   Results

In Figures 9.2 and 9.3 the measured high resolution LIF excitation spectrum of the origin of the $S_1 \leftarrow S_0$ transition of 4-ABN is shown. The absolute frequency of the band origin (0.0 on the scale of the figures) is at $33\,481.440\pm0.003$ cm^{-1}. The spectrum consists of about 800 well resolved lines with a linewidth of 26 MHz and was recorded in less than 10 minutes. In this way the drift of the interferometer during the scan was minimized.

The spectrum can immediately be identified as a b-type band. This indicates that the electronic transition moment vector in 4-ABN is parallel to the inertial b-axis (short axis polarized), as has also been observed for aniline [7] and benzonitrile [8].

After identification of the band type, we used the following procedure to analyze the data. A spectrum was simulated using an asymmetric rotor Hamiltonian and using rotational constants obtained from a crude geometrical structure. The spectrum obtained in this way, was then compared with the experimental spectrum. An initial assignment was made in the center part of the spectrum, which is the least dense part. The assigned lines were used as input for the fitting program. With the improved rotational constants the spectrum was simulated again and compared with the experimental spectrum. This procedure was repeated several times. At the end 350 lines were included in the fit and all parameters were varied simultaneously. All lines could be fitted within the experimental error.

The absolute precision of the UV data is limited by thermal drift of the frequency markers. The magnitude of this error can be determined by scanning the spectrum several times on various days. From the fit, we obtain the origin of the transition and the rotational constants A, B, and C in the ground state as well as in the excited state. The constants are listed in Table 9.1 together with the asymmetry parameters and the inertial defects.

The shape of the spectrum depends on the rotational temperature, and the linewidth of the
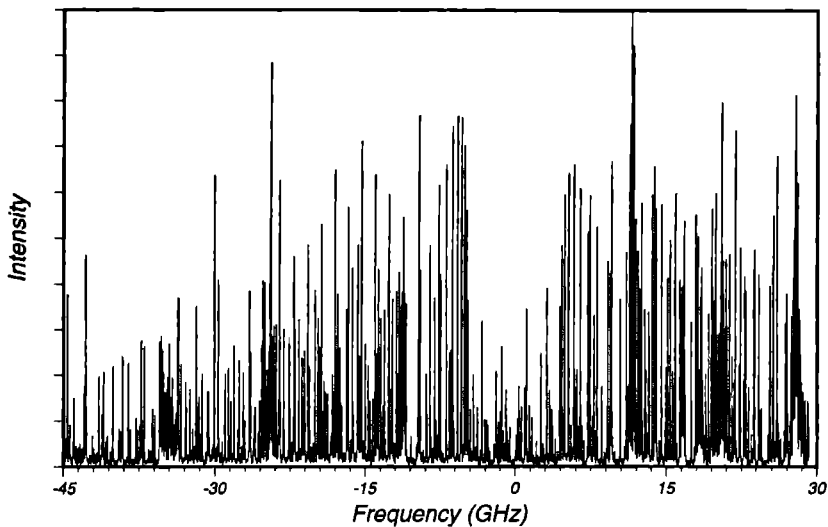
Figure 9.2: *High resolution LIF spectrum of the origin of the $S_1 \leftarrow S_0$ transition of 4-ABN. The absolute frequency of the origin (0.0 on the scale of the figure) is at $33\,481.440 \pm 0.003$ cm^{-1}.*
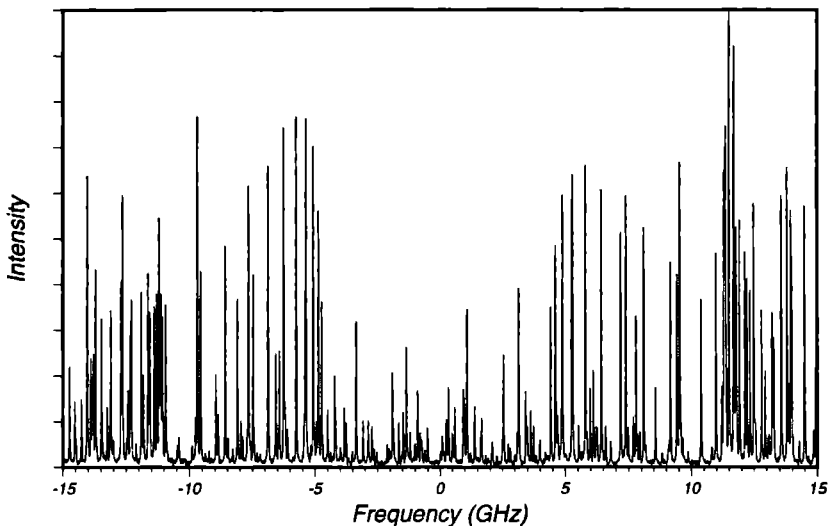

Figure 9.3: *Part of the high resolution LIF spectrum of the origin of the $S_1 \leftarrow S_0$ transition of 4-ABN. The spectrum is a pure b-type band.*

		Molecular Constants of 4-aminobenzonitrile			
	S_0		S_1		
			0	I_0^2	1_0^1
A''	5579.3(5)	ΔA	−316.61(6)	−323.97(5)	−323.99(10)
B''	990.26(9)	ΔB	10.849(3)	11.392(3)	11.082(7)
C''	841.39(8)	ΔC	0.095(1)	0.989(2)	0.557(5)
$\Delta I''$	−0.293(2)	$\Delta I'$	−0.281(2)	−0.878(3)	−0.608(9)
ν_0			33 481.440(3)	34 288.676(3)	34 297.760(3)

Table 9.1: *Molecular constants of 4-aminobenzonitrile; the rotational constants (in MHz) and the inertial defect ($\Delta I = I_c - I_b - I_a$, in amu Å^2) in the S_0 state, the differences of the rotational constants between the S_0 and S_1 states ($\Delta A = A' - A''$, etc.), and the inertial defect in the S_1 state. The constants are listed for three bands, which have their origin at the absolute frequency ν_0 (in cm^{-1}).*

individual rotational lines. The experimental spectrum could be best simulated with a rotational temperature of 3 K, and a linewidth of 26 MHz. The linewidth of our spectrometer is known to be 14 MHz owing to residual Doppler broadening, transit time effects, fluorescence collection optics and laser linewidth, leaving a contribution due to the finite excited state lifetime of 4-ABN. The lifetime of the origin can then be estimated to be 9±3 ns, which is slightly less than the reported value of 13.0 ns [3].

Besides the origin band, we have measured the rotationally resolved excitation spectra of two vibronic bands at 807 cm^{-1} and 816 cm^{-1} above the electronic origin. The first band has been assigned to the $\Delta v = 2$ transition in the amino group inversion mode, I_0^2, by Gibson *et al.* [2]. The signal to noise ratio of the high resolution spectrum of this band is worse than that of the spectrum of the origin band, for which there are two reasons. First, the Franck-Condon factor of the I_0^2 band is smaller. In the low resolution spectrum, this band is a factor two lower in intensity than the origin band [3]. Second, the power of the excitation laser is a factor 10–20 lower as a result of the use of a BBO crystal for generating UV, rather than the more efficient LiIO$_3$ which could be used to measure the origin band. The other vibronic band, at 816 cm^{-1}, has been assigned to the $\Delta v = 1$ transition in the ring breathing mode, 1_0^1 [2, 4]. Both vibronic bands are *b*-type bands. All lines in both spectra, could be assigned and fitted to an asymmetric rotor Hamiltonian. The rotational constants are presented in Table 9.1. The linewidths of the spectra are slightly larger than the linewidth observed in the origin band, indicating that the life times are slightly shorter. The linewidths of the I_0^2 and the 1_0^1 bands are 24 MHz, which results, after deconvolution, in a value for the life time of 9±4 ns. This value is in agreement with the reported 10.9 ns for the I_0^2 band, and 11.1 ns for the 1_0^1 band [3].

9.4 Discussion

Although it is impossible to determine the complete structure of 4-ABN from our data, we can derive a qualitative picture of the structure in the S_0 state and the structural changes upon excitation. The inertial defect in the S_0 state of 4-ABN is $-0.293(2)$ amu $Å^2$. This value can be compared to the values of benzonitrile, $+0.093(30)$ amu $Å^2$ [9], and aniline, $-0.408(1)$ amu $Å^2$ [10], for which the complete substitution structures have been determined (respectively, [9] and [11]). Benzonitrile is planar in the ground state. In aniline, the hydrogen atoms of the NH_2 group are not coplanar with the rest of the molecule. The angle β of aniline has been determined to be $37°$–$44°$ [11, 12, 10]. The inertial defect of 4-ABN is smaller than that of aniline, suggesting that the angle β of 4-ABN is slightly smaller (ca. $6°$).

The structure of 4-ABN in the crystal-phase (at 153 K) has been determined by Heine et al. [13]. Their conclusion was that the inversion angle β is $34(3)°$. The nitrogen atom of the amino group is located out of the benzene plane by $0.059(3)$ Å (in opposite direction to the amino hydrogen atoms). Furthermore, the cyano group is located out of the plane on the same side as the amino hydrogen atoms (C atom $0.020(3)$ Å, N atom $0.047(3)$ Å). From the positions of all atoms, we have calculated the rotational constants and the inertial defect (Table 9.2). Since bond lengths in the crystalline phase are always smaller than gas-phase bond lengths, the rotational constants of crystalline 4-ABN are larger than those of gas-phase 4-ABN. However, it is interesting to note that the inertial defects are equal. This indicates that the out-of-plane atomic positions in the gas-phase can be reasonable well described by the crystal-phase positions. The out-of-plane position of the nitrogen atoms give only a minor contribution to the inertial defect. We therefore conclude that the angle β of 4-ABN is roughly $34°$.

Upon electronic excitation to the origin of the S_1, the A constant of 4-ABN decreases with 5.7%, the B constant increases with 1.1%, while the C constant is practically unchanged. Comparison of the changes in rotational constants with those of aniline ($\Delta A=-5.9\%$, $\Delta B=+1.5\%$, $\Delta C=-1.0\%$ [7]), and benzonitrile ($\Delta A=-3.2\%$, $\Delta B=-2.3\%$, $\Delta C=-2.5\%$ [8]), shows that 4-ABN closely resembles aniline, rather than benzonitrile. The same conclusion was drawn by Gibson et al. based on the analysis of the vibrationally resolved electronic excitation and emission spectra [1, 2]. However, the inertial defect of aniline decreases upon excitation, while the inertial defect of 4-ABN remains constant.

Qualitatively, the changes in rotational constants can be explained by an expansion of the benzene ring (with the two C–C bonds parallel to the a-axis increasing less than the other four C–C bonds), a contraction of the C–N(amino) bond, and a slight reduction of the C–N(cyano) bond. Since the inertial defect in the S_1 state is almost identical to that of the S_0 state, the inversion angle β remains unaltered upon excitation. Another possibility is that β decreases (like in aniline), while another part of the molecule comes out of the benzene plane.

Exciting 4-ABN to the vibronic band at 807 or 816 cm^{-1}, shows a slight increase of the absolute values of the differences in rotational constants (compared to the origin). ΔA becomes more negative, while ΔB and ΔC become more positive. The inertial defects are larger, indicating that some atoms move (further) out of the benzene plane. Logical candidates are the amino hydrogen atoms and the cyano group. The band at 807 cm^{-1} has been assigned to the $\Delta v=2$ transition in the amino inversion mode, I_0^2 [2]. The associated increase of β can explain partially the increase in ΔA and ΔI. The other band, at 816 cm $^{-1}$, has been assigned to the $\Delta v=1$ transition in the ring vibrating mode, 1_0^1 [2, 4]. An expansion of the benzene ring alone would not change the inertial defect, so there is an additional out-of-plane motion.

Molecular Constants of 4-aminobenzonitrile			
	gas-phase	crystal-phase	PM3
A''	5579 3(5)	5756 4	5527 5
B''	990 26(9)	1006 8	994 7
C''	841 39(8)	857 3	843 8
ΔA	–316 61(6)		–155 3
ΔB	10 849(3)		6 4
ΔC	0 095(1)		0 3
$\Delta I''$	–0 293(2)	–0 28	–0 59
$\Delta I'$	–0 281(2)		–0 14

Table 9.2: *Rotational constants of 4-aminobenzonitrile Experimental values in the gas-phase (this work), and the crystal-phase [13] Theoretical values reported by Yu et al [4], obtained from semi-empirical calculations Rotational constants are in MHz, inertial defects in amu Å²*

The rotational constants of Table 9 1 can be used to test the results of theoretical calculations Yu *et al* [4] used the semi-empirical quantum chemical calculation PM3 to compute the geometry and the normal modes of 4-ABN in the S_0 and S_1 states The calculated normal modes were in good agreement with the experimental values [4] The calculated rotational constants can now be compared with the experimental constants of present study (Table 9 2) It is seen that the calculated ground state constants are in good agreement with the experimental values The agreement is worse for the excited state Furthermore, the calculations predict a decrease in the inertial defect which is not observed It is interesting to note that this decrease (although not that large) has been observed for aniline [7]

The results of present study can be useful for the analysis and interpretation of more complicated derivatives of 4-ABN An important derivative is 4-N,N-dimethylaminobenzonitrile (DMABN) This molecule is extensively studied because of its dual fluorescence in polar solvents The high resolution excitation spectrum of DMABN is heavily perturbed by torsional motions of the methyl groups [14]

Acknowledgements

References

1. E.M. Gibson, A.C. Jones, A.G. Taylor, W.G. Bouwman and D. Phillips, J. Phys. Chem. **92** (1988) 5449

2. E.M. Gibson, A.C. Jones and D. Phillips, Chem. Phys. Letters **146** (1988) 270

3. H. Yu, E. Joslin, B. Crystall, T. Smith, W. Sinclair and D. Phillips, J. Phys. Chem. **97** (1993) 8146

4. H. Yu, E. Joslin, S.M. Zain, H. Rzepa and D. Phillips, Chem. Phys. **178** (1993) 483

5. B.D. Howells, J. McCombie, T.F. Palmer, J.P. Simons and A. Walters, J. Chem. Soc. Faraday Trans. **88** (1992) 2595

6. S. Gerstenkorn and P. Luc, *Atlas du spectroscopie d'absorption de la molecule d'iode*, CNRS, Paris (1978)
   S. Gerstenkorn and P. Luc, Rev. Phys. Appl. **14** (1979) 791

7. E.R.Th. Kerstel, M. Becucci, G. Pietraperzia and E.M. Castellucci, to be published.

8. J.C.D. Brand and P.D. Knight, J. Mol. Spectrosc. **36** (1970) 328

9. B. Bak, D. Christensen, W.B. Dixon, L. Hansen-Nygaard and J. Rastrup-Andersen, J. Chem. Phys. **37** (1962) 2027

10. B. Kleibömer and D.H. Sutter, Z. Naturforsch. **43a** (1988) 561

11. D.G. Lister, J.K. Tyler, J.H. Høg and N.W. Larsen, J. Mol. Struct. **23** (1974) 253

12. M. Quack and M. Stockburger, J. Mol. Spectrosc. **43** (1972) 87

13. A. Heine, R. Herbst-Irmer, D. Stalke, W. Hühnle and K.A. Zachariasse, Acta Cryst. **B50** (1994) 363

14. G. Berden, unpublished results.
    D.W. Pratt, private communication.

Samenvatting

Hoge resolutie UV spectroscopie
aan aromatische moleculen

Het bestuderen van moleculen en moleculaire complexen in een supersone moleculaire bundel-expansie met behulp van een smalbandige ultraviolette (UV) laser levert gedetailleerde informatie over hun structuur en dynamica. Een supersone moleculaire bundel wordt gemaakt door de te bestuderen moleculen met een overmaat aan edelgas atomen door een klein gaatje (ongeveer 100 μm) te laten expanderen in een vacuüm tank. In deze expansie vindt een aanzienlijke reductie plaats van de vibratie- en rotatietemperatuur (de rotatietemperatuur is ongeveer 3 K). Deze lage temperaturen hebben twee voordelen. Ten eerste is het aantal bezette energietoestanden laag, zodat de waargenomen spectra eenvoudiger worden. Ten tweede kunnen door de lage interne energie zwak gebonden moleculaire klusters (complexen) ontstaan. Doordat de snelheid van alle moleculen en atomen in de bundel nagenoeg gelijk is, vinden geen botsingen plaats, waardoor de zwak gebonden klusters niet uit elkaar vallen.

Door de moleculaire bundel loodrecht te kruisen met een UV laserbundel, kunnen de te bestuderen moleculen of klusters energie opnemen waardoor ze in een electonisch aangeslagen toestand komen. De aangeslagen toestand bestaat slechts zeer kort. De moleculen gaan naar een lagere energietoestand, waarbij ze hun energie verliezen in de vorm van licht. Dat licht, laser geïnduceerde fluorescentie genaamd, wordt gedetecteerd als functie van de golflengte van de UV laserbundel.

Op deze wijze kan het electronisch rotatiespectrum van een molecuul worden opgemeten. Elke lijn in het spectrum zegt iets over de mate waarin het gehele molecuul roteert. Analyse van het gehele spectrum levert informatie op over de structuur van dit molecuul in de grondtoestand (de electronische toestand waarin het molecuul zich bevond voordat het aangeslagen was) en de structuurveranderingen die plaatsvinden als het molecuul aangeslagen wordt. Verder kan uit het spectrum de tijd bepaald worden die het molecuul in de aangeslagen toestand doorgebracht heeft (levensduur) en kan de richting van de electronenverplaatsing ten gevolge van de electronische excitatie bepaald worden (overgangsdipoolmoment).

In dit proefschrift worden aromatische moleculen bestudeerd. Dit zijn moleculen waarin een koolstofring (benzeenring) ingebouwd is. In hoofdstuk 2 is trifenylamine (TPA) onderzocht. Het rotatiespectrum is dat van een symmetrische top. Dit betekent dat TPA een drievoudige symmetrie-as heeft. Analyse van dit spectrum geeft de rotatieconstanten in de grondtoestand en de electronisch aangeslagen toestand. Hieruit kan worden afgeleid dat TPA een propeller-achtige vorm heeft. Verder is het Van der Waals complex van TPA met argon onderzocht. Het spectrum van dit zwak

gebonden kluster toont onmiddellijk aan dat het argon atoom op de symmetrie-as van TPA zit.

Hoofdstuk 3 beschrijft een microgolf-ultraviolet dubbel resonantie experiment aan 1-cyano-naftaleen. Door met behulp van microgolfstraling de bezetting van bepaalde energieniveaus in de electronische grondtoestand te veranderen, worden deze niveaus gemerkt. Rotatielijnen in het UV spectrum die een gevolg zijn van een overgang vanuit een gemerkt niveau, kunnen dan zichtbaar worden gemaakt. Hierdoor kan de analyse van het UV rotatiespectrum vergemakkelijkt worden.

De limiet van hoog opgeloste UV spectroscopie wordt bijna bereikt in het experiment dat beschreven is in hoofdstuk 4. Het rotatiespectrum van het Van der Waals complex van 1-cyano-naftaleen en triethylamine is gemeten en geanalyseerd. Omdat het complex zo enorm groot is, bevat het spectrum zoveel rotatielijnen dat het grootste deel van de lijnen elkaar overlappen. Desalniettemin kon de structuur van dit grote kluster bepaald worden.

Hoofdstuk 5 beschrijft experimenten aan 1-aminonaftaleen (1-AN). Dit molecuul bestaat uit een vlak deel, naftaleen, waaraan een amino-groep (NH_2) is bevestigd. Door de rotatiespectra van 1-AN te vergelijken met de spectra van 1-AN, waarin de waterstofatomen in de aminogroep zijn vervangen door deuteriumatomen, zijn de posities van deze waterstofatomen bepaald. Het blijkt dat deze atomen uit het naftaleenvlak komen en dat de afstand tot dit vlak afhangt van de electronische en vibrationele toestand waarin 1-AN zich bevindt.

In hoofdstuk 6 wordt aangetoond dat het molecuul 2H-benzotriazole bestaat. Tot dan toe was alleen het bestaan van 1H-benzotriazole aangetoond. De twee moleculen lijken veel op elkaar wat de geometrische structuur betreft. Het enige verschil is de positie van één waterstofatoom. Dit heeft echter grote consequenties voor de electronische structuur en dus voor de chemische activiteit van de twee moleculen.

De rotatiespectra van indole, indazole en benzimidazole, die getoond worden in hoofdstuk 7, vertonen abnormale intensiteiten. Ten gevolge van het electronisch aanslaan van deze moleculen treden structuursveranderingen op die zodanig zijn dat de richtingen van de hoofdtraagheidsassen van deze moleculen plotseling veranderen. Dit effect, dat assen-reorientatie genoemd wordt, zorgt voor veranderingen in de intensiteiten van de rotationale lijnen. Analyse van de frequenties van de rotationele lijnen levert de rotatieconstanten van elk molecuul in de grondtoestand en de aan-geslagen toestand. Analyse van de intensiteiten van de rotatielijnen geeft de verandering van de hoofdtraagheidsassen. Beide analyses geven zeer nauwkeurige structuur-parameters voor indole, indazole en benzimidazole, die gebruikt kunnen worden voor het testen van theoretische structuur-berekeningen.

Hoofdstuk 8 toont de hoog opgeloste spectra van fenol en van het fenol-water complex. Beide spectra zijn 'verstoord' door een interactie tussen de rotatie van het hele molecuul (of complex) en een interne beweging van een deel van dit molecuul (of complex). Uit de analyse van de spectra blijkt dat in fenol de OH-groep roteert om de C O binding. Als fenol electronisch aangeslagen wordt, verdwijnt deze interne beweging omdat de C–O binding sterker wordt. In het via een waterstofbrug gebonden fenol-water complex roteert het water molecuul om zijn eigen symmetrie-as en om de waterstofbinding. Een interne beweging zoals in het ongebonden fenol molecuul, vindt nu niet meer plaats.

Het laatste hoofdstuk van dit proefschrift toont de resulaten van een spectroscopische studie aan 4-aminobenzonitriel. De rotatiespectra van een aantal vibratiebanden in de aangeslagen toestand zijn gemeten en geanalyseerd om de structuur en structuurveranderingen van dit molecuul te bepalen.

Curriculum Vitae

Op 12 mei 1966 ben ik geboren te Tegelen. Na het behalen van het VWO diploma aan het "Blariacum College" te Blerick, ging ik in 1985 Natuurkunde studeren aan de Katholieke Universiteit Nijmegen (KUN). Mijn studie werd afgesloten met een stage op de afdeling Molecuul- en Laserfysica. Op 25 oktober 1989 mocht ik het doctoraal diploma Experimentele Natuurkunde in ontvangst nemen. Vervolgens verhuisde ik voor tien maanden naar Rome. Gedurende de eerste twee maanden verrichtte ik onderzoek in de groep van Prof. A. Giardini-Guidoni van de Universiteit "La Sapienza". Daarna werkte ik op het instituut ENEA (te Frascati) in de groep van Dr. R. Fantoni aan het opbouwen van een opstelling voor optische diagnostiek in een CVD reactor. Eind 1990 trad ik als onderzoeker-in-opleiding in dienst van de stichting voor Fundamenteel Onderzoek der Materie (FOM). Het promotie-onderzoek werd verricht op de afdeling Molecuul- en Laserfysica van de KUN, onder begeleiding van Dr. L. Meerts, Prof. J. Reuss en Prof. G. Meijer. De resultaten hiervan staan beschreven in dit proefschrift.

Publications

Luminescence and ESCA analysis of laser-ablated materials
A. Giardini-Guidoni, A. Morone, M. Snels, E. Desimoni, A.M. Salvi, R. Fantoni,
W.C.M. Berden and M. Giorgi
Applied Surface Science *46* (1990) 321

On-line gas-phase optical diagnostics in plasma CVD deposition of carbon films
R. Fantoni, M. Giorgi, A.G.G. Moliterni, W.C.M. Berden, V. Lazic, O. Martini and
F. Polla Mattiot
Journal of Materials Research *7* (1992) 1204

Spectroscopy on triphenylamine and its van der Waals complexes
G. Meijer, G. Berden, W.L. Meerts, H.E. Hunziker, M.S. de Vries and H.R. Wendt
Chemical Physics *163* (1992) 209

*High resolution laser induced fluorescence and microwave-ultraviolet double resonance
spectroscopy on 1-cyanonaphthalene*
G. Berden, W.L. Meerts and W. Kreiner
Chemical Physics *174* (1993) 247

*High resolution laser induced fluorescence study of a cage molecule,
1,4-diazabicyclo[2,2,2]octane, DABCO*
D. Consalvo, M. Drabbels, G. Berden, W.L. Meerts, D.H. Parker and J. Reuss
Chemical Physics *174* (1993) 267

*Rotationally resolved spectroscopy on the 1-cyanonaphthalene/triethylamine
van der Waals complex in a molecular beam*
G. Berden and W.L. Meerts
Chemical Physics Letters *224* (1994) 405

149

Rotationally resolved UV spectroscopy on the 2H-tautomer of benzotriazole in a molecular beam
G. Berden, E. Jalviste and W. Leo Meerts
Chemical Physics Letters *226* (1994) 305

Rotationally resolved UV spectroscopy of indole, indazole and benzimidazole, inertial axis reorientation in the $S_1(^1L_b) \leftarrow S_0$ transitions
G. Berden, W. Leo Meerts and E. Jalviste
To be published.

High resolution UV spectroscopy of phenol and the hydrogen bonded phenol-water cluster
G. Berden, W.L. Meerts, M. Schmitt and K. Kleinermanns
Journal of Chemical Physics, submitted.

High resolution fluorescence excitation spectroscopy of 1-aminonaphthalene. S_0 and S_1 geometries and $S_1 \leftarrow S_0$ transition moment orientations
G. Berden, W.L. Meerts, D.F. Plusquellic and D.W. Pratt
To be published.

Rotationally resolved UV spectroscopy of 4-aminobenzonitrile (4-ABN)
G. Berden, J. van Rooy, W.L. Meerts and K.A. Zachariasse
To be published.